Radiations by Finite-Sized Sources in Uniaxial Materials

LUMS

A Not-for-Profit University

Aamir Hayat

Department of Physics,

Syed Baber Ali School of Science and Engineering,

Lahore University of Management Sciences (LUMS),

Lahore, Pakistan

This dissertation is submitted in partial fulfillment of the requirements for the degree of Doctor of Philosophy

July 2020

Author's Declaration

I _____ hereby state that my PhD thesis titled

_____

is my own work and has not been submitted previously by me for taking any degree from LAHORE UNIVERSITY OF MANAGEMENT SCIENCES or anywhere else in the country/world.

At any time if my statement is found to be incorrect, even after my graduation, the university has the right to withdraw my PhD degree.

Name of Student: _____

Date: _____

Certificate of Approval

This is to certify that the research work presented in this thesis, entitled, **Radiations by Finite-Sized Sources in Uniaxial Materials** was conducted by Mr. **Aamir Hayat** under supervision of **Dr. Muhammad Faryad**.

No part of this has been submitted anywhere for any degree. This thesis is submitted to

Higher Education of Pakistan in partial fulfilment of the requirement for the Degree of Philosophy in the field of **Physics** for the Department of **Physics** for *"LAHORE UNIVERSITY OF MANAGEMENT SCIENCES"*.

Name of Student: **Aamir Hayat**   Signature:

Roll# **2015-12-0005**

Examination Committee:

    a) External Examiner 1:   Signature: _____

        Name & Designation: **Dr. Abdul Ghaffar, Associate Professor and Chair**

        Office Address: Department of Physics, University of Agriculture, Faisalabad

    b) Internal Examiner 1:   Signature: _____

        Name & Designation: **Dr. Muhammad Sabieh Anwar, Associate Professor and Dean SSE**

        Office Address Department of Physics, LUMS University, Lahore

    c) Internal Examiner 2:   Signature: _____

        Name & Designation: **Dr. Ata Ulhaq, Assistant Professor**

        Office Address: Department of Physics, LUMS University, Lahore

    d) Internal Examiner 3:   Signature: _____

        Name & Designation: **Dr. Muhammad Imran Cheema, Assistant Professor**

        Office Address: Department of Electrical Engineering, LUMS University, Lahore

    e) Internal Examiner 4:   Signature: _____

        Name & Designation: _____

        Office Address

    f) Internal Examiner 5:   Signature: _____

        Name & Designation: _____

Office Address

g) Internal Examiner 6:   Signature: _____

    Name & Designation: _____

    Office Address

Name of Supervisor: **Dr. Muhammad Faryad**   Signature: _____

Name of Dean/HOD: **Dr. Muhammad Faryad**   Signature: _____

SYED BABAR ALI SCHOOL OF SCIENCE AND ENGINEERING

Dissertation Approval

The members of the Committee approve the dissertation entitled **Radiations by Finite-Sized Sources in Uniaxial Materials**……by …**Aamir Hayat**…………,

defended on ……**31-07-2020**…………………………………………………………………………..

It is recommended that this dissertation be used in partial fulfillment of the requirements for the degree of Doctor of Philosophy from Department of Computer Science in Syed Babar Ali School of Science and Engineering.

_____
(Advisor)

_____
(External Examiner)

_____
(FDC Member)

_____
(FDC Member)

_____
(FDC Member)

Declaration

The work presented in this thesis was carried out in the period from **2015-2020** at Lahore University of Management Sciences under the supervision of **Dr. Muhammad Faryad** at the **Department of Physics**. I hereby declare that this submission is my own work and that, to the best of my knowledge and belief, contains no material previously published or written by another person, neither has it been accepted for the award of any other degree or diploma at a university or any other institute of higher learning, except where due acknowledgment has been made in the text.

Aamir Hayat

Date: July 31, 2020

Certificate

This is to certify that the thesis titled, "*Radiations by Finite-Sized Sources in Uniaxial Materials*" submitted by **Aamir Hayat** I.D. No: **2015-12-0005** in partial fulfillment of the requirements of Doctor of Philosophy embodies the work done by him under my supervision.

Supervisor
Dr. Muhammad Faryad
Assistant Professor
Lahore University of Management Sciences

Abstract

We present analytical results of fields radiated by finite-sized sources in unbounded uniaxial dielectric materials. Uniaxial materials are abundant in nature (rutile, calcite, quartz etc.) and can also be fabricated as periodic arrangement of thin sheets of different isotropic materials or as periodic arrangements of thin cylinders with their axis pointing in the same directions. Most modern metamaterials are also uniaxial due to dominant planar technology in electronics. Examples of uniaxial metamaterials include hyperbolic and zero-index materials. Analytical results of radiations from sources inside uniaxial materials are only available for point-sources. However, point-source is only a zeroth order approximation of actual radiators. In this thesis, the finite-sized sources are considered and approximate analytical results are derived. Finite-sized electric dipole and current loop are taken to find the next-order approximation of point-electric and point magnetic dipoles in uniaxial material. These results are obtained in the near zone and far zone for the two orientations of the finite-length dipole: when it is parallel to the optic axis and when it is perpendicular to the optic axis. These two orthogonal orientations can be used to construct solutions for an arbitrarily oriented dipole. When the electric dipole is parallel to the optic axis, only extraordinary waves are emitted. When the electric dipole is perpendicular this optic axis, both ordinary and extraordinary waves are emitted; however, the radiations are suppressed along the optic axis and no extraordinary waves are emitted in a direction perpendicular to both the electric dipole and the optic axis. A comparison with the point dipole showed that the directivity of the radiation pattern can be controlled using the length of the dipole. The radiations by a current loop in an unbounded uniaxial dielectric material with uniform current distribution are also studied. The closed-form expressions for the radiation in the far zone are found using the dyadic Green functions in the frequency domain. Analytical results are obtained when the axis of the loop was parallel to the optic axis and when it was perpendicular to the optic axis. Only ordinary waves are emitted when the axis of the loop is parallel to the optic axis in contrast to the electric dipole. When the axis of the loop is perpendicular to the optic axis, both the ordinary and the extraordinary waves are emitted. The results for different radii of the loop show that the radiation pattern strongly depends upon the size of the loop. A comparison of the finite-length dipole in the hyperbolic material with that of the uniaxial dielectric material showed that the radiation patterns are very different for the extraordinary waves but the patterns for the ordinary waves are similar. When the dipole and the optic axis are parallel, the extraordinary radiations are emitted along a cone in the hyperbolic material with the optic axis as its axis. When the dipole is perpendicular, no extraordinary radiation is emitted along the dipole, the optic axis, and perpendicular to the plane formed by the dipole and the optic axis. Furthermore, analytical results are obtained for the wire material in the zero-index regime. When the dipole is parallel, only the near field is significantly present and no radiations are emitted in the far field. When the dipole is perpendicular, the near field is negligible, but far field radiations are present, though only of the ordinary type.

List of Publications

1. A. Hayat and M. Faryad, "On the radiation from a Hertzian dipole of a finite length in the uniaxial dielectric medium," *OSA Continuum* **2** (4) 1411-1429 (2019); Erratum: **2** (10), 2855 (2019).

2. A. Hayat and M. Faryad, "Closed-form expressions for electromagnetic waves generated by a current loop in a uniaxial dielectric medium in the far zone," *J. Opt. Soc. Am. B* **36** (8), F9-F17 (2019).

3. A. Hayat and M. Faryad, "Radiation by a finite-length electric dipole in the hyperbolic media," *Phys. Rev. A* **101** (1), 013832 (2020).

Acknowledgements

Contents

List of Figures

Chapter 1

Introduction

Uniaxial materials have single axis of symmetry and can support electromagnetic waves with two orthogonal states of different phase velocities. These materials exist in nature and they can be prepared artificially from simple isotropic materials. The artificial fabrication can be achieved by stacking the layers of different isotropic materials periodically or by dispersing the parallel cylindrical inclusions in an isotropic host. Moreover, out of seven crystal systems, trigonal, tetragonal and hexagonal crystal systems are uniaxial. Also, many other crystals can be approximated very well as uniaxial materials.

In this thesis, we investigated radiation by finite-sized sources in uniaxial materials. Analytical results for near and far field are obtained. Radiation problems are important to understand radiation properties of radiators and scattering properties of inclusions and impurities. A small linear electric current element with uniform current distribution is called a dipole. We considered finite-length dipole because several electrically small sources of electromagnetic waves can be modeled as Hertzian dipoles of finite-length such as quantum dots or quantum wires. The finite-length dipole is also highly useful for helping analyze larger antennas which can be subdivided into short sections having uniform currents as large antennas can be thought of as composed of small sections with uniform current distribution on each small section. Our main goal is to provide analytical results for the finite-length dipole. We have also considered the current loop whose limiting case can be treated as point-magnetic dipole.

Uniaxial material are ubiquitous in optical components: birefringent filters, birefringent lenses, waveplates, birefringent interferometers, and nonlinear optical effect generators [1]. Several uniaxial crystals like quartz have been used to make specialized lenses, windows, and filters used in lasers, microscopes, telescopes, electronic sensors, and scientific instruments [2]. Uniaxial materials occupy an important place in optics because of their varied applications including imaging [3, 4], sensing [5], cloaking [6], waveguiding [7], and simulating space-time phenomena [8]. Artificially prepared

uniaxial materials that have unconventional material parameters, have been used to achieve unprecedented functionality in the control of electromagnetic and acoustic waves, such as superlensing and negative refraction [9]. The different values of the components of permittivity dyadic causes the dispersion relation of uniaxial materials to show elliptic or hyperbolic shapes. Hyperbolic materials show super-resolution in the far-zone through image magnification, negative refraction, and enhanced spontaneous emission (Purcell effect) [10]. Moreover, whenever the sign of material parameter changes, a topological transition occurs [9]. Also these are very important from the point of view of their applications in the field of nano imaging [11] , nano sensing [12], nano resonators [13], efficient absorbers [14], and subdiffraction imaging [15].

Upto the zeroth order, small sources of radiations can be modeled as point dipoles. Several authors have studied the radiations from point dipoles. For example, the radiation by a point dipole in unbounded uniaxial material is dealt in Refs. [16–18]. The radiation over a layered material with its optic axis lying perpendicular to the plane of stratification has been studied by Tsang *et al.* [19], Kong [20], Kwon and Wang [21], and Tang [22], while the same problem with point dipole embedded in the stratified material has been studied by Ali and Mahmoud [23]. Far field radiation emitted by an arbitrarily oriented point dipole which is placed in a two-layered uniaxially anisotropic material with its tilted optic axis is treated analytically with the use of dyadic Green function [24]. Here, two cases are discussed, when the dipole is placed over the two layered uniaxial material, and when it is embedded in a two layered uniaxial material [24].

This thesis deals with the next order of approximation of radiation sources in the uniaxial materials by taking into account their finite size. The generalization of both the electric and magnetic dipoles are considered. The size of the radiation sources plays critical role in the directivity of radiation. This is even more important in uniaxial materials because of a special direction (optic axis) is already present in the material.

This chapter is focused on a brief introduction of uniaxial materials, their types, and their applications which are discussed in Sec. 1.1 . The dyadic Green function and it's approximate form are briefly discussed in Secs. 1.2 and 1.3 as the study of radiations will be carried out with the help of dyadic Green functions. Moreover, the analytical results for the point-electric dipole in the near and far-zone in the uniaxial dielectric material are presented in Sec. 1.4. The overview of the thesis is presented in Sec. 1.5

In this thesis, $\exp(-i\omega t)$ time-dependence is implicit, where t is the time, ω is the angular frequency, and $i = \sqrt{-1}$. Moreover, ε_o, μ_o, and $k_o = \omega\sqrt{\varepsilon_o\mu_o}$, represent the free-space permittivity, permeability, and wavenumber respectively. Boldface letters represent vectors and symbols underlined

twice represent dyadics. The dyadic Green functions are represented by upper-case letters, that are underlined twice, such as $\underline{\underline{G}}$ and the scalar Green functions are represented by lower-case letters, for example g. The identity dyadic is represented as $\underline{\underline{I}}$.

1.1 Uniaxial materials

Materials having a single axis of symmetry that can support electromagnetic waves with two distinct states of polarization along each direction of propagation with different phase velocities are called uniaxial materials [16, 25–27]. Two distinct plane waves can propagate in each direction in a uniaxial material except in a direction parallel to $\pm\hat{\mathbf{c}}$ (where $\hat{\mathbf{c}}$ denotes the axis of symmetry). Whenever these waves propagate parallel to $\pm\hat{\mathbf{c}}$, both of these have the same phase speed and attenuation rate. The axis which is parallel to $\hat{\mathbf{c}}$ is called optic axis [26, 28]. Moreover, a wave that propagates with the same phase velocity in all directions in the uniaxial material is called an ordinary wave. Whereas, the wave whose phase velocity depends upon the direction of propagation and is different from the velocity of ordinary waves unless the wave is propagating along the optic axis of the material, is called the extraordinary wave [29]. Uniaxial dielectric materials exists in nature [30], e.g., rutile, calcite and quartz [31, 32], and they can also be fabricated artificially, e.g., a stack of thin films with alternating high and low refractive indices [33] as shown in Fig. 1.3, and electrically thin wires arranged periodically in a parallel manner as shown in Fig. 1.4 [34, 35].

1.1.1 Ordinary and extraordinary waves

Let us consider a monochromatic plane wave of an angular frequency ω propagating through uniaxial material with an electric field [29]

$$\mathbf{E}\left(\mathbf{r},\omega\right) = \mathbf{E}_{o}\left(\omega\right)\exp[i(\omega t - \mathbf{k}\cdot\mathbf{r})], \tag{1.1}$$

and the magnetic field

$$\mathbf{H}\left(\mathbf{r},\omega\right) = \mathbf{H}_{o}\left(\omega\right)\exp[i(\omega t - \mathbf{k}\cdot\mathbf{r})], \tag{1.2}$$

where $\mathbf{k} = \frac{\omega}{c}n\hat{\mathbf{s}}$ is the wave vector with $\hat{\mathbf{s}}$ as the unit vector representing the direction of propagation and n as the refractive index. Maxwell equations for the electric and magnetic field displacement vectors are

$$\nabla \times \mathbf{E} = -\frac{\partial \mathbf{B}}{\partial t}, \tag{1.3}$$

$$\nabla \times \mathbf{H} = \frac{\partial \mathbf{D}}{\partial t}, \tag{1.4}$$

where

$$\mathbf{D} = \underline{\underline{\varepsilon}} \cdot \mathbf{E}, \quad \mathbf{B} = \underline{\underline{\mu}} \cdot \mathbf{H}, \tag{1.5}$$

with

$$\underline{\underline{\varepsilon}} = \varepsilon_o \left[\varepsilon_b \underline{\underline{I}} + (\varepsilon_a - \varepsilon_b) \hat{\mathbf{c}} \hat{\mathbf{c}} \right], \quad \underline{\underline{\mu}} = \mu_o \mu_b \underline{\underline{I}}, \tag{1.6}$$

where ε_o, μ_o, $\underline{\underline{I}}$ and $\hat{\mathbf{c}}$ represents, the permittivity of free space, the permeability of the free space, identity dyadic, and unit vector in the direction of the optic axis, respectively.

Now by substituting Eqs. (1.1) and (1.2) along with Eq. (1.5) into Eqs. (1.3) and (1.4), respectively, we get

$$\mathbf{k} \times \mathbf{E}_o = \omega \underline{\underline{\mu}} \cdot \mathbf{H}_o, \tag{1.7}$$

$$\mathbf{k} \times \mathbf{H}_o = -\omega \underline{\underline{\varepsilon}} \cdot \mathbf{E}_o. \tag{1.8}$$

By eliminating $\mathbf{H}$ from Eqs. (1.7) and (1.8), we get

$$\mathbf{k} \times (\mathbf{k} \times \mathbf{E}_o) + \omega^2 \mu_o \mu_b \underline{\underline{\varepsilon}} \cdot \mathbf{E}_o = 0 \tag{1.9}$$

after using Eq. (1.6). In the principal coordinate system, the permittivity tensor is defined as

$$\underline{\underline{\varepsilon}} = \varepsilon_o \begin{pmatrix} \varepsilon_b & 0 & 0 \\ 0 & \varepsilon_b & 0 \\ 0 & 0 & \varepsilon_a \end{pmatrix}. \tag{1.10}$$

Substituting Eq. (1.10) into Eq. (1.9) and further simplification gives [29]

$$\begin{pmatrix} \omega^2 \mu_o \mu_b \varepsilon_b - k_y^2 - k_z^2 & k_x k_y & k_x k_z \\ k_y k_x & \omega^2 \mu_o \mu_b \varepsilon_b - k_x^2 - k_z^2 & k_y k_z \\ k_z k_x & k_z k_y & \omega^2 \mu_o \mu_b \varepsilon_a - k_x^2 - k_y^2 \end{pmatrix} \begin{pmatrix} E_x \\ E_y \\ E_z \end{pmatrix} = 0. \tag{1.11}$$

For non-trivial solution to exist, the determinant of the matrix in Eq. (1.11) must vanish. Therefore [29]

$$\begin{vmatrix} \omega^2 \mu_o \mu_b \varepsilon_b - k_y^2 - k_z^2 & k_x k_y & k_x k_z \\ k_y k_x & \omega^2 \mu_o \mu_b \varepsilon_b - k_x^2 - k_z^2 & k_y k_z \\ k_z k_x & k_z k_y & \omega^2 \mu \mu_b \varepsilon_a - k_x^2 - k_y^2 \end{vmatrix} = 0. \tag{1.12}$$

Equation (1.12) gives

$$\left(\frac{k_x^2 + k_y^2}{\varepsilon_a} + \frac{k_z^2}{\varepsilon_b} - \frac{\omega^2}{c^2}\right)\left(\frac{k^2}{\varepsilon_b} - \frac{\omega^2}{c^2}\right) = 0\,. \tag{1.13}$$

The first part of Eq. (1.13) represents an ellipsoid and the second part of the same equation represents a
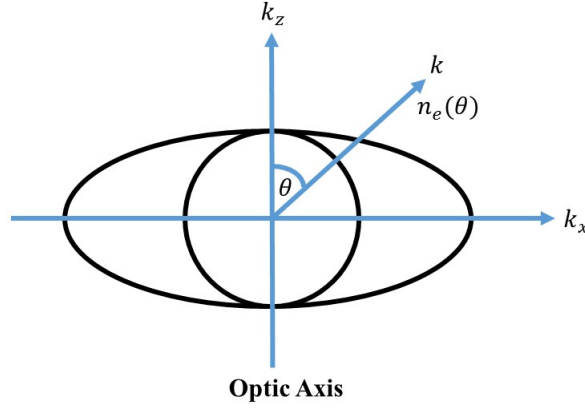
FIGURE 1.1: Schematic showing the intersection of xz plane with the normal surfaces of uniaxial material, when $n_e(\theta)$ is the refractive index of extraordinary wave.

sphere. The point where both of these shapes touch each other define the optic axis of the uniaxial material as shown in Fig. 1.1. When the wave propagates in the direction of the optic axis, it will experience the same refractive index and it's phase velocity remains the same for any polarization state [36]. Moreover, the spherical part in Eq. (1.13) tells us that the ordinary wave experience the same refractive index in all directions, that is $\sqrt{\varepsilon_b}$. The ordinary wave has same refractive index in all direction and obeys all laws of refraction, while extraordinary wave experiences refractive index $n_e(\theta)$, and it depends on the direction of propagation of wave. The phase velocity of both ordinary and extraordinary waves will be the same only along the optic axis [36]. Using the spherical coordinates system in ellipsoid part of Eq. (1.13), the most general relation for the refractive index $n_e(\theta)$ at different angle θ is given by [29].

$$\frac{1}{n_e^2(\theta)} = \frac{\cos^2\theta}{\varepsilon_b} + \frac{\sin^2\theta}{\varepsilon_a}\,. \tag{1.14}$$

It is clear that index of refraction varies from $n_e(\theta) = \sqrt{\varepsilon_b}$ for $\theta = 0^o$ to $n_e(\theta) = \sqrt{\varepsilon_a}$ for $\theta = 90^o$ as shown in Fig. 1.1 [29]. Also, on the basis of Eqs. (1.13) and (1.14), uniaxial material can be divided into two types (i) Positive uniaxial material for which $\mathrm{Re}(\varepsilon_b) < \mathrm{Re}(\varepsilon_a)$, (ii) Negative uniaxial material for

Possible materials formed by changing permittivities values			
Lossless dielectric	$\varepsilon_a'' = 0; \varepsilon_b'' = 0$	$\varepsilon_a' > 0; \varepsilon_b' > 0$	
Lossless hyperbolic	$\varepsilon_a'' = 0; \varepsilon_b'' = 0$	$\varepsilon_a' < 0; \varepsilon_b' > 0$ Type-I Hyperbolic	$\varepsilon_a' > 0; \varepsilon_b' < 0$ Type-II Hyperbolic
Lossy dielectric	$\varepsilon_a'' > 0; \varepsilon_b'' > 0$	$\varepsilon_a' > 0; \varepsilon_b' > 0$	
Lossy hyperbolic	$\varepsilon_a'' > 0; \varepsilon_b'' > 0$	$\varepsilon_a' < 0; \varepsilon_b' > 0$ Type-I Hyperbolic	$\varepsilon_a' > 0; \varepsilon_b' < 0$ Type-II Hyperbolic

TABLE 1.1: Classification of uniaxial materials based on real $(\varepsilon_b', \varepsilon_a')$ and imaginary $(\varepsilon_b'', \varepsilon_a'')$ values for the principal values of permittivity tensor.

which $\mathrm{Re}(\varepsilon_b) > \mathrm{Re}(\varepsilon_a)$ as depicted in Fig. 1.2. Rutile, quartz, and ice are positive uniaxial materials whereas calcite, beryl, and proustite are negative uniaxial materials [29].
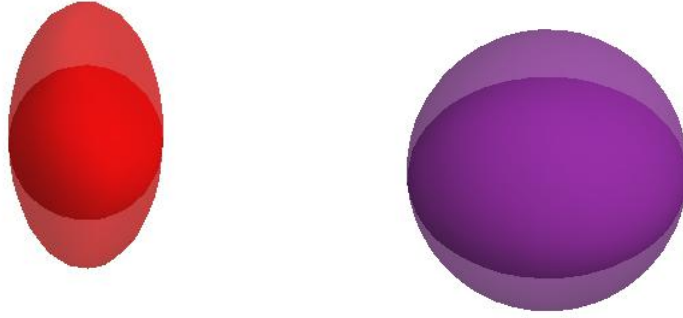
FIGURE 1.2: Normal surfaces of uniaxial material representing (left) positive uniaxial material with $\mathrm{Re}(\varepsilon_b) < \mathrm{Re}(\varepsilon_a)$ and (right) negative uniaxial material with $\mathrm{Re}(\varepsilon_b) > \mathrm{Re}(\varepsilon_a)$.

Let us define the wave vector for the uniaxial material as $\mathbf{k} = \frac{\omega}{c}(n + ik)\,\hat{\mathbf{s}}$, whose refractive index consists of both real and imaginary parts. Also, by choosing the principal permittivities of the permittivity tensor as $\varepsilon_b = \varepsilon_b' + i\varepsilon_b''$, and $\varepsilon_a = \varepsilon_a' + i\varepsilon_a''$, the modified form of Eq. (1.10) is given by [36]

$$\underline{\underline{\varepsilon}} = \varepsilon_o \begin{pmatrix} \varepsilon_b' + i\varepsilon_b'' & 0 & 0 \\ 0 & \varepsilon_b' + i\varepsilon_b'' & 0 \\ 0 & 0 & \varepsilon_a' + i\varepsilon_a'' \end{pmatrix}. \tag{1.15}$$

Different types of uniaxial material exist based on the real and imaginary part of the principal permittivities in Eq. (1.15). Some of these types are depicted in Table 1.1 [37]. In this thesis, we have dealt with ordinary uniaxial dielectric materials, hyperbolic, and zero-index uniaxial materials.

1.1.2   Stack material

Material which is formed by taking two or more isotropic materials arranged periodically in a parallel manner such as shown in Fig. 1.3 is known as stack material. In such a system, the two interesting situations can be considered: when the external electric field is directed either parallel or perpendicular to the planer interfaces. When the thickness of the layers is very small as compared to the wavelength, then this artificially prepared system acts as a homogeneous uniaxial material and can be described using equivalent parameters. The relations for the effective permittivity for the two principal polarizations are given by [34]
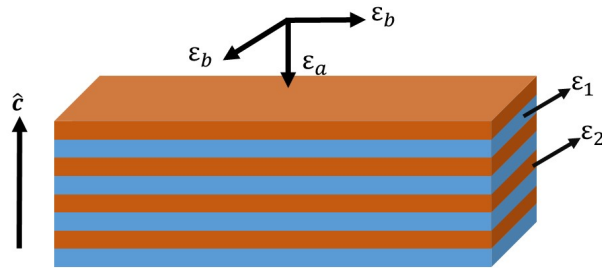
FIGURE 1.3: Electrically thin sheets of different isotropic materials arranged periodically in a parallel manner.

$$\varepsilon_a = f_1\varepsilon_1 + f_2\varepsilon_2$$
$$\varepsilon_b = \frac{\varepsilon_1\varepsilon_2}{f_2\varepsilon_1 + f_1\varepsilon_2}, \qquad (1.16)$$

where f_1 and f_2 are the volume filling fraction of material 1 and material 2, respectively. If we have more than one materials in each unit cell then

$$\varepsilon_a = \sum_i f_i\varepsilon_i$$
$$\varepsilon_b^{-1} = \sum_i f_i\varepsilon_i^{-1}, \qquad (1.17)$$

where $\sum f_i = 1$ should be fulfilled for entire composite. Therefore, the permittivity of layered composite is equal to the weighted arithmetic mean of the permittivities of all its constituents when the electric field is parallel to the interface, and the permittivity takes the value of the weighted harmonic mean of all the constituent permittivities when a perpendicular field is applied [34]. Many modern metamaterials are based on layered metal-dielectric composites.

1.1.3 Wire material

Uniaxial material can also be fabricated a parallel assemblies of wires as shown in Fig. 1.4. If we take the direction of the wires to be along the unit vector $\hat{\mathbf{c}}$ and assume $a \ll \lambda_o$, the relations for the effective permittivity along parallel and perpendicular directions are given by [38]

$$
\begin{aligned}
\varepsilon_a &= f\varepsilon_i + (1-f)\varepsilon_h \,, \\
\varepsilon_b &= \varepsilon_h \frac{(1+f)\varepsilon_i + (1-f)\varepsilon_h}{(1+f)\varepsilon_h + (1-f)\varepsilon_i} \,,
\end{aligned}
\tag{1.18}
$$

with ε_i and ε_h being the permittivity of wire inclusion and host materials, respectively. The permeability
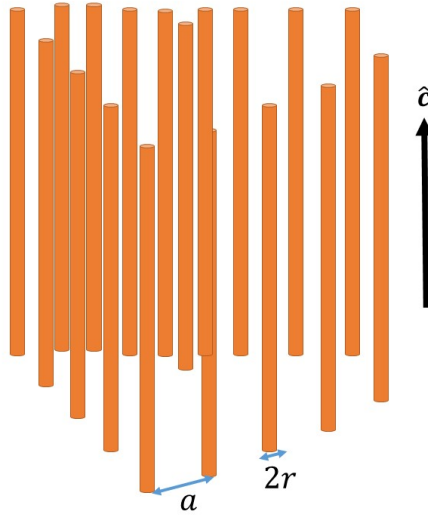
FIGURE 1.4: Thin thin rods of isotropic material arranged periodically to form uniaxial material.

of the wire material can taken as $\underline{\underline{\mu}} = \mu_o\mu_b\underline{\underline{I}}$ since all materials are taken to be non-magnetic. The parameter $f = \pi R^2/a^2$ is the surface concentration of the wire, with R the radius of the wire and a is the length of the unit cell of the material.

Constitutive elements of wire materials operating in the infrared and visible ranges are nanowires or nanorods [39]. Nanowires or nanorod-based composites have recently become a significant and

more interesting topic because of their unusual and counterintuitive optical properties that include subwavelength confinement of optical radiation, negative refraction, and modulation of photonic density of states [39–41]. Due to relatively low loss and ease of fabrication, nanowire composites found numerous applications in biosensing, acoustooptics, subwavelength imaging, and ultrafast all-optical processing, spanning visible to THz frequencies [42–46]. Wire material is a special class of uniaxial metamaterials that have homogeneous internal structure along one preselected direction.

1.1.4 Hyperbolic material

The permittivity dyadic $\underline{\underline{\varepsilon}}$ of the hyperbolic materials is given in Eq. (1.6) with

$$\varepsilon_a = \varepsilon_a' + i\varepsilon_a'', \tag{1.19}$$

and

$$\varepsilon_b = \varepsilon_b' + i\varepsilon_b''. \tag{1.20}$$
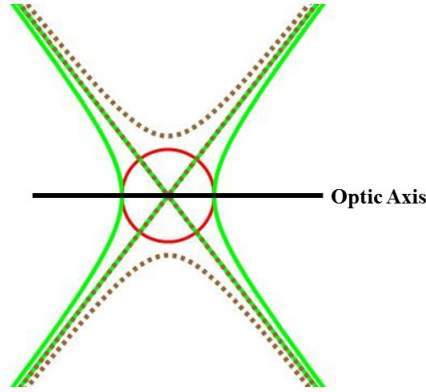
FIGURE 1.5: Intersection of xz plane with normal surface of a typical type-I hyperbolic material.

Therefore, there are two types of hyperbolic materials. Type-I materials are those for which $\varepsilon_a' < 0$, $\varepsilon_b' > 0$, and for type-II, we materials have $\varepsilon_a' > 0$, $\varepsilon_b' < 0$ [47]. As an example, we have presented intersection of xz plane with normal surface of a typical type-I lossless hyperbolic material by choosing different values of permittivities as shown in Fig. 1.5. In this material the ordinary wave experience the same refractive index in all the directions and it has less dissipation because only one permittivity has

negative value. Also, as the extraordinary wave experience the changing refractive index $n_e(\theta)$ in all directions except along the optic axis experience loss when the refractive index $n_e(\theta)$ goes to zero. In this region, the loss of extraordinary wave is maximum. Moreover, with changing the values of permittivities ε_b' and ε_a' the curve for $n_e(\theta)$ is not effected and it shows the position of the optic axis [36].

Hyperbolic material is a special case of uniaxial material in which the principal values of the permittivity dyadic $\underline{\underline{\varepsilon}}$ have opposite signs [27, 32] and the isofrequency surface of an extraordinary wave is a hyperboloid [47]. Due to the successful realization of hyperbolic materials using artificial photonic structures and metamaterials [48–52], interest in hyperbolic materials is now revived and rapidly increasing. Among the varieties of metamaterials proposed and fabricated, hyperbolic metamaterials are one of the most attractive class of metamaterials [53, 54] due to their unique hyperbolic dispersion [55, 56] enabling unusual electromagnetic responses, such as hyperlensing, cloaking phenomena [57–59], and broadband negative refraction [49, 60] without artificial magnetism, which is not very sensitive to structural disorder. Uniaxial hyperbolic metamaterials are multi-functional platforms to realize waveguiding, sensing, imaging, quantum and thermal engineering beyond conventional devices [61–64]. Hyperbolic material uses the concept of engineering the basic dispersion relation of waves to provide unique electromagnetic modes that can have a broad range of applications [65]. One can consider the hyperbolic metamaterial as a polaritonic crystal where the coupled states of light and matter give rise to a larger bulk density of electromagnetic states [66]. Some of the applications of hyperbolic metamaterials include negative refraction [67], sub-diffraction imaging [15], sub-wavelength modes [7], and spontaneous [68] and thermal emission engineering [69, 70].

It is much easier to produce hyperbolic material than double-negative media, as the only necessary criterion for hyperbolic material structures is that the motion of free electrons is restricted to be in one or two spatial directions. A few natural materials, including bismuth and graphite, exhibit hyperbolic dispersion in certain spectral ranges [32].

1.1.5 Zero-index material (ZIM)

Isotropic materials with either permittivity or permeability or both near zero are called zero-index material (ZIM) [71–73]. Isotropic ZIM can be fabricated as random mixture of electrically small inclusions of metal in dielectric host or other artificial nanostructure like split-ring resonators. In these materials $k \approx 0$ means that wave propagate with little spatial variation and infinite phase velocity [71]. In uniaxial ZIMs only one material parameter in the permittivity dyadic is taken to be near zero and the other parameter take uniaxial positive value. A uniaxial ZIM can be fabricated as photonic crystals of dielectric materials

[74] or as metal/dielectrics stack or wire material as discussed in earlier sections. In the effective-material regime ($a \ll \lambda_o$) and $f \ll 1$, we can choose the metallic wire with $Re(\varepsilon_i) < 0$ and dielectric host $\varepsilon_h > 0$ such that

$$\varepsilon_a \approx 0$$

to get

$$\underline{\underline{\varepsilon}} \approx \varepsilon_o \varepsilon_b (\underline{\underline{I}} - \hat{\mathbf{c}}\hat{\mathbf{c}}) \,. \tag{1.21}$$

from Eq. (1.6).

By choosing the appropriate values for the two constituents permittivities and filling fraction, a highly anisotropic material with one of the effective permittivity parameter approaches to zero and the other parameter approaches infinity simultaneously, can be created very easily [34]. Such a composite metal-dielectric layered media have found many applications in several versions of superlenses and hyperlenses [4, 75–77]. In such media, as the electromagnetic wave will possess a small wave number, leading to a very diminutive phase variation (that is, homogeneous field). Due to such an intriguing property, ZIMs have been investigated extensively for various applications, for instance, manipulating transmission in a ZIM waveguide with defects [78, 79], obtaining desired directive radiation or multi-beams [80, 81], enhancing radiation efficiency [82–84], squeezing or bending EM wave in a sub-wavelength ENZ channel [73], and unidirectional transmission [85].

1.2 Dyadic Green functions

A function which represents the solution of inhomogenous linear differential equation for which the source is localized both in space and time is known as Green function. A source function which is localized both in space and time is called a point source and impulse, respectively. It is useful in finding the solution for a source that involves finite spatial and temporal domain by representing the source as a dense distribution of impulsive point sources [25].

Green functions can be expressed in scalar, tensors, or dyadic form. Dyadic is mostly used in electromagnetism. A function that maps a vector source into vector solution of a differential equation is known as dyadic Green function. There are several physical processes which require dyadic Green functions, e.g., radiations emitted by a current source in a material and generation of elastodynamics waves by a mechanical source in a material [25, 26].

Several research articles, books and chapters have been written on dyadic Green functions in electromagnetism [16, 25, 26]. The dyadic Green functions for the uniaxial materials have been derived earlier [16, 17, 25, 26] and are reproduced here for completeness. Let us begin with the time-harmonic Maxwell equations [16, 26]

$$\nabla \times \mathbf{H}(\mathbf{r}) + i\omega \mathbf{D}(\mathbf{r}) = \mathbf{J}_e(\mathbf{r}) \,, \tag{1.22}$$

$$\nabla \times \mathbf{E}(\mathbf{r}) - i\omega \mathbf{B}(\mathbf{r}) = \mathbf{J}_m(\mathbf{r}) \,, \tag{1.23}$$

$$\nabla \cdot \mathbf{D}(\mathbf{r}) = \rho_e(\mathbf{r}) \,, \tag{1.24}$$

$$\nabla \cdot \mathbf{B}(\mathbf{r}) = \rho_m(\mathbf{r}) \,, \tag{1.25}$$

where $\mathbf{J}_e(\mathbf{r})$, $\mathbf{J}_m(\mathbf{r})$, $\rho_e(\mathbf{r})$ and $\rho_m(\mathbf{r})$ is the electric current density, magnetic current density, the electric charge density and magnetic charge density, respectively, and these are related by the continuity equations $\nabla \cdot \mathbf{J}_e(\mathbf{r}) - i\omega\rho_e(\mathbf{r}) = 0$ and $\nabla \cdot \mathbf{J}_m(\mathbf{r}) - i\omega\rho_m(\mathbf{r}) = 0$. The frequency domain constitutive relations of a uniaxial dielectric material can be written as

$$\mathbf{D}(\mathbf{r}) = \underline{\underline{\varepsilon}} \cdot \mathbf{E}(\mathbf{r}) \,, \quad \mathbf{B}(\mathbf{r}) = \mu_o \mu_b \mathbf{H}(\mathbf{r}) \,, \tag{1.26}$$

with the permittivity dyadic $\underline{\underline{\varepsilon}}$ given in Eq. (1.6). Since Eqs. (1.22) and (1.23) are linear in $\mathbf{E}$ and $\mathbf{H}$, the electric and magnetic field phasors can be written in terms of the dyadic Green functions as

$$\mathbf{E}(\mathbf{r}) = \iiint\limits_{V'} \left[\underline{\underline{G}}^{ee}(\mathbf{R}) \cdot \mathbf{J}_e(\mathbf{r}') + \underline{\underline{G}}^{em}(\mathbf{R}) \cdot \mathbf{J}_m(\mathbf{r}') \right] d^3\mathbf{r}' \,, \tag{1.27}$$

$$\mathbf{H}(\mathbf{r}) = \iiint\limits_{V'} \left[\underline{\underline{G}}^{me}(\mathbf{R}) \cdot \mathbf{J}_e(\mathbf{r}') + \underline{\underline{G}}^{mm}(\mathbf{R}) \cdot \mathbf{J}_m(\mathbf{r}') \right] d^3\mathbf{r}' \,, \tag{1.28}$$

where V' is the volume occupied by the electric current density $\mathbf{J}_e(\mathbf{r}')$ and

$$\mathbf{R} = \mathbf{r} - \mathbf{r}' \,. \tag{1.29}$$

The electric dyadic Green function $\underline{\underline{G}}^{ee}(\mathbf{R})$ and magnetoelectric dyadic Green function $\underline{\underline{G}}^{me}(\mathbf{R})$ can be found as [25, 26]

$$
\begin{aligned}
\underline{\underline{G}}^{ee}(\mathbf{R}) = {}& i\omega\mu_o\mu_b\Bigg\{ g_e(\mathbf{R})\varepsilon_a\underline{\underline{\varepsilon}}_r^{-1}\left[1 - \frac{1}{ik_on_oR_e} - \frac{1}{(k_on_oR_e)^2}\right] \\
& -g_e(\mathbf{R})\left[1 - \frac{3}{ik_on_oR_e} - \frac{3}{(k_on_oR_e)^2}\right]\frac{\varepsilon_a^2(\underline{\underline{\varepsilon}}_r^{-1}\cdot\mathbf{R})(\underline{\underline{\varepsilon}}_r^{-1}\cdot\mathbf{R})}{R_e^2} \\
& +\frac{1}{\varepsilon_b}\left[\varepsilon_b g_o(\mathbf{R}) - \varepsilon_a g_e(\mathbf{R})\right]\underline{\underline{K}}(\mathbf{R}) \\
& +\frac{Rg_o(\mathbf{R}) - R_e g_e(\mathbf{R})}{ik_on_o(\mathbf{R}\times\hat{\mathbf{c}})\cdot(\mathbf{R}\times\hat{\mathbf{c}})}\left[\underline{\underline{I}} - \hat{\mathbf{c}}\hat{\mathbf{c}} - 2\underline{\underline{K}}(\mathbf{R})\right]\Bigg\},
\end{aligned}
\tag{1.30}
$$

$$
\begin{aligned}
\underline{\underline{G}}^{me}(\mathbf{R}) = {}& \frac{\varepsilon_a}{\varepsilon_b}(1 - ik_on_oR_e)g_e(\mathbf{R})\frac{(\mathbf{R}\times\hat{\mathbf{c}})[\mathbf{R}\times(\mathbf{R}\times\hat{\mathbf{c}})]}{R_e^2(\mathbf{R}\times\hat{\mathbf{c}})\cdot(\mathbf{R}\times\hat{\mathbf{c}})} \\
& +\left[g_e(\mathbf{R}) - g_o(\mathbf{R})\right](\mathbf{R}\cdot\hat{\mathbf{c}})\frac{[\hat{\mathbf{c}}\times(\mathbf{R}\times\hat{\mathbf{c}})](\mathbf{R}\times\hat{\mathbf{c}}) + (\mathbf{R}\times\hat{\mathbf{c}})[\hat{\mathbf{c}}\times(\mathbf{R}\times\hat{\mathbf{c}})]}{[(\mathbf{R}\times\hat{\mathbf{c}})\cdot(\mathbf{R}\times\hat{\mathbf{c}})]^2} \\
& -(1 - ik_on_oR)g_o(\mathbf{R})\frac{[\mathbf{R}\times(\mathbf{R}\times\hat{\mathbf{c}})](\mathbf{R}\times\hat{\mathbf{c}})}{R^2[(\mathbf{R}\times\hat{\mathbf{c}})\cdot(\mathbf{R}\times\hat{\mathbf{c}})]},
\end{aligned}
\tag{1.31}
$$

where

$$
\underline{\underline{K}}(\mathbf{R}) = \frac{(\mathbf{R}\times\hat{\mathbf{c}})(\mathbf{R}\times\hat{\mathbf{c}})}{(\mathbf{R}\times\hat{\mathbf{c}})\cdot(\mathbf{R}\times\hat{\mathbf{c}})},
\tag{1.32}
$$

$$
\underline{\underline{\varepsilon}}_r^{-1} = \frac{1}{\varepsilon_b}\underline{\underline{I}} - \left(\frac{1}{\varepsilon_b} - \frac{1}{\varepsilon_a}\right)\hat{\mathbf{c}}\hat{\mathbf{c}},
\tag{1.33}
$$

and

$$
n_o = \sqrt{\varepsilon_b}\sqrt{\mu_b}, \quad k_o = \omega\sqrt{\mu_o\varepsilon_o}.
\tag{1.34}
$$

The scalar Green functions

$$
g_o(\mathbf{R}) = \frac{\exp(ik_on_oR)}{4\pi R} \quad\text{and}\quad g_e(\mathbf{R}) = \frac{\exp(ik_on_oR_e)}{4\pi R_e}
\tag{1.35}
$$

represent ordinary and extraordinary waves, respectively, and

$$
R_e = \sqrt{\frac{\varepsilon_a}{\varepsilon_b}(\mathbf{R}\times\hat{\mathbf{c}})\cdot(\mathbf{R}\times\hat{\mathbf{c}}) + (\mathbf{R}\cdot\hat{\mathbf{c}})^2}.
\tag{1.36}
$$

Let us note that the ordinary waves propagate with the same phase velocity in all directions in the uniaxial material and the extraordinary waves have their phase velocity dependent upon the direction of propagation which is different from that of the phase velocity of the ordinary waves unless the waves are propagating along the optic axis of the material [26]. Similarly, the dyadic Green $\underline{\underline{G}}^{mm}(\mathbf{R})$ can be found

directly by solving equation [25]

$$\left[\left(\nabla \times \underline{\underline{I}}\right) \cdot \underline{\underline{\varepsilon}}_r^{-1} \cdot \left(\nabla \times \underline{\underline{I}}\right) - k_o^2 \mu_b \underline{\underline{I}}\right] \cdot \underline{\underline{G}}^{mm}(\mathbf{R}) = i\omega\varepsilon_o \underline{\underline{I}}\delta(\mathbf{R}) \,, \tag{1.37}$$

as

$$\begin{aligned}
\underline{\underline{G}}^{mm}(\mathbf{R}) &= i\omega\varepsilon_o\varepsilon_b\Bigg\{g_o(\mathbf{R})\Big[1 + \frac{i}{k_o n_o R} - \frac{1}{(k_o n_o R)^2}\Big]\underline{\underline{I}} \\
&\quad -g_o(\mathbf{R})\Big[1 + \frac{3i}{k_o n_o R} - \frac{3}{(k_o n_o R)^2}\Big]\hat{\mathbf{R}}\hat{\mathbf{R}} \\
&\quad -\frac{1}{\varepsilon_b}\Big[\varepsilon_b g_o(\mathbf{R}) - \varepsilon_a g_e(\mathbf{R})\Big]\underline{\underline{K}}(\mathbf{R}) \\
&\quad +\frac{Rg_o(\mathbf{R}) - R_e g_e(\mathbf{R})}{ik_o n_o(\mathbf{R}\times\hat{\mathbf{c}})\cdot(\mathbf{R}\times\hat{\mathbf{c}})}\Big[\underline{\underline{I}} - \hat{\mathbf{c}}\hat{\mathbf{c}} - 2\underline{\underline{K}}(\mathbf{R})\Big]\Bigg\} \,.
\end{aligned} \tag{1.38}$$

By using Eq. (1.38), the magnetoelectric dyadic Green function $\underline{\underline{G}}^{em}(\mathbf{R})$ can be found directly from equation [25]

$$\underline{\underline{G}}^{em}(\mathbf{R}) = -\frac{1}{i\omega\varepsilon_o}\underline{\underline{\varepsilon}}_r^{-1} \cdot \big[\,\nabla \times \underline{\underline{G}}^{mm}(\mathbf{R})\big] \,, \tag{1.39}$$

as

$$\begin{aligned}
\underline{\underline{G}}^{em}(\mathbf{R}) &= \frac{\varepsilon_a}{\varepsilon_b}(1 - ik_o n_o R_e)g_e(\mathbf{R})\frac{[\mathbf{R}\times(\mathbf{R}\times\hat{\mathbf{c}})](\mathbf{R}\times\hat{\mathbf{c}})}{R_e^2(\mathbf{R}\times\hat{\mathbf{c}})\cdot(\mathbf{R}\times\hat{\mathbf{c}})} \\
&\quad +\Big[g_e(\mathbf{R}) - g_o(\mathbf{R})\Big](\mathbf{R}\cdot\hat{\mathbf{c}})\frac{[\hat{\mathbf{c}}\times(\mathbf{R}\times\hat{\mathbf{c}})](\mathbf{R}\times\hat{\mathbf{c}}) + (\mathbf{R}\times\hat{\mathbf{c}})[\hat{\mathbf{c}}\times(\mathbf{R}\times\hat{\mathbf{c}})]}{[(\mathbf{R}\times\hat{\mathbf{c}})\cdot(\mathbf{R}\times\hat{\mathbf{c}})]^2} \\
&\quad -(1 - ik_o n_o R)g_o(\mathbf{R})\frac{(\mathbf{R}\times\hat{\mathbf{c}})[\mathbf{R}\times(\mathbf{R}\times\hat{\mathbf{c}})]}{R^2[(\mathbf{R}\times\hat{\mathbf{c}})\cdot(\mathbf{R}\times\hat{\mathbf{c}})]} \,.
\end{aligned} \tag{1.40}$$

It can be seen that Eq. (1.40) can also be obtained by taking the transpose of Eq. (1.31).

1.3 Approximate dyadic Green function

Usually, we are interested in the far-field and near-field of a source. This can be achieved using approximate dyadic Green function in the near and far zone. In the near zone, $R \ll \lambda$ and $R \ll D$ where D is measure of size of source. In the far zone, $R \gg \lambda$ and $R \gg D$. Radiations in far zone appears as if the light travels along straight lines. Similarly, light scattered or reflected by an object seem to travel from the object to an observer along straight lines, known as optical rays. These lines are the flow lines of the energy in the radiation field. Therefore, fields in far zone are transfer electromagnetic fields. In close vicinity of the source, however, these flow lines are in general curves, and intricate field line patterns may

appear. Such structures can be found when the flow of radiation is resolved on a scale smaller than a wavelength. Therefore, fields in near zone looks like that of electrostatic and magnetostatic fields.

In the near zone, the dyadic Green function can be approximated by retaining terms proportional to $1/R^3$ since we have $k_o n_o R_e \ll 1$ and $k_o n_o R \ll 1$, which means that we are observing radiation at a distance which is much smaller than the wavelength. Therefore, Eqs. (1.30) and (1.31) can be written as

$$\underline{\underline{G}}^{ee}(\mathbf{R}) \approx \frac{i\varepsilon_a}{4\pi\omega\varepsilon_o\varepsilon_b} \left(\frac{3\varepsilon_a \left(\underline{\underline{\varepsilon}}_r^{-1} \cdot \mathbf{R} \right) \left(\underline{\underline{\varepsilon}}_r^{-1} \cdot \mathbf{R} \right)}{R_e^5} - \frac{\underline{\underline{\varepsilon}}_r^{-1}}{R_e^3} \right) \tag{1.41}$$

and

$$\underline{\underline{G}}^{me}(\mathbf{R}) \approx 0 \tag{1.42}$$

in the near zone.

In the far zone, our point of observation is at a distance which is much greater than the wavelength of the radiation, that is, $k_o n_o R_e \gg 1$ and $k_o n_o R \gg 1$. Therefore, to compute the electromagnetic field in the far zone, we retain the terms proportional to $1/R$. So, Eq. (1.30) can be approximated as

$$
\begin{aligned}
\underline{\underline{G}}^{ee}(\mathbf{R}) \approx{}& i\omega\mu_o\mu_b \left\{ g_e(\mathbf{R})\varepsilon_a\underline{\underline{\varepsilon}}_r^{-1} - g_e(\mathbf{R})\frac{\varepsilon_a^2(\underline{\underline{\varepsilon}}_r^{-1} \cdot \mathbf{R})(\underline{\underline{\varepsilon}}_r^{-1} \cdot \mathbf{R})}{R_e^2} \right. \\
& \left. + \frac{1}{\varepsilon_b}\left[\varepsilon_b g_o(\mathbf{R}) - \varepsilon_a g_e(\mathbf{R}) \right]\underline{\underline{K}}(\mathbf{R}) \right\}.
\end{aligned}
\tag{1.43}
$$

Using the identity [25, 26]

$$\underline{\underline{\varepsilon}}_r^{-1} - \frac{\varepsilon_a(\underline{\underline{\varepsilon}}_r^{-1} \cdot \mathbf{R})(\underline{\underline{\varepsilon}}_r^{-1} \cdot \mathbf{R})}{R_e^2} - \frac{1}{\varepsilon_b}\underline{\underline{K}}(\mathbf{R}) = \frac{\left[\mathbf{R} \times (\mathbf{R} \times \hat{\mathbf{c}})\right]\left[\mathbf{R} \times (\mathbf{R} \times \hat{\mathbf{c}})\right]}{\varepsilon_b R_e^2 (\mathbf{R} \times \hat{\mathbf{c}}) \cdot (\mathbf{R} \times \hat{\mathbf{c}})}, \tag{1.44}$$

Eq. (1.43) can be rearranged as

$$\underline{\underline{G}}^{ee}(\mathbf{R}) = i\omega\mu_o\mu_b \left\{ g_e(\mathbf{R})\frac{\varepsilon_a\left[\mathbf{R} \times (\mathbf{R} \times \hat{\mathbf{c}})\right]\left[\mathbf{R} \times (\mathbf{R} \times \hat{\mathbf{c}})\right]}{\varepsilon_b R_e^2 (\mathbf{R} \times \hat{\mathbf{c}}) \cdot (\mathbf{R} \times \hat{\mathbf{c}})} + g_o(\mathbf{R})\underline{\underline{K}}(\mathbf{R}) \right\}. \tag{1.45}$$

Similarly, Eq. (1.31) can be written as

$$\underline{\underline{G}}^{me}(\mathbf{R}) \approx ik_o n_o \left\{ g_o(\mathbf{R})\frac{[\mathbf{R} \times (\mathbf{R} \times \hat{\mathbf{c}})](\mathbf{R} \times \hat{\mathbf{c}})}{R(\mathbf{R} \times \hat{\mathbf{c}}) \cdot (\mathbf{R} \times \hat{\mathbf{c}})} - \frac{\varepsilon_a}{\varepsilon_b}g_e(\mathbf{R})\frac{(\mathbf{R} \times \hat{\mathbf{c}})[\mathbf{R} \times (\mathbf{R} \times \hat{\mathbf{c}})]}{R_e[(\mathbf{R} \times \hat{\mathbf{c}}) \cdot (\mathbf{R} \times \hat{\mathbf{c}})]} \right\} \tag{1.46}$$

in the far zone.

1.4 Radiation by point dipoles in uniaxial material

In this section, the radiation from a point electric and a magnetic dipole are discussed. For both the cases electric and magnetic field were evaluated by dyadic Green function in Refs. [25, 26, 86]. However, we also compute the radiation pattern in the far zone for later comparison with finite-sized sources.

1.4.1 Radiation by a point-electric dipole

The radiation from the monochromatic sources can be studied with dyadic Green function. Let us consider a point electric dipole having a dipole moment p_o and located at the origin. The electric density for the point electric dipole is given by [25]

$$\mathbf{J}_e(\mathbf{r}) = -i\omega\mathbf{p}_o\delta(\mathbf{r}), \quad \mathbf{J}_m(\mathbf{r}) = 0\,. \tag{1.47}$$

As the detailed derivation are given in Ref. [25], we present the final results of the electric and magnetic fields in the near and far zones. The electric field and the magnetic field of a point electric dipole when we are very close to the dipole, i.e., $k_o n_o r \ll 1$ and $k_o n_o r_e \ll 1$ are given by [25]

$$\mathbf{E}(\mathbf{r}) = \frac{1}{4\pi\varepsilon_o r_e^3}\frac{\varepsilon_a}{\varepsilon_b}\left[\frac{\varepsilon_a\left(\underset{=}{\varepsilon_r^{-1}}\cdot\mathbf{r}\right)\left(\underset{=}{\varepsilon_r^{-1}}\cdot\mathbf{r}\right)}{r_e^2} - \underset{=}{\varepsilon_r^{-1}}\right]\cdot\mathbf{p}_o \quad,$$

$$\mathbf{H}(\mathbf{r}) = 0 \quad, \tag{1.48}$$

where

$$r_e = \sqrt{\frac{\varepsilon_a}{\varepsilon_b}(\mathbf{r}\times\hat{\mathbf{c}})\cdot(\mathbf{r}\times\hat{\mathbf{c}}) + (\mathbf{r}\cdot\hat{\mathbf{c}})^2}\,. \tag{1.49}$$

Similarly in the far zone, the electric and magnetic fields are given by [25]

$$\begin{aligned}
\mathbf{E}(\mathbf{r}) &= \omega^2\mu_o\mu_b\Bigg\{g_e(\mathbf{r},0)\frac{\varepsilon_a}{\varepsilon_b}\frac{[\mathbf{r}\times(\mathbf{r}\times\hat{\mathbf{c}})][\mathbf{r}\times(\mathbf{r}\times\hat{\mathbf{c}})]}{r_e^2(\mathbf{r}\times\hat{\mathbf{c}})\cdot(\mathbf{r}\times\hat{\mathbf{c}})} + g_o(\mathbf{r},0)\underline{\underline{K}}(\mathbf{r}) \\
&\quad + \frac{rg_o(\mathbf{r},0) - r_e g_e(\mathbf{r},0)}{ik_o n_o(\mathbf{r}\times\hat{\mathbf{c}})\cdot(\mathbf{r}\times\hat{\mathbf{c}})}\left[\underline{\underline{I}} - \hat{\mathbf{c}}\hat{\mathbf{c}} - 2\underline{\underline{K}}(\mathbf{r})\right]\Bigg\}\cdot\mathbf{p}_o\,,
\end{aligned} \tag{1.50}$$

$$\mathbf{H}(\mathbf{r}) = \omega k_o n_o\Bigg\{-g_e(\mathbf{r},0)\frac{\varepsilon_a}{\varepsilon_b}\frac{(\mathbf{r}\times\hat{\mathbf{c}})[\mathbf{r}\times(\mathbf{r}\times\hat{\mathbf{c}})]}{r_e(\mathbf{r}\times\hat{\mathbf{c}})\cdot(\mathbf{r}\times\hat{\mathbf{c}})} + g_o(\mathbf{r},0)\frac{[\mathbf{r}\times(\mathbf{r}\times\hat{\mathbf{c}})](\mathbf{r}\times\hat{\mathbf{c}})}{r(\mathbf{r}\times\hat{\mathbf{c}})\cdot(\mathbf{r}\times\hat{\mathbf{c}})}\Bigg\}\cdot\mathbf{p}_o\,. \tag{1.51}$$

The above results are approximate results in the far zone. Now, suppose the point electric dipole is oriented parallel to the optic axis, i.e., $\mathbf{p}_o = p_o \hat{\mathbf{c}}$, then the electric and magnetic fields become [25]

$$
\begin{aligned}
\mathbf{E}(\mathbf{r}) \;=\; \omega^2 p_o \mu_o \mu_b \Bigg\{ & \left[1 + \frac{i}{k_o n_o r_e} - \frac{1}{(k_o n_o r_e)^2} \right] \hat{\mathbf{c}} \\
& - \left[1 + \frac{3i}{k_o n_o r_e} - \frac{3}{(k_o n_o r_e)^2} \right] \frac{\varepsilon_a (\hat{\mathbf{c}} \cdot \mathbf{r})(\underline{\varepsilon}_r^{-1} \cdot \mathbf{r})}{r_e^2} \Bigg\} g_e(\mathbf{r}, 0) \,,
\end{aligned}
\tag{1.52}
$$

and

$$
\mathbf{H}(\mathbf{r}) = i\omega p_o \frac{\varepsilon_a}{\varepsilon_b}(1 - ik_o n_o r_e) \frac{(\mathbf{r} \times \hat{\mathbf{c}})}{r_e^2} g_e(\mathbf{r}, 0) \,,
\tag{1.53}
$$

respectively. As we see that only $g_e(\mathbf{r}, 0)$ is present in both Eqs. (1.52) and (1.53), it means that when the electric dipole is aligned parallel to the direction of the optic axis only extraordinary wave is emitted.

The time-averaged power radiated per unit solid angle by the point dipole is given by [87, 88]

$$
\frac{dP}{d\Omega} = \frac{1}{2} \hat{\mathbf{r}} \cdot \mathrm{Re}(\mathbf{E} \times \mathbf{H}^*) \mathrm{r}^2 \,.
\tag{1.54}
$$

When both the optic axis and the point electric dipole are parallel to the z axis, the time-averaged power radiated per unit solid angle can be found by substituting Eqs. (1.50) and (1.51) into Eq. (1.54) as

$$
\frac{dP}{d\Omega} = \frac{k_o^4 \mu_b n_o p_o^2 c \varepsilon_d^2}{32 \pi^2 \varepsilon_o \Theta^5} \sin^2 \theta
\tag{1.55}
$$

in the spherical coordinates, where

$$
\varepsilon_d = \frac{\varepsilon_a}{\varepsilon_b}, \quad \Theta = \sqrt{\cos^2 \theta + \varepsilon_d \sin^2 \theta}.
\tag{1.56}
$$

We have used the following equation for transforming Cartesian coordinates to spherical coordinates

$$
x = r \sin\theta \cos\phi, \quad y = r \sin\theta \sin\phi, \quad z = r \cos\theta \,.
\tag{1.57}
$$

When the point dipole is parallel to the z axis and the optic axis parallel to the x axis, the time-averaged power per unit solid angle can be found in two parts because we have both ordinary and extraordinary wave since the electric field and magnetic field satisfy the orthogonality relations [29]

$$
\hat{\mathbf{r}} \cdot (\mathbf{E}_e \times \mathbf{H}_o^*) = 0, \quad \hat{\mathbf{r}} \cdot (\mathbf{E}_o \times \mathbf{H}_e^*) = 0 \,.
\tag{1.58}
$$

We can find the total radiated power by adding the radiated power of ordinary and extraordinary wave separately, i.e.,

$$\frac{dP}{d\Omega} = \frac{dP_o}{d\Omega} + \frac{dP_e}{d\Omega} \, , \tag{1.59}$$

where

$$\frac{dP_o}{d\Omega} = \frac{1}{2}\hat{\mathbf{r}} \cdot \text{Re}(\mathbf{E_o} \times \mathbf{H_o^*})\text{r}^2 \, , \tag{1.60}$$

and

$$\frac{dP_e}{d\Omega} = \frac{1}{2}\hat{\mathbf{r}} \cdot \text{Re}(\mathbf{E_e} \times \mathbf{H_e^*})\text{r}^2 \, . \tag{1.61}$$

Now the time-averaged power radiated by the point dipole for ordinary wave can be found by substituting the ordinary part of Eqs. (1.50) and (1.51) into Eq. (1.60), and further by using Eq. (1.57) to convert into spherical coordinates as

$$\frac{dP_o}{d\Omega} = \frac{k_o^4 \mu_b n_o p_o^2 c}{32\pi^2 \varepsilon_o} \frac{\sin^2\theta \sin^2\phi}{\sin^2\theta \sin^2\phi + \cos^2\theta} \, . \tag{1.62}$$

Similarly, the time-averaged power radiated by the point-electric dipole for extraordinary wave can be found by substituting the extraordinary part of Eqs. (1.50) and (1.51) into Eq. (1.61), and further by using Eq. (1.57) to convert into spherical coordinates as

$$\frac{dP_e}{d\Omega} = \frac{k_o^4 \mu_b n_o p_o^2 c \varepsilon_d^2}{32\pi^2 \varepsilon_o \Phi^5} \frac{\sin^2\theta \cos^2\phi \cos^2\theta}{\sin^2\theta \sin^2\phi + \cos^2\theta} \, , \tag{1.63}$$

where

$$\Phi(\theta,\phi) = \sqrt{\sin^2\theta \cos^2\phi + \varepsilon_d\Big(\sin^2\theta \sin^2\phi + \cos^2\theta\Big)} \, . \tag{1.64}$$

The total time-averaged power radiated per unit solid angle by the point dipole can be found by substituting Eqs. (1.62) and (1.63) into Eq. (1.59) as

$$\frac{dP}{d\Omega} = \frac{k_o^4 \mu_b n_o p_o^2 c}{32\pi^2 \varepsilon_o} \left(\frac{\varepsilon_d^2 \cos^2\theta \cos^2\phi}{\Phi^5} + \sin^2\phi \right) \frac{\sin^2\theta}{\sin^2\theta \sin^2\phi + \cos^2\theta} . \tag{1.65}$$

The far-field radiation patterns of extraordinary waves emitted by a point electric dipole aligned with the optic axis (z axis) are shown in Fig. 1.6. The dipole is placed in uniaxial material (rutile) with $p_0 = 1/\omega$, $\varepsilon_a = 8.427$, $\varepsilon_b = 6.843$, $\mu_b = 1$, $\lambda_o = 0.584\,\mu\text{m}$ [29]. The plot is given only for $0 \leq \theta \leq \pi$ and $\pi/2 \leq \phi \leq 3\pi/2$ for easier visualization since the pattern is independent of ϕ, as can be seen from Eq. (1.55). The figure shows that the pattern is like that of a dipole in an isotropic material.

When the dipole is perpendicular to the optic axis, the radiation pattern of ordinary and extraordinary waves are shown in Fig. 1.7 on left and right, respectively. It is clear from the left figure that the radiations

FIGURE 1.6: Far-field radiation pattern of a point dipole given by Eq. (1.55), when it is oriented parallel to the optic axis (z axis) and lying in a uniaxial material (rutile) with $p_0 = 1/\omega$, $\varepsilon_a = 8.427$, $\varepsilon_b = 6.843$, $\mu_b = 1$, $\lambda_o = 0.584\,\mu$m. The plot is given for $0 \le \theta \le \pi$ and $\pi/2 \le \phi \le 3\pi/2$.

in the direction of optic axis are suppressed, though not zero. The radiation pattern of the extraordinary wave from the dipole perpendicular to the optic axis are shown in Fig. 1.7 (right). The figure shows that the emission is directive along the optic axis, though the radiations are suppressed along the optic axis in a plane perpendicular to the dipole. Furthermore, there are no radiations emitted along the y axis, a direction perpendicular to both the dipole and the optic axis.

FIGURE 1.7: Far-field radiation pattern of (left) ordinary waves given by Eq. (1.62) and (right) extraordinary waves given by Eq. (1.63), when the point dipole is oriented along z axis and the optic axis along x axis for a uniaxial material (rutile) with $p_0 = 1/\omega$, $\varepsilon_a = 8.427$, $\varepsilon_b = 6.843$, $\mu_b = 1$, $\lambda_o = 0.584\,\mu$m. The plot is given for $0 \le \theta \le \pi$ and $\pi/2 \le \phi \le 3\pi/2$.

1.4.2 Radiation by a point-magnetic dipole

Now, let us consider a point-magnetic dipole located at the origin with dipole moment m_o and the current density given by [25]

$$\mathbf{J}_e(\mathbf{r}) = 0, \quad \mathbf{J}_m(\mathbf{r}) = -i\omega\mathbf{m}_o\delta(\mathbf{r}). \tag{1.66}$$

The electric and magnetic fields in the near zone given by [25]

$$\mathbf{H}(\mathbf{r}) = 0,$$
$$\mathbf{E}(\mathbf{r}) = \frac{1}{4\pi\mu_o\mu_b r^3}\left[3\hat{\mathbf{r}}(\hat{\mathbf{r}}\cdot\mathbf{m}_o) - \mathbf{m}_o\right]. \tag{1.67}$$

It is clear from Eq. (1.67) that it represents the magneto static field because the magnetic field is present in the absence of ω, i.e., for $\omega \to 0$. Moreover, when we are very far away from the dipole, the approximate electric and magnetic fields are given by [25]

$$\mathbf{E}(\mathbf{r}) = \omega k_o n_o \left\{ g_o(\mathbf{r},0)\frac{(\mathbf{r}\times\hat{\mathbf{c}})\left[\mathbf{r}\times(\mathbf{r}\times\hat{\mathbf{c}})\right]}{r(\mathbf{r}\times\hat{\mathbf{c}})\cdot(\mathbf{r}\times\hat{\mathbf{c}})} - g_e(\mathbf{r},0)\frac{\varepsilon_a}{\varepsilon_b}\frac{\left[\mathbf{r}\times(\mathbf{r}\times\hat{\mathbf{c}})\right](\mathbf{r}\times\hat{\mathbf{c}})}{r_e(\mathbf{r}\times\hat{\mathbf{c}})\cdot(\mathbf{r}\times\hat{\mathbf{c}})} \right\}\cdot\mathbf{m}_o, \tag{1.68}$$

and

$$\mathbf{H}(\mathbf{r}) = \omega^2\varepsilon_o\varepsilon_b\left\{ g_o(\mathbf{r},0)\left(\underline{I} - \hat{\mathbf{r}}\hat{\mathbf{r}}\right) - \frac{1}{\varepsilon_b}\left[\varepsilon_b g_o(\mathbf{r},0) - \varepsilon_a g_o(\mathbf{r},0)\right]\underline{\underline{K}}(\mathbf{r}) \right\}\cdot\mathbf{m}_o. \tag{1.69}$$

Only the terms proportional to $1/r$ were retained in Eqs. (1.68) and (1.69) under the far zone approximation, which is valid when we are far away from the source.

As a special case, when the dipole is aligned along the direction of the optic axis, i.e., $\mathbf{m} = m_o\hat{\mathbf{c}}$, then the electric and magnetic fields are in most general form can be written as [25]

$$\mathbf{E}(\mathbf{r}) = -i\omega m_o(1 - ik_o n_o r)\frac{(\mathbf{r}\times\hat{\mathbf{c}})}{r^2}g_o(\mathbf{r},0), \tag{1.70}$$

and

$$\mathbf{H}(\mathbf{r}) = \omega^2 m_o\varepsilon_o\varepsilon_b\left\{ \left[1 + \frac{i}{k_o n_o r} - \frac{1}{(k_o n_o r)^2}\right]\hat{\mathbf{c}} - \left[1 + \frac{3i}{k_o n_o r} - \frac{3}{(k_o n_o r)^2}\right]\hat{\mathbf{r}}(\hat{\mathbf{r}}\cdot\hat{\mathbf{c}}) \right\}g_o(\mathbf{r},0). \tag{1.71}$$

Equations (1.70) and (1.71) show that only ordinary wave is emitted by a point magnetic dipole because $g_e(\mathbf{r},0)$ is absent in both equations. If we compare these equations with Eqs. (1.52) and (1.53), we can see that when the electric and magnetic dipole are aligned parallel to the direction of the optic axis, they only emit extraordinary and ordinary wave, respectively.

When both the optic axis and the point-magnetic dipole are parallel to the z axis, the time-averaged power radiated per unit solid angle can be found by substituting Eqs. (1.68) and (1.69) into Eq. (1.54) as

$$\frac{dP}{d\Omega} = \frac{k_o^4 \varepsilon_b n_o m_o^2 c}{32 \mu_o \pi^2} \sin^2 \theta \qquad (1.72)$$

in the spherical coordinates.

When the point magnetic dipole is parallel to the z axis and the optic axis is parallel to the x axis, the time-averaged power radiated by the point-magnetic dipole for ordinary wave can be found by substituting the ordinary part of Eqs. (1.68) and (1.69) into Eq. (1.60), and further by using Eq. (1.57) to convert into spherical coordinates as

$$\frac{dP_o}{d\Omega} = \frac{k_o^4 \varepsilon_b n_o m_o^2 c}{32 \mu_o \pi^2} \frac{\sin^2 \theta \cos^2 \theta \cos^2 \phi}{\sin^2 \theta \sin^2 \phi + \cos^2 \theta} . \qquad (1.73)$$

Similarly, the time-averaged power radiated by the point magnetic dipole for extraordinary wave can be found by substituting the extraordinary part of Eqs. (1.68) and (1.69) into Eq. (1.61), and further by using Eq. (1.57) to convert into spherical coordinates as

$$\frac{dP_e}{d\Omega} = \frac{k_o^4 \varepsilon_b n_o m_o^2 c \varepsilon_d^2}{32 \mu_o \pi^2 \Phi^3} \frac{\sin^2 \theta \sin^2 \phi}{\sin^2 \theta \sin^2 \phi + \cos^2 \theta} . \qquad (1.74)$$

The total time-averaged power radiated per unit solid angle by the point magnetic dipole can be found by substituting Eqs. (1.73) and (1.74) into Eq. (1.59) as

$$\frac{dP}{d\Omega} = \frac{k_o^4 \varepsilon_b n_o m_o^2 c}{32 \mu_o \pi^2} \left(\cos^2 \theta \cos^2 \phi + \frac{\varepsilon_d^2 \sin^2 \phi}{\Phi^3} \right) \frac{\sin^2 \theta}{\sin^2 \theta \sin^2 \phi + \cos^2 \theta}. \qquad (1.75)$$

The far-field radiation patterns of ordinary waves emitted by a point magnetic dipole with its axis aligned with the optic axis (z axis) are shown in Fig. 1.8. The point-magnetic dipole is placed in rutile with $p_0 = 1/\omega$, $\varepsilon_a = 8.427$, $\varepsilon_b = 6.843$, $\mu_b = 1$, and $\lambda_o = 0.584 \, \mu$m [29]. We have plotted Eq. (1.72) only for $0 \leq \theta \leq \pi$ and $\pi/2 \leq \phi \leq 3\pi/2$ because it is easier to visualize the pattern since it is independent of ϕ. The figure shows that the pattern is the same as that of a point dipole in an isotropic material [26]. Let us note that no radiations exist along the optic axis which also happens to be the axis of the loop in this case.

When the axis of the point-magnetic dipole is perpendicular to the optic axis, the radiation pattern of the ordinary and extraordinary waves are shown in Fig. 1.9 on left and right, respectively. Its clear
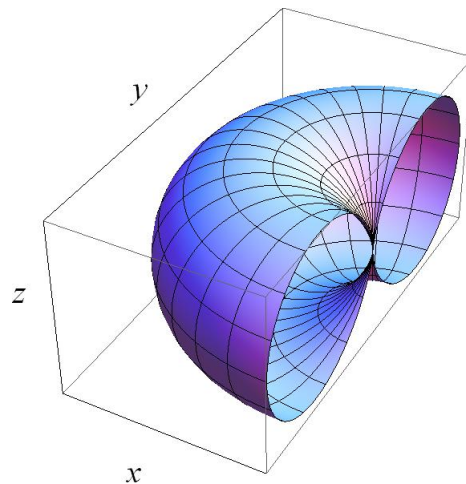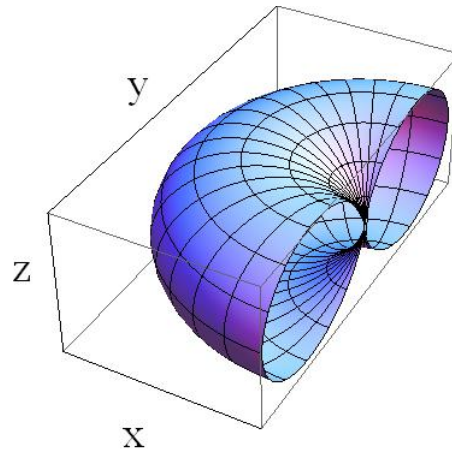
FIGURE 1.8: Far-field radiation pattern of a point magnetic dipole given by Eq. (1.72), when it is oriented parallel to the optic axis (z axis) and lying in a uniaxial material (rutile) with $p_0 = 1/\omega$, $\varepsilon_a = 8.427$, $\varepsilon_b = 6.843$, $\mu_b = 1$, $\lambda_o = 0.584\,\mu\text{m}$ [29]. The plot is given for $0 \leq \theta \leq \pi$ and $\pi/2 \leq \phi \leq 3\pi/2$.
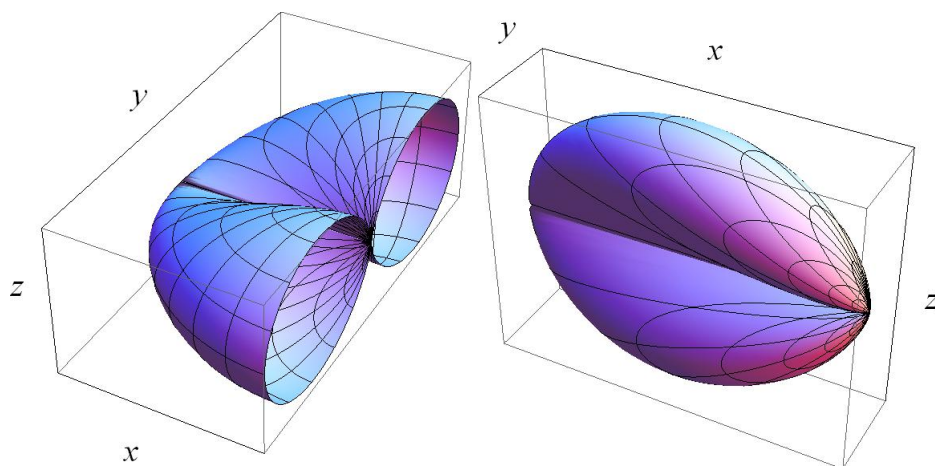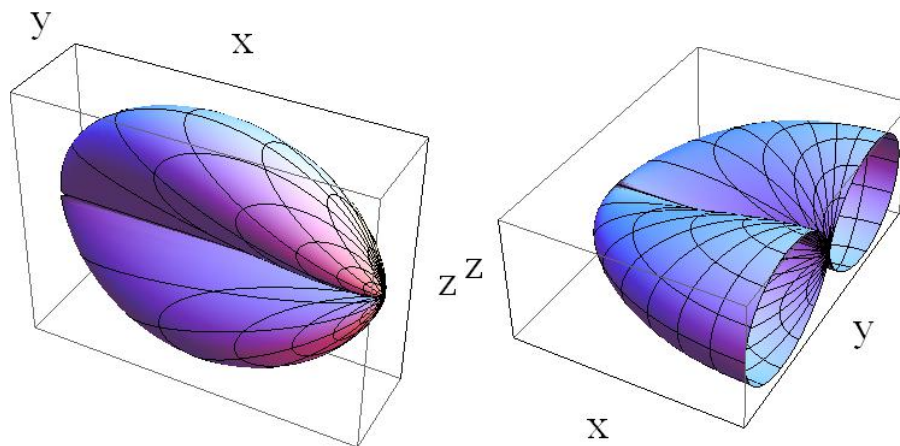

FIGURE 1.9: Far-field radiation pattern of (left) ordinary waves given by Eq. (1.73) and (right) extraordinary waves given by Eq. (1.74), when the point magnetic dipole is oriented along z axis and the optic axis along x axis for a uniaxial material (rutile) with $p_0 = 1/\omega$, $\varepsilon_a = 8.427$, $\varepsilon_b = 6.843$, $\mu_b = 1$, $\lambda_o = 0.584\,\mu\text{m}$ [29]. The plot is given for $0 \leq \theta \leq \pi$ and $\pi/2 \leq \phi \leq 3\pi/2$.

from the figure that the radiations are directed toward the optic axis for the ordinary wave and these are suppressed along the optic axis for the extraordinary waves.

1.4.3   Comparison of point-electric and point-magnetic dipole

When both the optic axis and the dipole (electric or magnetic) are parallel to each other, the radiation pattern is similar for both the dipoles. However, when the optic axis is along the x axis and the dipole (electric or magnetic) is along the z axis the radiation pattern for both the ordinary and extraordinary wave is reversed.

1.5 Overview of thesis

The main goal of this thesis is to study the radiation problems of finite-sized sources placed in the uniaxial materials. In Chapter 2, we have analyazed a finite-length electric dipole. Analytical results are presented in the near and far zone when the dipole is placed in the uniaxial dielectric material. When the dipole is parallel and perpendicular to the optic axis. In Chapter 3, a finite-sized current loop is taken up to mimic finite-sized magnetic dipole. The elegant closed form are derived in the far-zone when the loop axis is parallel and perpendicular to the optic axis. In Chapter 4, the radiations by a finite-length electric dipole are studies in the hyperbolic material. The strong dependence upon the length of the dipole is found. In Chapter 5, analytical results are presented for the finite-length electric dipole when it is placed in uniaxial zero-index material. The wire-medium in the zero-index regime is considered for analysis. Finally, conlusions and future directions are presented in Chapter 6

Chapter 2

Hertzian electric dipole in uniaxial dielectric material

In this chapter, the radiation by an extended linear source in the unbounded uniaxial dielectric material with uniform current distribution is studied. The exact as well as approximate fields in the near and far zones are found analytically using the dyadic Green functions in the frequency domain. Elegant closed-form results are obtained when the Hertzian dipole is parallel and perpendicular to the optic axis of the uniaxial material. When the dipole is parallel to the optic axis, only extraordinary waves are emitted. When the dipole is perpendicular to the optic axis, both ordinary and extraordinary waves are emitted; however, the radiations are suppressed along the optic axis and no extraordinary waves are emitted in a direction perpendicular to both the electric dipole and the optic axis. A comparison with the point dipole showed that the directivity of the radiation pattern can be controlled using the length of the Hertzian dipole.

The plan of the chapter is as follow: The introduction and the relevant literature review is presented in Sec. 2.1. The case of the electric dipole oriented parallel to the optic axis, when both the optic axis and the dipole are parallel to the x axis, is presented in Sec. 2.2. The case of the dipole oriented parallel to the optic axis, when both the optic axis and the dipole are parallel to the z axis, is presented in Sec. 2.3. The case of the dipole perpendicular to the optic axis is presented in Sec. 2.4. The representative numerical results are discussed in Sec. 2.5 and are compared with a point dipole in Sec. 2.6. Finally, the concluding remarks are presented in Sec. 2.7.

This chapter is based on "A. Hayat and M. Faryad, On the radiation from a Hertzian dipole of a finite length in the uniaxial dielectric material, *OSA Continuum* **2**, 1411-1429 (2019)"

2.1   Introduction

A small linear electric current element with uniform current distribution is called a Hertzian dipole. Several electrically small sources of electromagnetic waves can be modeled as Hertzian dipoles such as quantum dots or quantum wires. The length of the Hertzian dipole is usually short as compared to the wavelength of electromagnetic waves emitted by that dipole [24, 89]. The Hertzian dipole is also highly useful for helping analyze larger antennas which can be subdivided into short sections having uniform currents as large antennas can be thought of as composed of small sections with uniform current distribution on each small section [89].

To the zeroth order, small sources of radiations can be modeled as point dipoles. Therefore, several authors have studied the radiations from point dipoles. For example, the radiation by a point dipole in unbounded uniaxial material is dealt in Refs. [16–18]. The radiation over a layered material with its optic axis lying perpendicular to the plane of stratification has been studied by Tsang *et al.* [19], Kong [20], Kwon and Wang [21], and Tang [22], while the same problem with point dipole embedded in the stratified material has been studied by Ali and Mahmoud [23]. Far field radiation emitted by an arbitrarily oriented point dipole which is placed in a two-layered uniaxially anisotropic material with its tilted optic axis is treated analytically with the use of dyadic Green function[24]. Here two cases are discussed, when the dipole is placed over the two layered uniaxial material, and when it is embedded in a two layered uniaxial material [24].

Most of the analytical work on radiation by sources inside the uniaxial materials has been done for point dipoles, which are the zeroth order approximation of real sources. For the next approximation, it is important to consider the radiation from sources with finite length. The simplest case for this type of source is a Hertzian dipole with constant current density phasor over the length of the source. This is the problem addressed in this chapter. However, unlike the point dipole, when the integration is trivial, the results cannot be obtained in closed form for general Hertzian dipole. Therefore, we solved for two cases of the orientation of the Hertzian dipole: (i) When the dipole is parallel to the optic axis and (ii) when the dipole is perpendicular to the optic axis. A generally oriented dipole can always be broken into two vector components, one along and one perpendicular to the optic axis. Therefore, our formulation can be used to construct the solution of generally oriented Hertzian dipole by simple vector superposition. Let us note that the extended sources have been dealt with for radiation in the uniaxial material numerically [18] and using integral equations [90], and using approximation [91]. Moreover, the radiation resistance of an electrically-small electric and magnetic dipole has been studied in a cold uniaxial plasma [92]. However, our aim is to find closed-form and rigorous solutions of an extended linear dipole in this chapter.

2.2 Dipole and optic axis parallel to x axis

Let us begin with the simpler case when both the electric dipole and the optic axis are parallel to the x axis as shown in Fig. 2.1 with the electric current density

$$\mathbf{J}_e(\mathbf{r}') = \begin{cases} -i\omega p_o \delta(y')\delta(z')\hat{\mathbf{x}}, & |x'| \leq L, \\ 0, & |x'| > L. \end{cases} \tag{2.1}$$

FIGURE 2.1: Schematic showing a dipole (thick line) oriented parallel to the optic axis $\hat{\mathbf{c}} = \hat{\mathbf{x}}$. The field point P is located at position vector $\mathbf{r}$ with respect to the origin.

2.2.1 Near field

The near-field of the Hertzian dipole parallel to the optic axis can be computed by substituting the near-field approximation of the dyadic Green function (1.41) and the electric current density (2.1) into Eq. (1.27) to get

$$\mathbf{E}(\mathbf{r}) = \frac{\varepsilon_d p_o}{4\pi\varepsilon_o} \int_{-L}^{L} \left[\frac{3\varepsilon_a(\underline{\underline{\varepsilon}}_r^{-1} \cdot \mathbf{R}_x)(\underline{\underline{\varepsilon}}_r^{-1} \cdot \mathbf{R}_x) \cdot \hat{\mathbf{x}}}{R_{ex}^5} - \frac{\underline{\underline{\varepsilon}}_r^{-1} \cdot \hat{\mathbf{x}}}{R_{ex}^3} \right] dx', \tag{2.2}$$

where

$$\varepsilon_d = \varepsilon_a/\varepsilon_b, \tag{2.3}$$

$$R_{ex} = \sqrt{\varepsilon_d(y^2 + z^2) + (x - x')^2}, \tag{2.4}$$

and

$$\mathbf{R_x} = (x - x')\hat{\mathbf{x}} + y\hat{\mathbf{y}} + z\hat{\mathbf{z}}. \tag{2.5}$$

Using Eqs. (1.33) and (2.5), we can get the following identities

$$\underline{\underline{\varepsilon}}_r^{-1} \cdot \mathbf{R}_x = \frac{1}{\varepsilon_b}(y\hat{\mathbf{y}} + z\hat{\mathbf{z}}) + \frac{1}{\varepsilon_a}(x - x')\hat{\mathbf{x}}, \tag{2.6}$$

$$\underline{\underline{\varepsilon}}_r^{-1} \cdot \hat{\mathbf{x}} = \frac{1}{\varepsilon_a}\hat{\mathbf{x}}. \tag{2.7}$$

Substituting Eqs. (2.6) and (2.7) into Eq. (2.2), we get

$$\mathbf{E}(\mathbf{r}) = \frac{\varepsilon_d p_o}{4\pi\varepsilon_o\varepsilon_a}\left\{ 3\varepsilon_d(y\hat{\mathbf{y}} + z\hat{\mathbf{z}}) \int_{-L}^{L} \frac{(x - x')}{\left[\varepsilon_d(y^2 + z^2) + (x - x')^2\right]^{\frac{5}{2}}} dx' + 3\hat{\mathbf{x}} \right.$$

$$\left. \times \int_{-L}^{L} \frac{(x - x')^2}{\left[\varepsilon_d(y^2 + z^2) + (x - x')^2\right]^{\frac{5}{2}}} dx' - \hat{\mathbf{x}} \int_{-L}^{L} \frac{1}{\left[\varepsilon_d(y^2 + z^2) + (x - x')^2\right]^{\frac{3}{2}}} dx' \right\}, \tag{2.8}$$

that gives

$$\mathbf{E}(\mathbf{r}) = \frac{\varepsilon_d p_o}{4\pi\varepsilon_o\varepsilon_b}\left\{ y\hat{\mathbf{y}} + z\hat{\mathbf{z}}\left(\frac{1}{\left[\varepsilon_d(y^2 + z^2) + (x - L)^2\right]^{\frac{3}{2}}} - \frac{1}{\left[\varepsilon_d(y^2 + z^2) + (x + L)^2\right]^{\frac{3}{2}}} \right) \right.$$

$$\left. + \frac{\hat{\mathbf{x}}}{\varepsilon_d}\left(\frac{L - x}{\left[\varepsilon_d(y^2 + z^2) + (x - L)^2\right]^{\frac{3}{2}}} + \frac{L + x}{\left[\varepsilon_d(y^2 + z^2) + (x + L)^2\right]^{\frac{3}{2}}} \right) \right\}. \tag{2.9}$$

Since $\mathbf{H}(\mathbf{r}) = 0$ in the near-field, Eq. (2.9) effectively represents the electrostatic field of a line of charge in the uniaxial material parallel to the optic axis.

2.2.2 Far field

The electric and magnetic fields in the far field can be found by the substitution of Eqs. (1.43) and (2.1) into Eq. (1.27), to get

$$\mathbf{E}(\mathbf{r}) = \omega^2\mu_o\mu_b p_o\left\{ \int_{-L}^{L} g_e(\mathbf{R}_x)\left[\varepsilon_a\underline{\underline{\varepsilon}}_r^{-1} \cdot \hat{\mathbf{x}} - \frac{\varepsilon_a^2(\underline{\underline{\varepsilon}}_r^{-1} \cdot \mathbf{R}_x)(\underline{\underline{\varepsilon}}_r^{-1} \cdot \mathbf{R}_x) \cdot \hat{\mathbf{x}}}{R_{ex}^2} \right] dx' \right\}, \tag{2.10}$$

which can be written as

$$
\begin{aligned}
\mathbf{E}(\mathbf{r}) \;=\;& \frac{\omega^2 \mu_o \mu_b p_o}{4\pi} \left[\hat{\mathbf{x}} \int_{-L}^{L} \frac{\exp(ik_o n_o R_{ex})}{R_{ex}} dx' - \varepsilon_d (y\hat{\mathbf{y}} + z\hat{\mathbf{z}}) \int_{-L}^{L} \frac{(x-x')\exp(ik_o n_o R_{ex})}{R_{ex}^3} dx' \right. \\
&\left. -\hat{\mathbf{x}} \int_{-L}^{L} \frac{(x-x')^2 \exp(ik_o n_o R_{ex})}{R_{ex}^3} dx' \right],
\end{aligned}
\tag{2.11}
$$

using Eqs. (1.35), (2.6) and (2.7), where R_{ex} is given by Eq. (2.4).

Since our point of observation is far away from the dipole, i.e., $r_e \gg x'$, which means that our distance from the dipole is much greater than the size of the dipole. So, in this limit, we neglect the square and higher order terms in the binomial expansion of Eq. (2.4) and approximate as

$$
R_{ex} \simeq r_e - \frac{x}{r_e} x'
\tag{2.12}
$$

in the exponential factor, where

$$
r_e = \sqrt{x^2 + \varepsilon_d(y^2 + z^2)}.
\tag{2.13}
$$

In the denominator of Eq. (2.11), we can approximate $R_{ex} \simeq r_e$. Thereafter, Eq. (2.11) becomes

$$
\mathbf{E}(\mathbf{r}) \simeq \frac{\omega^2 \mu_o \mu_b p_o}{4\pi} \exp(ik_o n_o r_e) \left[\left(\frac{I_1}{r_e} - \frac{I_3}{r_e^3} \right) \hat{\mathbf{x}} - \varepsilon_d \left(\frac{y\hat{\mathbf{y}} + z\hat{\mathbf{z}}}{r_e^3} \right) I_2 \right],
\tag{2.14}
$$

where the integrals I_1 to I_3 are derived in the appendix.

Using the transformation from Cartesian to spherical coordinates given in Eq. (1.57), we can rewrite Eq. (2.13) as

$$
r_e = r \sqrt{\sin^2 \theta \cos^2 \phi + \varepsilon_d \left(\sin^2 \theta \sin^2 \phi + \cos^2 \theta \right)} = r\Phi(\theta, \phi).
\tag{2.15}
$$

Now by substituting the solutions of integrals I_1, I_2 and I_3 along with Eqs. (1.57) and (2.15) into Eq. (2.14), the final expression of the electric field in spherical coordinates is given by

$$
\begin{aligned}
\mathbf{E}(\mathbf{r}) \;=\;& \frac{k_o \mu_b p_o \varepsilon_d}{2\pi \varepsilon_o n_o r} \frac{\exp(ik_o n_o r\Phi)}{\Phi^2} \left[\frac{(\sin^2 \theta \sin^2 \phi + \cos^2 \theta)}{\sin\theta\cos\phi} \hat{\mathbf{x}} \right. \\
&\left. - \sin\theta\sin\phi\hat{\mathbf{y}} - \cos\theta\hat{\mathbf{z}} \right] \sin\left(\frac{k_o L n_o \sin\theta\cos\phi}{\Phi} \right).
\end{aligned}
\tag{2.16}
$$

The expression of the magnetic field can be found by using Eqs. (1.46) and (2.1) in Eq. (1.28) as

$$\mathbf{H}(\mathbf{r}) = -k_o n_o \omega p_o \varepsilon_d \int_{-L}^{L} g_e(\mathbf{R}_x) \frac{(\mathbf{R}_x \times \hat{\mathbf{x}})[\mathbf{R}_x \times (\mathbf{R}_x \times \hat{\mathbf{x}})] \cdot \hat{\mathbf{x}}}{R_{ex}(\mathbf{R}_x \times \hat{\mathbf{x}}) \cdot (\mathbf{R}_x \times \hat{\mathbf{x}})} dx' .$$

(2.17)

Using Eq. (1.35) we get

$$\mathbf{H}(\mathbf{r}) = \frac{k_o n_o \omega p_o \varepsilon_d}{4\pi} (-y\hat{\mathbf{z}} + z\hat{\mathbf{y}}) \int_{-L}^{L} \frac{\exp(ik_o n_o R_{ex})}{R_{ex}^2} dx' ,$$

(2.18)

after making use of the following

$$\mathbf{R}_x \times \hat{\mathbf{x}} = -y\hat{\mathbf{z}} + z\hat{\mathbf{y}}, \quad [\mathbf{R}_x \times (\mathbf{R}_x \times \hat{\mathbf{x}})] \cdot \hat{\mathbf{x}} = -(y^2 + z^2).$$

(2.19)

Using Eqs. (2.12) in the exponential term and $R_{ex} = r_e$ in the denominator of Eq. (2.18), we get

$$\mathbf{H}(\mathbf{r}) = \frac{k_o n_o \omega p_o \varepsilon_d}{4\pi} \frac{\exp(ik_o n_o r_e)}{r_e^2} (-y\hat{\mathbf{z}} + z\hat{\mathbf{y}}) I_1 .$$

(2.20)

By substituting the value of I_1 into Eq. (2.20), transforming to the spherical coordinates and ignoring $1/r^2$ terms we get

$$\mathbf{H}(\mathbf{r}) = \frac{k_o p_o c \varepsilon_d}{2\pi r} \frac{\exp(ik_o n_o r \Phi)}{\Phi \sin\theta \cos\phi} \Big(\cos\theta \hat{\mathbf{y}} - \sin\theta \sin\phi \hat{\mathbf{z}} \Big) \sin\Big(\frac{k_o L n_o \sin\theta \cos\phi}{\Phi} \Big) .$$

(2.21)

From Eqs. (2.16) and (2.21), we can see that only extraordinary waves propagate in this case. Furthermore, the electric and magnetic fields are perpendicular to each other, as is usually the case of radiation in the far zone.

Using the expressions for $\mathbf{E}$ and $\mathbf{H}$ from Eqs. (2.16) and (2.21) in Eq. (1.54), the time-averaged power radiated per unit solid angle by the Hertzian dipole is given by

$$\frac{dP}{d\Omega} = \frac{k_o^2 \mu_b p_o^2 c \varepsilon_d^2}{8\pi^2 \varepsilon_o n_o} \frac{(\sin^2\theta \sin^2\phi + \cos^2\theta)}{\Phi^3 \sin^2\theta \cos^2\phi} \sin^2\Big(\frac{k_o L n_o \sin\theta \cos\phi}{\Phi} \Big) .$$

(2.22)

When we substitute $\varepsilon_d = 1$, $\Phi = 1$, we get the results for the isotropic material.
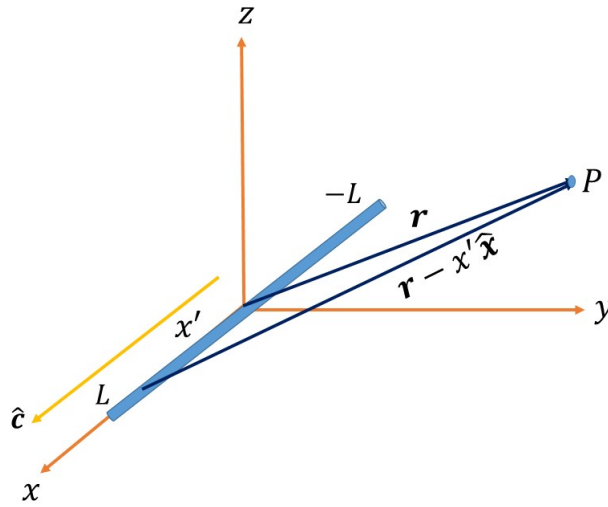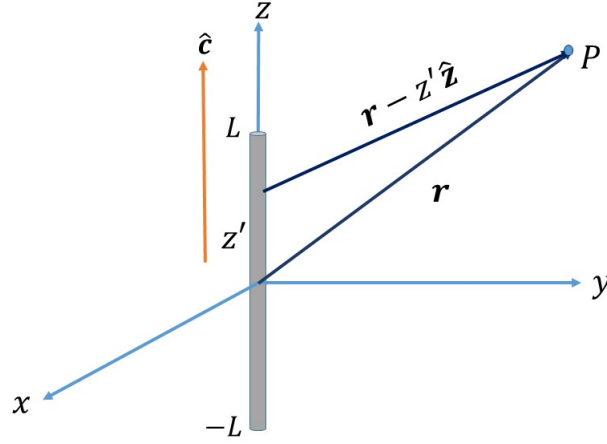
FIGURE 2.2: Schematic showing a dipole (thick vertical line) oriented parallel to the optic axis $\hat{\mathbf{c}} = \hat{\mathbf{z}}$. The field point P is located at a position vector $\mathbf{r}$ with respect to the center of the dipole.

2.3 Dipole and optic axis parallel to z axis

In the previous section, we had the dipole and the optic axis parallel to the x axis. In the following section, we will present the results for the dipole to be parallel to the z axis, but the optic axis would still be parallel to the x axis. The reason is that an arbitrarily oriented dipole can be resolved into a dipole parallel to and perpendicular to the optic axis. Therefore, the results of the previous section and the following section can be used to construct solutions of an arbitrarily oriented Hertzian dipole. However, in this section, we present the results of for a Hertzian dipole when the optic axis is parallel to the z axis so that the results of the next section and this section can be compared for the case of isotropic material for consistency check.

When the dipole and the optic axis are parallel to the z axis as shown in Fig. 2.2, the expression for the electric field is given by

$$\mathbf{E}(\mathbf{r}) = \frac{k_o\mu_b p_o\varepsilon_d}{2\pi\varepsilon_o n_o r} \frac{\exp(ik_o n_o r\Theta)}{\Theta^2} \left[\frac{\sin^2\theta}{\cos\theta}\hat{\mathbf{x}} - \sin\theta\cos\phi\hat{\mathbf{y}} - \sin\theta\sin\phi\hat{\mathbf{z}}\right] \sin\left(\frac{k_o L n_o\cos\theta}{\Theta}\right), \quad (2.23)$$

and the expression for magnetic field is given by

$$\mathbf{H}(\mathbf{r}) = \frac{k_o p_o c\varepsilon_d}{2\pi r} \frac{\exp(ik_o n_o r\Theta)}{\Theta\cos\theta}\left(-\sin\theta\cos\phi\hat{\mathbf{z}} + \sin\theta\sin\phi\hat{\mathbf{y}}\right)\sin\left(\frac{k_o L n_o\cos\theta}{\Theta}\right). \quad (2.24)$$

The power distribution then is given by

$$\frac{dP}{d\Omega} = \frac{k_o^2 \mu_b p_o^2 c \varepsilon_d^2}{8\pi^2 \varepsilon_o n_o} \frac{\sin^2 \theta}{\Theta^3 \cos^2 \theta} \sin^2 \left(\frac{k_o L n_o \cos \theta}{\Theta} \right). \tag{2.25}$$

The result is independent of ϕ as should be the case since the dipole and the optic axis are both along the z axis and the problem has azimuthal symmetry. The far field for the isotropic material can be obtained by setting $\varepsilon_d = 1$ and $\Theta = 1$.

2.4 Dipole parallel to z axis and optic axis parallel to x axis

Let us now consider the case when the Hertzian dipole is perpendicular to the optics axis, as shown schematically in Fig. 2.3. For this electric dipole, the current density can be written as

$$\mathbf{J}_e(\mathbf{r}) = \begin{cases} -i\omega p_o \delta(x')\delta(y')\hat{\mathbf{z}}', & |z'| \leq L, \\ 0, & |z'| > L. \end{cases} \tag{2.26}$$
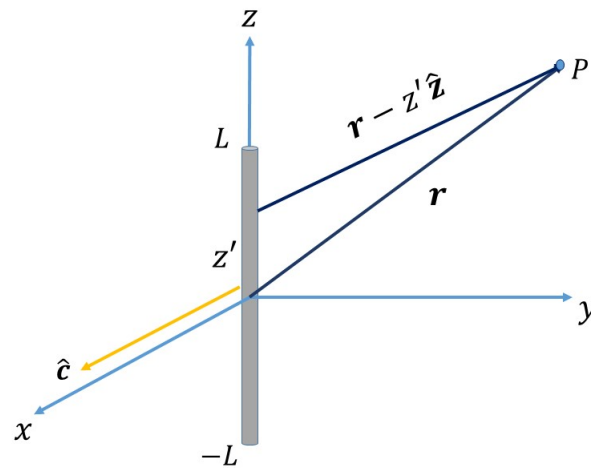
FIGURE 2.3: Schematic showing a dipole (thick vertical line) oriented perpendicular to the optic axis $\hat{\mathbf{c}} = \hat{\mathbf{x}}$. The field point P is located at a position vector $\mathbf{r}$ with respect to the center of the dipole.

2.4.1 Near field

In the near field, the expression of electric field is found by substitution of Eqs. (1.41) and (2.26) into Eq. (1.27) as

$$\mathbf{E}(\mathbf{r}) = \frac{\varepsilon_d p_o}{4\pi\varepsilon_o} \int\limits_{-L}^{L} \left[\frac{3\varepsilon_a(\underline{\underline{\varepsilon}}_r^{-1} \cdot \mathbf{R}_z)(\underline{\underline{\varepsilon}}_r^{-1} \cdot \mathbf{R}_z) \cdot \hat{\mathbf{z}}}{R_{ez}^5} - \frac{\underline{\underline{\varepsilon}}_r^{-1} \cdot \hat{\mathbf{z}}}{R_{ez}^3} \right] dz', \tag{2.27}$$

where

$$\mathbf{R}_z = x\hat{\mathbf{x}} + y\hat{\mathbf{y}} + (z - z')\hat{\mathbf{z}} \tag{2.28}$$

and

$$R_{ez} = \sqrt{x^2 + \varepsilon_d y^2 + \varepsilon_d (z - z')^2} \,. \tag{2.29}$$

After simplification, we get

$$\begin{aligned}
\mathbf{E}(\mathbf{r}) &= \frac{3\varepsilon_d^2 p_o}{4\pi\varepsilon_o\varepsilon_a} \Bigg\{ \left(x\hat{\mathbf{x}} + \varepsilon_d y\hat{\mathbf{y}} \right) \int\limits_{-L}^{L} \frac{(z - z')}{[x^2 + \varepsilon_d y^2 + \varepsilon_d (z - z')^2]^{\frac{5}{2}}} dz' \\
&\quad + \hat{\mathbf{z}}\varepsilon_d \int\limits_{-L}^{L} \frac{(z - z')^2}{[x^2 + \varepsilon_d y^2 + \varepsilon_d (z - z')^2]^{\frac{5}{2}}} dz' - \frac{\hat{\mathbf{z}}}{3} \int\limits_{-L}^{L} \frac{1}{[x^2 + \varepsilon_d y^2 + \varepsilon_d (z - z')^2]^{\frac{3}{2}}} dz' \Bigg\},
\end{aligned}$$

which gives

$$\begin{aligned}
\mathbf{E}(\mathbf{r}) &= \frac{3\varepsilon_d^2 p_o}{4\pi\varepsilon_o\varepsilon_a} \Bigg[\left(x\hat{\mathbf{x}} + \varepsilon_d y\hat{\mathbf{y}} \right) \Bigg\{ \frac{1}{[x^2 + \varepsilon_d y^2 + \varepsilon_d (z - L)^2]^{\frac{3}{2}}} - \frac{1}{[x^2 + \varepsilon_d y^2 + \varepsilon_d (z + L)^2]^{\frac{3}{2}}} \Bigg\} \\
&\quad + \frac{\hat{\mathbf{z}}\varepsilon_d}{(x^2 + \varepsilon_d y^2)} \Bigg\{ \frac{(z - L)^2}{[x^2 + \varepsilon_d y^2 + \varepsilon_d (z - L)^2]^{\frac{3}{2}}} - \frac{(z + L)^2}{[x^2 + \varepsilon_d y^2 + \varepsilon_d (z + L)^2]^{\frac{3}{2}}} \Bigg\} \\
&\quad + \frac{\hat{\mathbf{z}}}{3(x^2 + \varepsilon_d y^2)} \Bigg\{ \frac{(z - L)}{[x^2 + \varepsilon_d y^2 + \varepsilon_d (z - L)^2]^{\frac{1}{2}}} - \frac{(z + L)}{[x^2 + \varepsilon_d y^2 + \varepsilon_d (z + L)^2]^{\frac{1}{2}}} \Bigg\} \Bigg]. \tag{2.30}
\end{aligned}$$

Let us recall that $\mathbf{H}(\mathbf{r}) \approx 0$ in the near zone.

2.4.2 Far field except at optic axis

In the far field, the expression of electric field can be found by substituting Eqs. (1.45) and (2.26) into Eq. (1.27), and its simplified expression is given by

$$
\mathbf{E}(\mathbf{r}) = \frac{\omega^2 \mu_o \mu_b p_o}{4\pi} \Bigg\{ \varepsilon_d \int_{-L}^{L} \frac{\left[(x^2 y \hat{\mathbf{y}} - x y^2 \hat{\mathbf{x}})(z - z') + x^2 \hat{\mathbf{z}}(z - z')^2 - x \hat{\mathbf{x}}(z - z')^3 \right]}{y^2 + (z - z')^2}
$$

$$
\times \frac{\exp(i k_o n_o R_{ez})}{R_{ez}^3} dz' + \int_{-L}^{L} \left(\frac{y^2 \hat{\mathbf{z}} - y(z - z') \hat{\mathbf{y}}}{y^2 + (z - z')^2} \right) \frac{\exp(i k_o n_o R_z)}{R_z} dz' \Bigg\}. \tag{2.31}
$$

To solve these integrals we use far field approximation. Using Eq. (1.36) with $\hat{\mathbf{c}} = \hat{\mathbf{x}}$, we get

$$
R_{ez} = \left[r_e^2 + \varepsilon_d z'(z' - 2z) \right]^{\frac{1}{2}}, \tag{2.32}
$$

where r_e is given by Eq. (2.13).

In the far-field, our point of observation is far away from the dipole, i.e., $r_e \gg z'$, so in this limit, we can neglect the higher order terms in z'/r_e in the binomial expansion of (2.32) and have

$$
R_{ez} \simeq r_e - \varepsilon_d \frac{z z'}{r_e} \tag{2.33}
$$

in the exponential term, whereas we can approximate $R_{ez} \simeq r_e$ in the denominator. Similarly,

$$
R_z = \left[r^2 + z'(z' - 2z) \right]^{\frac{1}{2}} \tag{2.34}
$$

can be approximated as

$$
R_z \simeq r - \frac{z z'}{r} \tag{2.35}
$$

in the exponential term and $R_z \simeq r$ in the denominator. Furthermore,

$$
y^2 + (z - z')^2 \sim y^2 + z^2 \tag{2.36}
$$

since $y^2 + z^2 >> L$ in the far field at a point other than the optic axis. Therefore, Eq. (2.31) becomes

$$
\mathbf{E}(\mathbf{r}) \simeq \frac{\omega^2 \mu_o \mu_b p_o}{4\pi} \Bigg\{ \frac{\varepsilon_d \exp(i k_o n_o r_e)}{r_e^3 (y^2 + z^2)} \left[(x^2 y \hat{\mathbf{y}} - x y^2 \hat{\mathbf{x}}) I_4 + x^2 \hat{\mathbf{z}} I_5 - x \hat{\mathbf{x}} I_6 \right]
$$

$$
+ \frac{\exp(i k_o n_o r)}{r(y^2 + z^2)} \left(y^2 \hat{\mathbf{z}} I_7 - y \hat{\mathbf{y}} I_8 \right) \Bigg\}, \tag{2.37}
$$

where the integrals I_4 to I_8 are derived in the appendix.

After substituting the solutions of integrals I_4 to I_8 in Eq. (2.37) and using Eq. (1.57), the final expression for the electric field is

$$\mathbf{E} = \mathbf{E}_o + \mathbf{E}_e \,, \tag{2.38}$$

where

$$\mathbf{E}_o(\mathbf{r}) = \frac{k_o\mu_b p_o}{2\pi\varepsilon_o n_o r}\left(-\hat{\mathbf{y}} + \tan\theta\sin\phi\hat{\mathbf{z}}\right)\frac{\exp(ik_o n_o r)\sin\theta\sin\phi}{(\sin^2\theta\sin^2\phi + \cos^2\theta)}\sin(k_o n_o L\cos\theta) \tag{2.39}$$

represents the ordinary wave and

$$
\begin{aligned}
\mathbf{E}_e(\mathbf{r}) &= \frac{k_o\mu_b p_o}{2\pi\varepsilon_o n_o r}\Big[-(\sin^2\theta\sin^2\phi + \cos^2\theta)\hat{\mathbf{x}} + \sin^2\theta\cos\phi\sin\phi\hat{\mathbf{y}} \\
&\quad + \sin\theta\cos\theta\cos\phi\hat{\mathbf{z}}\Big]\frac{\exp(ik_o n_o r\Phi)\sin\theta\cos\phi}{\Phi^2(\sin^2\theta\sin^2\phi + \cos^2\theta)}\sin\left(\frac{\varepsilon_d k_o n_o L\cos\theta}{\Phi}\right)
\end{aligned}
\tag{2.40}
$$

represents the extraordinary wave.

Now the expression for the magnetic field in the far field with $\hat{\mathbf{c}} = \hat{\mathbf{x}}$ can be found by substituting Eqs. (1.46) and (2.26) into Eq. (1.28) as

$$
\begin{aligned}
\mathbf{H}(\mathbf{r}) &= k_o n_o\omega p_o\int_{-L}^{L}\Bigg\{g_o(\mathbf{R}_z)\frac{[\mathbf{R}_z\times(\mathbf{R}_z\times\hat{\mathbf{x}})](\mathbf{R}_z\times\hat{\mathbf{x}})\cdot\hat{\mathbf{z}}}{R_z(\mathbf{R}_z\times\hat{\mathbf{x}})\cdot(\mathbf{R}_z\times\hat{\mathbf{x}})} \\
&\quad -\varepsilon_d g_e(\mathbf{R}_z)\frac{(\mathbf{R}_z\times\hat{\mathbf{x}})[\mathbf{R}_z\times(\mathbf{R}_z\times\hat{\mathbf{x}})]\cdot\hat{\mathbf{z}}}{R_{ez}(\mathbf{R}_z\times\hat{\mathbf{x}})\cdot(\mathbf{R}_z\times\hat{\mathbf{x}})}\Bigg\}dz' \,.
\end{aligned}
\tag{2.41}
$$

Using Eq. (1.35) in Eq. (2.41), we get

$$
\begin{aligned}
\mathbf{H}(\mathbf{r}) &= \frac{k_o n_o\omega p_o}{4\pi}\Bigg\{\int_{-L}^{L}\frac{\exp(ik_o n_o R_z)}{R_z^2}\frac{[-xy^2\hat{\mathbf{y}} + y^3\hat{\mathbf{x}} - xy(z-z')\hat{\mathbf{z}} + y(z-z')^2\hat{\mathbf{x}}]}{y^2 + (z-z')^2}dz' \\
&\quad -\varepsilon_d\int_{-L}^{L}\frac{\exp(ik_o n_o R_{ez})}{R_{ez}^2}\frac{[-xy(z-z')\hat{\mathbf{z}} + x(z-z')^2\hat{\mathbf{y}}]}{y^2 + (z-z')^2}dz'\Bigg\} \,.
\end{aligned}
\tag{2.42}
$$

Just like the electric field, the magnetic field in the far field can be approximated as

$$
\begin{aligned}
\mathbf{H}(\mathbf{r}) &\simeq \frac{k_o n_o\omega p_o}{4\pi}\Bigg\{\frac{\exp(ik_o n_o r)}{r^2(y^2 + z^2)}\Big[(y^3\hat{\mathbf{x}} - xy^2\hat{\mathbf{y}})I_7 - xy\hat{\mathbf{z}}I_8 + y\hat{\mathbf{x}}I_9\Big] \\
&\quad -\frac{\varepsilon_d\exp(ik_o n_o r_e)}{r_e^2(y^2 + z^2)}\left(-xy\hat{\mathbf{z}}I_4 + x\hat{\mathbf{y}}I_5\right)\Bigg\} \,,
\end{aligned}
\tag{2.43}
$$

where the integral I_9 in the far zone is derived in the appendix.

Substituting the values of I_4, I_7, I_8, and I_9 in Eq. (2.43) along with the use of Eqs. (1.57) and (2.15), the final expression for the magnetic field is given by

$$\mathbf{H} = \mathbf{H}_o + \mathbf{H}_e , \qquad (2.44)$$

where $\mathbf{H}_o$ represents the ordinary wave given by

$$\begin{aligned}
\mathbf{H}_o(\mathbf{r}) \quad = \quad & \frac{k_o p_o c}{2\pi r} \Big[(\sin^2\theta \sin^2\phi + \cos^2\theta)\hat{\mathbf{x}} - \sin^2\theta\cos\phi\sin\phi\hat{\mathbf{y}} \\
& - \sin\theta\cos\theta\cos\phi\hat{\mathbf{z}} \Big] \frac{\exp(ik_o n_o r)\sin\theta\sin\phi}{\cos\theta(\sin^2\theta\sin^2\phi + \cos^2\theta)} \sin(k_o n_o L\cos\theta) ,
\end{aligned} \qquad (2.45)$$

and $\mathbf{H}_e$ represents the extraordinary wave given by

$$\mathbf{H}_e(\mathbf{r}) \quad = \quad \frac{k_o p_o c}{2\pi r} \Big(-\cos\theta\hat{\mathbf{y}} + \sin\theta\sin\phi\hat{\mathbf{z}} \Big) \frac{\exp(ik_o n_o r\Phi)\sin\theta\cos\phi}{\Phi(\sin^2\theta\sin^2\phi + \cos^2\theta)} \sin\left(\frac{\varepsilon_d k_o n_o L\cos\theta}{\Phi}\right) . \qquad (2.46)$$

Substituting the expression for $\mathbf{E}_o$ and $\mathbf{H}_o$ from Eqs. (2.39) and (2.45) into Eq. (1.60) and converting into spherical coordinates, we get

$$\frac{dP_o}{d\Omega} = \frac{k_o^2 \mu_b p_o^2 c}{8\pi^2 \varepsilon_o n_o} \frac{\sin^2\theta\sin^2\phi}{\cos^2\theta(\sin^2\theta\sin^2\phi + \cos^2\theta)} \sin^2(k_o n_o L\cos\theta) . \qquad (2.47)$$

Similarly, by substituting the expression for $\mathbf{E}_e$ and $\mathbf{H}_e$ from Eqs. (2.40) and (2.46) into Eq. (1.61) and converting into spherical coordinates, we get

$$\frac{dP_e}{d\Omega} = \frac{k_o^2 \mu_b p_o^2 c}{8\pi^2 \varepsilon_o n_o} \frac{\sin^2\theta\cos^2\phi}{\Phi^3(\sin^2\theta\sin^2\phi + \cos^2\theta)} \sin^2\left(\frac{\varepsilon_d k_o L n_o\cos\theta}{\Phi}\right) . \qquad (2.48)$$

The total time-averaged power radiated per unit solid angle by the dipole is given by substituting Eqs. (2.47) and (2.48) into Eq. (1.59) as

$$\begin{aligned}
\frac{dP}{d\Omega} \quad = \quad & \frac{k_o^2 \mu_b p_o^2 c}{8\pi^2 \varepsilon_o n_o} \frac{\sin^2\theta}{(\sin^2\theta\sin^2\phi + \cos^2\theta)} \left[\frac{\cos^2\phi}{\Phi^3} \sin^2\left(\frac{\varepsilon_d k_o L n_o\cos\theta}{\Phi}\right) \right. \\
& \left. + \frac{\sin^2\phi}{\cos^2\theta} \sin^2(k_o n_o L\cos\theta) \right] .
\end{aligned} \qquad (2.49)$$

When we substitute $\varepsilon_d = 1$ (giving $\Phi = 1$), Eqs. (2.25) and (2.49) reduce to the exactly same results.

2.4.3 Far field at optic axis

At the optic axis (x axis), $\mathbf{R} = R\hat{\mathbf{x}} = R\hat{\mathbf{c}}$ ($\theta = \pi/2$, $\phi = 0, \pi$) and the fields and the power has to be computed carefully using the limiting procedure [25]. The dyadic Green functions at the optic axis in the far zone are given by [25]

$$\underline{\underline{G}}^{ee}(\mathbf{R}) = i\omega\mu_o\mu_b \left[\left(\varepsilon_a\underline{\underline{\varepsilon}}_r^{-1} - \hat{\mathbf{R}}\hat{\mathbf{R}} \right) + \frac{\varepsilon_b - \varepsilon_a}{2\varepsilon_b} \left(\underline{\underline{I}} - \hat{\mathbf{c}}\hat{\mathbf{c}} \right) \right] g_o(\mathbf{R}) \tag{2.50}$$

and

$$\underline{\underline{G}}^{me}(\mathbf{R}) = \frac{ik_o n_o(\varepsilon_d + 1)}{2} g_o(\mathbf{R})\hat{\mathbf{c}} \times \underline{\underline{I}} \,. \tag{2.51}$$

The expression for electric field can be found by substituting Eqs. (2.26) and (2.50) with $\hat{\mathbf{R}} = \hat{\mathbf{x}}$ in Eq. (1.27), and is given by

$$\mathbf{E}(\mathbf{r}) = \frac{k_o^2 \mu_b p_o L}{4\pi\varepsilon_o}(\varepsilon_d + 1)\frac{\exp(ik_o n_o r)}{r}\hat{\mathbf{z}} \,. \tag{2.52}$$

Similarly, the expression for the magnetic field can be found by substituting Eqs. (2.26) and (2.51) in Eq. (1.28), and is given by

$$\mathbf{H}(\mathbf{r}) = -\frac{k_o^2 n_o p_o cL}{4\pi}(\varepsilon_d + 1)\frac{\exp(ik_o n_o r)}{r}\hat{\mathbf{y}} \,. \tag{2.53}$$

Now by substituting Eqs. (2.52) and (2.53) into Eq. (1.54), the expression of the time-averaged power radiated per unit solid angle by the dipole is given by

$$\frac{dP}{d\Omega} = \frac{k_o^4 \mu_b n_o p_o^2 cL^2}{32\pi^2 \varepsilon_o}(\varepsilon_d + 1)^2 \,. \tag{2.54}$$

When we substitute $\varepsilon_d = 1$, Eqs. (2.25) with $\phi = 0$ and $\theta = \pi/2$ give the same result as of Eq. (2.54) for the isotropic material.

2.5 Numerical results and discussion

The analytical results obtained for the far-field radiation patterns given by Eqs. (2.22), (2.25), (2.47)-(2.49), and (2.54) constitute the main results and their elegant closed forms make them usable as it is. To illustrate their use, we present representative numerical results for radiations in rutile with $\varepsilon_a = 8.427$, $\varepsilon_b = 6.843$, $\mu_b = 1$ at $\lambda_o = 0.584\,\mu$m [29] for a dipole with $p_0 = 1/\omega$ and length $L = 0.1\lambda_o$ and $0.2\lambda_o$.

The far-field radiation patterns of extraordinary waves emitted by a Hertzian dipole aligned with the optic axis (z axis) are shown in Fig. 2.4. The dipole is placed in uniaxial material (rutile) when
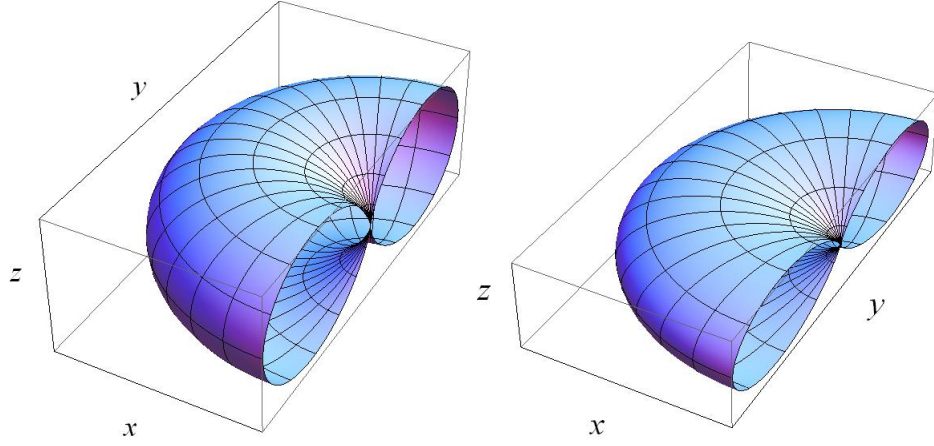
FIGURE 2.4: Far-field radiation pattern of a Hertzian dipole given by Eq. (2.25), which is oriented parallel to the optic axis (z axis) and lying in a uniaxial material (rutile) with $p_0 = 1/\omega$, $\varepsilon_a = 8.427$, $\varepsilon_b = 6.843$, $\mu_b = 1$, $\lambda_o = 0.584\,\mu$m [29], and (left) $L = 0.1\lambda_o$, (right) $L = 0.2\lambda_o$. The plot is given for $0 \leq \theta \leq \pi$ and $\pi/2 \leq \phi \leq 3\pi/2$.
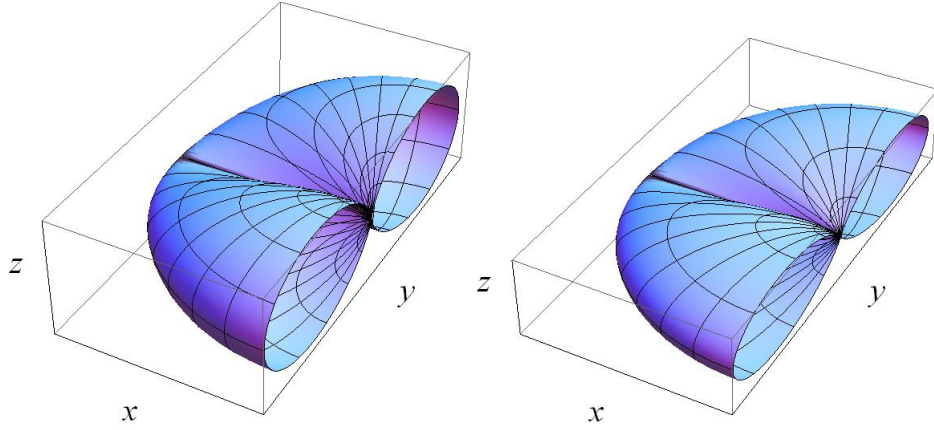
FIGURE 2.5: Far-field radiation pattern of ordinary waves given by Eq. (2.47) when the dipole is oriented along z axis and the optic axis along x axis for a uniaxial material (rutile) with $\varepsilon_a = 8.427$, $\varepsilon_b = 6.843$, $\mu_b = 1$, $\lambda_o = 0.584\,\mu$m [29], and (left) $L = 0.1\lambda_o$, (right) $L = 0.2\lambda_o$. The plot is given for $0 \leq \theta \leq \pi$ and $\pi/2 \leq \phi \leq 3\pi/2$. The pattern is symmetric about xz plane.

$L = 0.1\lambda_o$ and $L = 0.2\lambda_o$. The plot is given only for $0 \leq \theta \leq \pi$ and $\pi/2 \leq \phi \leq 3\pi/2$ for easier visulaization since the pattern is independent of ϕ, as can be seen from Eq. (2.25). The figure shows that the pattern is like that of a dipole in an isotropic material and its directivity increases as the length of the dipole increases.

When the dipole is perpendicular to the optic axis, the radiation pattern of ordinary waves are shown in Fig. 2.5 for the same material with $L = 0.1\lambda_o$ and $L = 0.2\lambda_o$. Again the plot is provided only for $0 \leq \theta \leq \pi$ and $\pi/2 \leq \phi \leq 3\pi/2$ since the pattern as given by Eq. (2.47) is symmetric around xz plane as it should be since the dipole and the optic axis define this plane. Its clear from the figure that the
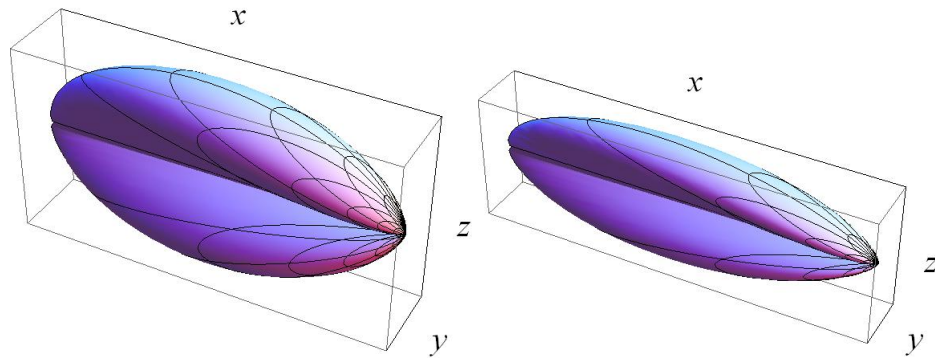
FIGURE 2.6: Same as Fig. 2.5 except that the pattern is that of extraordinary waves given by Eq. (2.48).

radiations in the direction of optic axis are suppressed, though not zero. When we increase the length of dipole, the radiation profile becomes more directive in a direction perpendicular to the dipole.

The radiation pattern of the extraordinary wave from the dipole perpendicular to the optic axis are shown in Fig. 2.6. The figure shows that the emission is highly directive along the optic axis, though the radiations are suppressed along the optic axis in a plane perpendicular to the dipole. Furthermore, there are no radiations emitted along the y axis, a direction perpendicular to both the dipole and the optic axis. When the length of the dipole is increased, the directivity of the radiations increases much more than the previous two cases. The figure shows strong dependence of radiation pattern on length of the dipole even when it is a fraction of the wavelength.

2.6 Comparison with the point dipole

To compare the results of the Hertzian dipole with those of a point dipole, let us consider a point-electric dipole with the electric current density as given in Eq. (1.47) and the plots are given in Fig. 1.6 and 1.7. The following results are very helpful in comparing the finite-sized and the point dipole:

- Let us note that $L \to 0$ in Eq. (2.25) results in the same form as that of Eq. (1.55). Similarly, the Hertzian-dipole results of Eq. (2.49) reduce to the same form as the point dipole of Eq. (1.65) when $L \to 0$ in Eq. (2.49).

- For comparison of the radiation patterns of the point dipole and the Hertzian dipole, the far-field radiation pattern of the point dipole are presented in Fig. 1.6 and 1.7 when the dipole is, respectively, parallel and perpendicular to the optics axis, for the same parameters as those for the Hertzian dipole. A comparison of Fig. 1.6 with Fig. 2.4 shows that the both pattern looks similar, but the

directivity is enhanced by the increase in length $2L$ of the Hertzian dipole. The comparison of Fig. 1.7 with Figs. 2.5 and 2.6 draws the same conclusion that the Hertzian dipole allows the control of directivity of the radiation by choosing the length of the dipole.

2.7 Concluding remarks

The near-field electric field and the far-field radiation pattern of a Hertzian dipole in uniaxial dielectric material were analytically derived and the far-field numerical results were presented for a chosen uniaxial material. The dipole was taken to be along and perpendicular to the optic axis. When the dipole was parallel to the optic axis, only extraordinary waves were emitted in the far field. When the dipole was perpendicular to the optic axis, both ordinary and extraordinary waves were emitted but the radiations along the optic axis were suppressed for both the ordinary and extraordinary waves. For the latter case, there was no emission of extraordinary waves perpendicular to the dipole and the optic axis in the far field. For all the cases, the directivity of the radiation pattern increased significantly with the increase in the length of the dipole. A comparison with the results of the point dipole showed that the the length of the Hertzian dipole plays a significant role in the directivity of the radiation pattern.

2.8 Appendix

In this appendix, we present the derivations of the integrals used in the formulation of the far-field radiations. In general, we solved the integrals in the Cartesian coordinates, converted them into the spherical coordinates, and then retained only the leading term.

Let us begin with

$$I_1 = \int_{-L}^{L} \exp\left(-isxx'\right)dx' = \frac{2\sin(sLx)}{sx}, \tag{2.55}$$

where

$$s = \frac{k_o n_o}{r_e}. \tag{2.56}$$

By substituting the expressions for x and r_e from Eqs. (1.57) and (2.15) into Eq. (2.55), we get

$$I_1 = \frac{2\Phi}{k_o n_o \sin\theta\cos\phi} \sin\left(\frac{k_o n_o L \sin\theta\cos\phi}{\Phi}\right). \tag{2.57}$$

The second integral is

$$
\begin{aligned}
I_2 &= \int_{-L}^{L} (x - x') \exp\left(-isxx'\right) dx' \\
&= \frac{-2isLx\cos(Lsx) + 2(i + sx^2)\sin(Lsx)}{s^2 x^2}.
\end{aligned}
\tag{2.58}
$$

By substituting the expressions for x and r_e from Eqs. (1.57) and (2.15) into Eq. (2.58) and keeping only the dominant term as $r \to \infty$, we get

$$
I_2 = \frac{2r\Phi}{k_o n_o} \sin\left(\frac{k_o n_o L \sin\theta \cos\phi}{\Phi}\right).
\tag{2.59}
$$

The third integral is

$$
\begin{aligned}
I_3 &= \int_{-L}^{L} (x - x')^2 \exp\left(-isxx'\right) dx' \\
&= \frac{i}{s^3 x^3} \Big\{ \exp(-isLx)[-2 - 2is(L - x)x + s^2(L - x)^2 x^2)] \\
&\quad - \exp(isLx)[-2 + 2is(L + x)x + s^2(L + x)^2 x^2] \Big\}.
\end{aligned}
\tag{2.60}
$$

By converting to spherical coordinates and retaining only the dominant term as $r \to \infty$, we get

$$
I_3 = \frac{2r^2 \Phi \sin\theta \cos\phi}{k_o n_o} \sin\left(\frac{k_o n_o L \sin\theta \cos\phi}{\Phi}\right).
\tag{2.61}
$$

The fourth integral is

$$
\begin{aligned}
I_4 &= \int_{-L}^{L} (z - z') \exp\left(-is\varepsilon_d zz'\right) dz' \\
&= \frac{-2i\varepsilon_d sLz \cos(\varepsilon_d Lsz) + 2(i + \varepsilon_d sz^2)\sin(\varepsilon_d Lsz)}{\varepsilon_d^2 s^2 z^2}.
\end{aligned}
\tag{2.62}
$$

By substituting the expressions for z and r_e from Eqs. (1.57) and (2.15) into Eq. (2.62) and keeping only the dominant term as $r \to \infty$, we get

$$
I_4 = \frac{2r\Phi}{\varepsilon_d k_o n_o} \sin\left(\frac{\varepsilon_d k_o n_o L \cos\theta}{\Phi}\right).
\tag{2.63}
$$

The fifth integral is

$$
\begin{aligned}
I_5 &= \int_{-L}^{L} (z - z')^2 \exp\left(-is\varepsilon_d zz'\right) dz' \\
&= \frac{i}{s^3 z^3 \varepsilon_d^3} \Big\{ \exp(-isLz\varepsilon_d)[-2 - 2is(L - z)z\varepsilon_d + s^2(L - z)^2 z^2 \varepsilon_d^2] \\
&\quad - \exp(isLz\varepsilon_d)[-2 + 2is(L + z)z\varepsilon_d + s^2(L + z)^2 z^2 \varepsilon_d^2] \Big\}.
\end{aligned}
\tag{2.64}
$$

By converting to spherical coordinates and retaining only the dominant term as $r \to \infty$, we get

$$
I_5 = \frac{2r^2 \Phi \cos\theta}{\varepsilon_d k_o n_o} \sin\left(\frac{\varepsilon_d k_o n_o L \cos\theta}{\Phi}\right).
\tag{2.65}
$$

The sixth integral is

$$
\begin{aligned}
I_6 &= \int_{-L}^{L} (z - z')^3 \exp\left(-is\varepsilon_d zz'\right) dz' \\
&= \frac{1}{s^4 z^4 \varepsilon_d^4} \Big\{ \exp(-isLz\varepsilon_d)\Big[6 + i6s(L - z)z\varepsilon_d - 3s^2(L - z)^2 z^2 \varepsilon_d^2 - is^3(L - z)^3 z^3 \varepsilon_d^3\Big] \\
&\quad - \exp(isLz\varepsilon_d)\Big[6 - i6s(L + z)z\varepsilon_d - 3s^2(L + z)^2 z^2 \varepsilon_d^2 + is^3(L + z)^3 z^3 \varepsilon_d^3\Big] \Big\}.
\end{aligned}
\tag{2.66}
$$

By converting to spherical coordinates and retaining only the dominant term as $r \to \infty$, we get

$$
I_6 = \frac{2r^3 \Phi \cos^2\theta}{\varepsilon_d k_o n_o} \sin\left(\frac{\varepsilon_d k_o n_o L \cos\theta}{\Phi}\right).
\tag{2.67}
$$

The seventh integral

$$
I_7 = \int_{-L}^{L} \exp\left(-i\tau zz'\right) dz'
\tag{2.68}
$$

is similar to I_1 with

$$
\tau = \frac{k_o n_o}{r}.
\tag{2.69}
$$

Performing integration and keeping only the dominant term as $r \to \infty$, the final expression for I_7 in spherical coordinates is

$$
I_7 = \frac{2 \sin(k_o n_o L \cos\theta)}{k_o n_o \cos\theta}.
\tag{2.70}
$$

The eighth integral is similar to I_4, so

$$I_8 = \int_{-L}^{L} (z - z') \exp(-i\tau z z') dz' = \frac{2r \sin(k_o n_o L \cos \theta)}{k_o n_o} \ . \tag{2.71}$$

The integral I_9 is similar to I_5 so

$$I_9 = \int_{-L}^{L} (z - z')^2 \exp(-i\tau z z') dz' = \frac{2r^2 \cos \theta \sin(k_o n_o L \cos \theta)}{k_o n_o} \ . \tag{2.72}$$

Chapter 3

Current loop in uniaxial dielectric material

In this chapter, the radiations by a current loop in an unbounded uniaxial dielectric material with uniform current distribution are studied. The closed-form expressions for the radiation in the far zone are found using the dyadic Green functions in the frequency domain. Analytical results are obtained when the axis of the loop was parallel to the optic axis and when it was perpendicular to the optic axis. Only ordinary waves are emitted when the axis of the loop is parallel to the optic axis. When the axis of the loop is perpendicular to the optic axis, both the ordinary and the extraordinary waves are emitted. The results for different radii of the loop show that the radiation pattern strongly depends upon the size of the loop.

The plan of the chapter is as follow: The introduction and relevant literature review is presented in Sec. 3.1. The closed-form results are presented in Sec. 3.2 when the axis of the loop is parallel with the optic axis of the uniaxial material. In Sec. 3.3, the axis of the loop is perpendicular to the optic axis. A comparison with a point-magnetic dipole is presented in Sec. 3.4. The results and concluding remarks are presented in Sec. 3.5 and Sec. 3.7, respectively.

This chapter is based on "A. Hayat and M. Faryad, Closed-form expressions for electromagnetic waves generated by a current loop in a uniaxial dielectric material in the far zone, *J. Opt. Soc. Am. B* **36**, F9-F17 (2019)"

3.1 Introduction

The radiation by point-magnetic dipoles in the uniaxial materials have been studied by several authors [17, 25]. Radiation due to a point-magnetic dipole in a hyperbolic uniaxial media is studied by Alkina and Sautbekov [93]. These studies have been carried out for electrically small current loop or a point-magnetic dipole. However, the point-magnetic dipole cannot exist because magnetic monopoles do not exist. Since the magnetic dipoles might be needed to model real radiation sources in uniaxial materials like quantum dots, wires, and sheets, the radiation characteristics of a current loop with arbitrary radius is needed. Therefore, we set out to find the radiation characteristics of an electric current loop which effectively models the magnetic dipole. Because the radius of loop is taken to be arbitrary in this chapter, the problem taken up can be used to model real extended radiation sources. Furthermore, the modeling of the magnetic dipole with a current loop enable direct realization of the magnetic dipole in addition to providing a generalization of the fields in an isotropic material to the simplest anisotropic material, i.e., uniaxial dielectric material. In this chapter, we develop closed-form results of electromagnetic fields for the finite-sized loop when the loop's symmetry axis is either parallel or perpendicular to the optic axis of the material.

Let us note that electromagnetic waves generated by extended sources in the uniaxial material has been tackled numerically [18] and integral equations for generalized electric and magnetic currents have also been obtained [90]. However, our aim in this chapter is to obtain closed-form results. Also, the current distribution of a thin conducting loop inside a uniaxial material when the optic axis of the material and symmetry axis of the loop are the same have also been studied [94]. Electrodynamics characteristics of loop antennas which are placed over the surface of uniaxial anisotropic cylinder is studied by Kudrin *et al*. [95]. Radiation as well as scattering from a microstrip patch antenna on a uniaxial material is studied by Pozar [96]. Furthermore, the problem of determining the current distribution on a loop of a thin strip coiled into a ring was studied by Zaboronkova [97].

3.2 Loop axis and optic axis parallel to z-axis

Consider a constant current-loop of radius a as shown in Fig. 3.1. The loop lies wholly in the xy plane and carries constant current I_0. Since the optic axis is along the z axis, $\hat{\mathbf{c}} = \hat{\mathbf{z}}$. The electric current density phasor in spherical coordinates is given by

$$\mathbf{J}_e(\mathbf{r}) = \frac{I_0}{a}\delta(r-a)\delta(\theta - \frac{\pi}{2})\hat{\phi}, \tag{3.1}$$

$$\mathbf{J}_m(\mathbf{r}) = 0. \tag{3.2}$$

The electric field in the far zone can be computed by substituting Eqs. (1.45) and (3.1) into Eq. (1.27) to
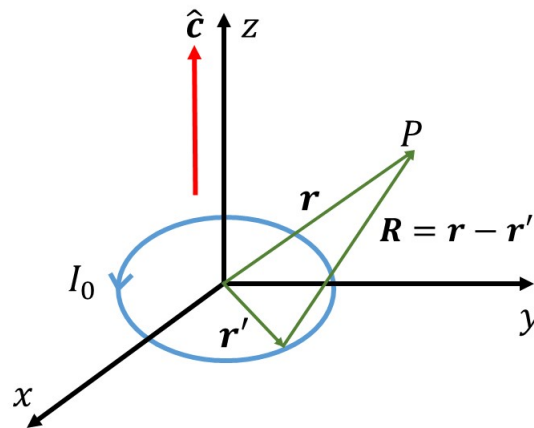
FIGURE 3.1: Schematic showing a current loop with radius a and lies parallel to optic axis with $\hat{\mathbf{c}} = \hat{\mathbf{z}}$
.

get

$$\mathbf{E}(\mathbf{r}) = i\omega\mu_o\mu_b I_0 a \int_0^{2\pi} \left\{ g_o(\tilde{\mathbf{R}})\frac{(\tilde{\mathbf{R}}\times\hat{\mathbf{z}})(\tilde{\mathbf{R}}\times\hat{\mathbf{z}})\cdot\hat{\phi}'}{(\tilde{\mathbf{R}}\times\hat{\mathbf{z}})\cdot(\tilde{\mathbf{R}}\times\hat{\mathbf{z}})} + g_e(\tilde{\mathbf{R}})\frac{\varepsilon_d\left[\tilde{\mathbf{R}}\times\left(\tilde{\mathbf{R}}\times\hat{\mathbf{z}}\right)\right]\left[\tilde{\mathbf{R}}\times\left(\tilde{\mathbf{R}}\times\hat{\mathbf{z}}\right)\right]\cdot\hat{\phi}'}{R_{ez}^2\left(\tilde{\mathbf{R}}\times\hat{\mathbf{z}}\right)\cdot\left(\tilde{\mathbf{R}}\times\hat{\mathbf{z}}\right)} \right\}d\phi', \tag{3.3}$$

where

$$\tilde{\mathbf{R}} = (x - x')\hat{\mathbf{x}} + (y - y')\hat{\mathbf{y}} + z\hat{\mathbf{z}}, \tag{3.4}$$

and

$$\varepsilon_d = \varepsilon_a/\varepsilon_b, \tag{3.5}$$

$$\hat{\phi}' = -\sin\phi'\hat{\mathbf{x}} + \cos\phi'\hat{\mathbf{y}}. \tag{3.6}$$

Using the transformation given in Eq. (1.57), we can write Eq. (3.4) as

$$\tilde{\mathbf{R}} = (x - a\cos\phi')\hat{\mathbf{x}} + (y - a\sin\phi')\hat{\mathbf{y}} + z\hat{\mathbf{z}}, \tag{3.7}$$

here we replaced only the prime coordinates with their spherical expression and leave the un-prime coordinates unchanged.

Since the fields in Eq. (3.3) are a superposition of the ordinary and the extraordinary waves. We evaluate the fields for both of them separately. The expression for extraordinary field from Eq. (3.3) can be written as

$$
\begin{aligned}
\mathbf{E}_e(\mathbf{r}) &= \frac{iaI_0\omega\mu_o\mu_b\varepsilon_d}{4\pi} \int\limits_0^{2\pi} \frac{\exp(ik_o n_o R_{ez})}{r_{ez}^3} \Bigg[z(x\sin\phi' - y\cos\phi')\hat{\mathbf{z}} \\
&+ \frac{z^2(xy\cos\phi' - x^2\sin\phi' - ay\cos^2\phi' + ax\cos\phi'\sin\phi')\hat{\mathbf{x}}}{(\mathbf{r}\times\hat{\mathbf{z}})^2} \\
&+ \frac{z^2(y^2\cos\phi' - xy\sin\phi' - ay\cos\phi'\sin\phi' + ax\sin^2\phi')\hat{\mathbf{y}}}{(\mathbf{r}\times\hat{\mathbf{z}})^2} \Bigg] d\phi',
\end{aligned} \tag{3.8}
$$

where in the denominator we replaced $\tilde{\mathbf{R}}$ with $\mathbf{r}$, and R_{ez} with r_{ez}. However, in the exponential term, we must approximate

$$R_{ez} \approx r_{ez} - \frac{\varepsilon_d r a \sin\theta \cos(\phi - \phi')}{r_{ez}}, \tag{3.9}$$

where

$$r_{ez} = r\Theta \qquad (3.10)$$

and

$$\Theta = \sqrt{\cos^2\theta + \varepsilon_d \sin^2\theta}\,. \qquad (3.11)$$

Since the electric field phasor must be independent of ϕ due to the symmetry of current distribution about the z axis, let us determine it by setting $\phi = 0$. By substituting Eq. (3.9) and $\phi = 0$ in Eq. (3.8), we get

$$
\begin{aligned}
\mathbf{E}_e(\mathbf{r}) &= \frac{i\omega a I_0 \mu_o \mu_b \varepsilon_d}{4\pi r_{ez}^3} \exp(ik_o n_o r_{ez}) \Bigg\{ xz \int_0^{2\pi} \sin\phi' \exp\big(-is\cos\phi'\big) d\phi' \hat{\mathbf{z}} \\
&\quad + \frac{z^2}{x^2}\left[ax \int_0^{2\pi} \sin\phi' \cos\phi' \exp\big(-is\cos\phi'\big) d\phi' - x^2 \int_0^{2\pi} \sin\phi' \exp\big(-is\cos\phi'\big) d\phi' \right]\hat{\mathbf{x}} \\
&\quad + \frac{az^2}{x} \int_0^{2\pi} \sin^2\phi' \exp\big(-is\cos\phi'\big) d\phi' \hat{\mathbf{y}} \Bigg\},
\end{aligned}
\qquad (3.12)
$$

where

$$s = \frac{k_o n_o a \varepsilon_d \sin\theta}{\Theta}\,. \qquad (3.13)$$

After solving the integrals, the final expression of $\mathbf{E}_e$ in spherical coordinates is given by

$$\mathbf{E}_e(\mathbf{r}) = \frac{iI_0 a\mu_o\mu_b c}{2n_0 \Theta^2 r^2} \exp(ik_o n_o r_{ez}) \frac{\cos^2\theta}{\sin^2\theta} J_1\left(\left|\frac{k_o n_o a\varepsilon_d \sin\theta}{\Theta}\right|\right)\hat{\mathbf{y}}\,. \qquad (3.14)$$

Since the final expression contain $1/r^2$ terms only,

$$\mathbf{E}_e(\mathbf{r}) \approx 0 \qquad (3.15)$$

in the far zone.

The part of Eq. (3.3) representing the ordinary wave is given by

$$\mathbf{E}_o(\mathbf{r}) = \frac{i\omega\mu_o\mu_b I_0 a}{4\pi} \int_0^{2\pi} \frac{\exp\left(ik_o n_o \tilde{R}\right)}{r} \frac{(\tilde{\mathbf{R}} \times \hat{\mathbf{z}})(\tilde{\mathbf{R}} \times \hat{\mathbf{z}}) \cdot \hat{\phi}'}{(\mathbf{r} \times \hat{\mathbf{z}})^2} d\phi', \qquad (3.16)$$

for $r \gg a$ by approximating $\tilde{R}$ as r in the denominator. But, Eq. (3.7) is approximated as

$$\tilde{R} = r - a\sin\theta\cos\phi', \qquad (3.17)$$

to be used in the exponential term in the far zone. With the substitutions of Eqs. (3.6), (3.7) and (3.17), Eq. (3.16) can be written as

$$
\begin{aligned}
\mathbf{E}_o(\mathbf{r}) &= \frac{i\omega\mu_o\mu_b I_0 a}{4\pi r} \frac{\exp(ik_o n_o r)}{x^2} \Bigg\{ \bigg[x^2 \int_0^{2\pi} \cos\phi' \exp(-i\tau\cos\phi')d\phi' \\
&\quad + a^2 \int_0^{2\pi} \cos^3\phi' \exp(-i\tau\cos\phi')d\phi' - 2xa \int_0^{2\pi} \cos^2\phi' \exp(-i\tau\cos\phi')d\phi' \bigg] \hat{\mathbf{y}} \\
&\quad + \bigg[ax \int_0^{2\pi} \sin\phi'\cos\phi' \exp(-i\tau\cos\phi')d\phi' - a^2 \int_0^{2\pi} \sin\phi'\cos^2\phi' \exp(-i\tau\cos\phi')d\phi' \bigg] \hat{\mathbf{x}} \\
&\quad - \bigg[ax \int_0^{2\pi} \sin^2\phi' \exp(-i\tau\cos\phi')d\phi' - a^2 \int_0^{2\pi} \sin^2\phi'\cos\phi' \exp(-i\tau\cos\phi')d\phi' \bigg] \hat{\mathbf{y}} \\
&\quad - a^2 \int_0^{2\pi} \sin^3\phi' \exp(-i\tau\cos\phi')d\phi'\hat{\mathbf{x}} \Bigg\},
\end{aligned}
\qquad (3.18)
$$

where τ is given by

$$\tau = k_o n_o a\sin\theta. \qquad (3.19)$$

After solving integrals and retaining the terms proportional to $1/r$, the final expression for ordinary wave is given by

$$\mathbf{E}_o(\mathbf{r}) = \frac{\omega\mu_o\mu_b I_0 a}{2} \frac{\exp(ik_o n_o r)}{r} J_1\left(k_o n_o a\sin\theta\right)\hat{\mathbf{y}}. \qquad (3.20)$$

The expression for the magnetic field can be computed by substituting Eqs. (1.46) and (3.1) in Eq. (1.28) as

$$
\mathbf{H}(\mathbf{r}) = \frac{ik_o n_o I_o a}{4\pi} \int\limits_0^{2\pi} \left\{ \frac{\exp\left(ik_o n_o \tilde{R}\right)}{\tilde{R}} \frac{[\tilde{\mathbf{R}} \times (\tilde{\mathbf{R}} \times \hat{\mathbf{z}})](\tilde{\mathbf{R}} \times \hat{\mathbf{z}}) \cdot \hat{\phi}'}{\tilde{R}(\tilde{\mathbf{R}} \times \hat{\mathbf{z}}) \cdot (\tilde{\mathbf{R}} \times \hat{\mathbf{z}})} \right.
$$
$$
\left. - \frac{\varepsilon_d \exp(ik_o n_o R_{ez})}{R_{ez}} \frac{(\tilde{\mathbf{R}} \times \hat{\mathbf{z}})[\tilde{\mathbf{R}} \times (\tilde{\mathbf{R}} \times \hat{\mathbf{z}})] \cdot \hat{\phi}'}{R_{ez}[(\tilde{\mathbf{R}} \times \hat{\mathbf{z}}) \cdot (\tilde{\mathbf{R}} \times \hat{\mathbf{z}})]} \right\} d\phi' . \tag{3.21}
$$

With the substitutions of Eqs. (3.6), (3.7) and (3.9) in the numerator with $\phi = 0$ and $R_{ez} \approx r_{ez}$ and

$$
(\tilde{\mathbf{R}} \times \hat{\mathbf{z}}) \cdot (\tilde{\mathbf{R}} \times \hat{\mathbf{z}}) = x^2 , \tag{3.22}
$$

in the denominator of Eq. (3.21), the extraordinary part of magnetic field is given by

$$
\mathbf{H}_e(\mathbf{r}) = \frac{ik_o n_o I_o a \varepsilon_d}{4\pi r_{ez}^2} \frac{\exp(ik_o n_o r_{ez})}{x^2} \left[axz \int\limits_0^{2\pi} \sin^2 \phi' \exp\left(-is \cos \phi'\right) d\phi' \right] \hat{\mathbf{x}} . \tag{3.23}
$$

After performing the integration and converting into spherical coordinates, we get

$$
\mathbf{H}_e(\mathbf{r}) = \frac{iI_o a \cos\theta}{2r^2 \Theta^2 \sin^2 \theta} \exp(ik_o n_o r_{ez}) J_1 \left(\left| \frac{k_o n_o a \varepsilon_d \sin\theta}{\Theta} \right| \right) \hat{\mathbf{x}} . \tag{3.24}
$$

Since the final expression contain terms with $1/r^2$, we have

$$
\mathbf{H}_e(\mathbf{r}) \approx 0 \tag{3.25}
$$

in the far zone.

With the use of Eqs. (3.6) and (3.7) in the numerator, Eq. (3.17) in the exponential term, and $\tilde{R} \approx r$ and Eq. (3.22) in the denominator of Eq. (3.21) with $\phi = 0$, we get

$$
\begin{aligned}
\mathbf{H}_o(\mathbf{r}) = {} & \frac{ik_o n_o I_o a}{4\pi r^2} \frac{\exp(ik_o n_o r)}{x^2} \left\{ \left[\left(x^3 + a^2 x + 2a^3 x \right) \times \int_0^{2\pi} \cos\phi' \exp\!\left(-i\tau\cos\phi'\right) d\phi' \right. \right. \\
& \left. - \left(a^4 + a^2 x^2 \right) \int_0^{2\pi} \exp\!\left(-i\tau\cos\phi'\right) d\phi' - 2ax^2 \int_0^{2\pi} \cos^2\phi' \exp\!\left(-i\tau\cos\phi'\right) d\phi' \right] \hat{\mathbf{z}} \\
& - \left[\left(x^2 z + a^3 z \right) \int_0^{2\pi} \cos\phi' \exp\!\left(-i\tau\cos\phi'\right) d\phi' - a^2 xz \int_0^{2\pi} \exp\!\left(-i\tau\cos\phi'\right) d\phi' \right. \\
& \left. \left. - axz \int_0^{2\pi} \cos^2\phi' \exp\!\left(-i\tau\cos\phi'\right) d\phi' \right] \hat{\mathbf{x}} \right\} .
\end{aligned}
\tag{3.26}
$$

By finding the solution of the integrals, transforming the Cartesian coordinates to the spherical coordinates and retaining the terms proportional to $1/r$ only, we get

$$
\mathbf{H}_o(\mathbf{r}) = \frac{k_o n_o I_o a}{2r} \exp(ik_o n_o r) \left(\sin\theta \hat{\mathbf{z}} - \cos\theta \hat{\mathbf{x}} \right) J_1 \left(k_o n_o a \sin\theta \right) .
\tag{3.27}
$$

From Eqs. (3.20) and (3.27), it is clear that only ordinary wave is radiated when the axis of the loop and the optic axis are parallel to each other. Furthermore, both the fields are perpendicular to each other, as is usually the case of radiation in the far zone.

The time-averaged power radiated per unit solid angle by the current loop can be found by substituting Eqs. (3.20) and (3.27) in Eq. (1.60), we get

$$
\frac{dP_o}{d\Omega} = \frac{k_o^2 n_o I_o^2 a^2 \mu_o \mu_b c}{8} J_1^2 \left(k_o n_o a \sin\theta \right) .
\tag{3.28}
$$

The above result is independent of ε_a since the ordinary waves are polarized perpendicular to the optic axis, as is also evident from Eq. (3.20).

3.3 Loop axis parallel to z-axis and optic axis parallel to x-axis

Let us now consider the case when the axis of the current loop and the optic axis are perpendicular to each other, as shown schematically in Fig. 3.2. For this current loop, the current densities are the same as given in Eqs. (3.1) and (3.2) but $\hat{\mathbf{c}} = \hat{\mathbf{x}}$ for the uniaxial dielectric material.
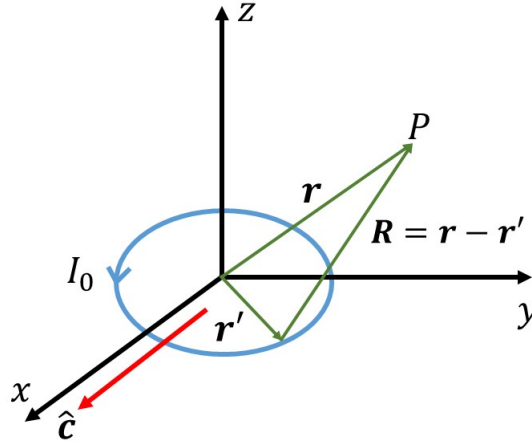
FIGURE 3.2: Schematic showing a current loop with its axis oriented perpendicular to the optic axis with $\hat{\mathbf{c}} = \hat{\mathbf{x}}$

.

We are interested in finding the fields at point P which is far away from the loop. The electric field can be computed by substituting Eqs. (1.35), (1.45), and (3.1) in Eq. (1.27) as

$$\mathbf{E}(\mathbf{r}) = \frac{i\omega\mu_o\mu_b I_0 a}{4\pi} \int\limits_0^{2\pi} \left\{ \frac{\varepsilon_d \exp(ik_o n_o R_{ex})}{R_{ex}} \frac{\left[\tilde{\mathbf{R}} \times \left(\tilde{\mathbf{R}} \times \hat{\mathbf{x}}\right)\right] \left[\tilde{\mathbf{R}} \times \left(\tilde{\mathbf{R}} \times \hat{\mathbf{x}}\right)\right] \cdot \hat{\phi}'}{R_{ex}^2 \left(\tilde{\mathbf{R}} \times \hat{\mathbf{x}}\right) \cdot \left(\tilde{\mathbf{R}} \times \hat{\mathbf{x}}\right)} \right.$$
$$\left. + \frac{\exp\left(ik_o n_o \tilde{R}\right)}{\tilde{R}} \frac{\left(\tilde{\mathbf{R}} \times \hat{\mathbf{x}}\right) \left(\tilde{\mathbf{R}} \times \hat{\mathbf{x}}\right) \cdot \hat{\phi}'}{\left(\tilde{\mathbf{R}} \times \hat{\mathbf{x}}\right) \cdot \left(\tilde{\mathbf{R}} \times \hat{\mathbf{x}}\right)} \right\} d\phi', \tag{3.29}$$

where R_{ex} is given by

$$R_{ex} = \sqrt{\varepsilon_d(\tilde{\mathbf{R}} \times \hat{\mathbf{x}}) \cdot (\tilde{\mathbf{R}} \times \hat{\mathbf{x}}) + (\tilde{\mathbf{R}} \cdot \hat{\mathbf{x}})^2}. \tag{3.30}$$

For $R \gg a$, the expression of R_{ex} in the spherical coordinates can be approximated from Eq. (3.30) and

is given by

$$R_{ex} = r_{ex} - \frac{ax \cos \phi' + a\varepsilon_d y \sin \phi'}{r_{ex}} , \qquad (3.31)$$

where r_{ex} is

$$r_{ex} = r \Phi (\theta, \phi) \qquad (3.32)$$

with

$$\Phi (\theta, \phi) = \sqrt{\sin^2 \theta \cos^2 \phi + \varepsilon_d \left(\sin^2 \theta \sin^2 \phi + \cos^2 \theta \right)} . \qquad (3.33)$$

In order to get Eq. (3.31) in a simplified form, we introduce the following change of variables

$$x = \eta \cos \alpha \sin \beta, \quad y\varepsilon_d = \eta \sin \alpha \sin \beta . \qquad (3.34)$$

Hence, Eq. (3.31) is given by

$$R_{ex} = r_{ex} - s_1 \cos \left(\alpha - \phi' \right) , \qquad (3.35)$$

where

$$s_1 = \frac{k_o n_o a \eta \sin \beta}{r \Phi} . \qquad (3.36)$$

By substituting Eqs. (3.6) and (3.7) in the numerator and Eq. (3.35) in the exponential term with

$R_{ex} \approx r_{ex}$ and

$$(\tilde{\mathbf{R}} \times \hat{\mathbf{x}}) \cdot (\tilde{\mathbf{R}} \times \hat{\mathbf{x}}) = y^2 + z^2 \qquad (3.37)$$

in the denominator of Eq. (3.29) as

$$
\begin{aligned}
\mathbf{E}_e(\mathbf{r}) \;=\; & \frac{-i\omega\mu_o\mu_b I_0 a\varepsilon_d}{4\pi(y^2+z^2)}\frac{\exp(ik_o n_o r_{ex})}{r_{ex}^3}\Bigg\{\Bigg[\left(xy^3+xyz^2\right)\int_0^{2\pi}\cos\phi'\exp\big[-is_1\cos(\alpha-\phi')\big]d\phi'\\
& +(y^4+2y^2z^2+z^4)\int_0^{2\pi}\sin\phi'\exp\big[-is_1\cos(\alpha-\phi')\big]d\phi'\Bigg]\hat{\mathbf{x}}\\
& -\Bigg[x^2y^2\int_0^{2\pi}\cos\phi'\exp\big[-is_1\cos(\alpha-\phi')\big]d\phi'+(xy^3+xyz^2)\\
& \times\int_0^{2\pi}\sin\phi'\exp\big[-is_1\cos(\alpha-\phi')\big]d\phi'\Bigg]\hat{\mathbf{y}}-\Bigg[x^2yz\int_0^{2\pi}\cos\phi'\exp\big[-is_1\cos(\alpha-\phi')\big]d\phi'\\
& +(xy^2z+xz^3)\int_0^{2\pi}\sin\phi'\exp\big[-is_1\cos(\alpha-\phi')\big]d\phi'\Bigg]\hat{\mathbf{z}}\Bigg\},
\end{aligned}
$$

(3.38)

where we have retained only those terms which are proportional to $1/r$ and ignored higher order terms in the far zone limit. After finding the solution of integrals and further simplification gives us

$$
\begin{aligned}
\mathbf{E}_e(\mathbf{r}) \;=\; & \frac{\omega\mu_o\mu_b I_0 a\varepsilon_d}{2(y^2+z^2)}\frac{\exp(ik_o n_o r\Phi)}{r^3\Phi^3}\left\{-(y^2+z^2)\hat{\mathbf{x}}+xy\hat{\mathbf{y}}+xz\hat{\mathbf{z}}\right\}J_1\left(\frac{k_o n_o a\eta\sin\beta}{r\Phi}\right)\\
& \times\left[xy\cos\alpha+(y^2+z^2)\sin\alpha\right].
\end{aligned}
$$

(3.39)

With the use of Eq. (3.34), the simplified form of Eq. (3.39) is given by

$$
\mathbf{E}_e(\mathbf{r})=\frac{\omega\mu_o\mu_b I_0 a\varepsilon_d}{2(y^2+z^2)}\frac{y\exp(ik_o n_o r\Phi)}{r^2\Phi\sin\theta\rho_d}\left[-(y^2+z^2)\hat{\mathbf{x}}+xy\hat{\mathbf{y}}+xz\hat{\mathbf{z}}\right]J_1\left(\frac{k_o n_o a\rho_d\sin\theta}{\Phi}\right),\quad (3.40)
$$

with

$$
\rho_d=\sqrt{\cos^2\phi+\varepsilon_d^2\sin^2\phi}\,.
$$

(3.41)

To evaluate the ordinary part of the electric field from Eq. (3.29), we can approximate $\tilde{R}$ from Eq. (3.7)

for the exponential term as

$$\tilde{R} = r - a \sin\theta \cos\left(\phi - \phi'\right) , \tag{3.42}$$

and for denominator it is approximated as $\tilde{R} \approx r$.

Substituting Eqs. (3.6) and (3.7) in the numerator, Eq. (3.42) in the exponential term, and Eq.

(3.37) with $\tilde{R} \approx r$ in the denominator of Eq. (3.29) and retaining only the terms proportional to $1/r$, we

get

$$
\begin{aligned}
\mathbf{E}_o(\mathbf{r}) &= \frac{i\omega\mu_o\mu_b I_0 a}{4\pi(y^2 + z^2)} \frac{\exp(ik_o n_o r)}{r} \Bigg\{ \left[-yz \int_0^{2\pi} \cos\phi' \exp\left[-i\tau\cos(\phi - \phi')\right] d\phi' \right. \\
&\quad \left. + az \int_0^{2\pi} \sin\phi' \cos\phi' \exp\left[-i\tau\cos(\phi - \phi')\right] d\phi' \right] \hat{\mathbf{z}} \\
&\quad + z^2 \int_0^{2\pi} \cos\phi' \exp\left[-i\tau\cos(\phi - \phi')\right] d\phi' \hat{\mathbf{y}} \Bigg\} .
\end{aligned}
\tag{3.43}
$$

Solving integrals and further simplification gives us

$$\mathbf{E}_o(\mathbf{r}) = \frac{\omega\mu_o\mu_b I_0 a}{2(y^2 + z^2)} \frac{\exp(ik_o n_o r)}{r} \left(-yz\hat{\mathbf{z}} + z^2\hat{\mathbf{y}} \right) \cos\phi J_1 \left(k_o n_o a \sin\theta \right) . \tag{3.44}$$

Now the expression for the magnetic field can be obtained by substituting Eqs. (1.35), (1.46) and

(3.1) in Eq. (1.28) as

$$
\begin{aligned}
\mathbf{H}(\mathbf{r}) &= \frac{ik_o n_o I_o a}{4\pi} \int_0^{2\pi} \Bigg\{ \frac{\exp\left(ik_o n_o \tilde{R}\right)}{\tilde{R}} \frac{[\tilde{\mathbf{R}} \times (\tilde{\mathbf{R}} \times \hat{\mathbf{x}})](\tilde{\mathbf{R}} \times \hat{\mathbf{x}}) \cdot \hat{\phi}'}{\tilde{R}(\tilde{\mathbf{R}} \times \hat{\mathbf{x}}) \cdot (\tilde{\mathbf{R}} \times \hat{\mathbf{x}})} - \frac{\varepsilon_d \exp(ik_o n_o R_{ex})}{R_{ex}} \\
&\quad \times \frac{(\tilde{\mathbf{R}} \times \hat{\mathbf{x}})[\tilde{\mathbf{R}} \times (\tilde{\mathbf{R}} \times \hat{\mathbf{x}})] \cdot \hat{\phi}'}{R_{ex}(\tilde{\mathbf{R}} \times \hat{\mathbf{x}}) \cdot (\tilde{\mathbf{R}} \times \hat{\mathbf{x}})} \Bigg\} d\phi' .
\end{aligned}
\tag{3.45}
$$

The extraordinary part of the magnetic field can be extracted from Eq. (3.45) by substituting Eqs. (3.6)

and (3.7) in the numerator, Eq. (3.42) in the exponential term, and Eq. (3.37) with $R_{ex} \approx r_{ex}$ in the denominator, and retaining only the terms proportional to $1/r$, we get

$$
\begin{aligned}
\mathbf{H}_e(\mathbf{r}) &= -\frac{ik_o n_o I_0 a \varepsilon_d}{4\pi(y^2 + z^2)} \frac{\exp(ik_o n_o r_{ex})}{r_{ex}^2} \Biggl\{ \Biggl[-xy^2 \int_0^{2\pi} \cos\phi' \exp\bigl[-is_1 \cos(\alpha - \phi')\bigr] d\phi' \\
&\quad -(y^3 + yz^2) \int_0^{2\pi} \sin\phi' \exp\bigl[-is_1 \cos(\alpha - \phi')\bigr] d\phi' \Biggr] \hat{\mathbf{z}} + \Biggl[xyz \int_0^{2\pi} \cos\phi' \exp\bigl[-is_1 \cos(\alpha - \phi')\bigr] d\phi' \\
&\quad +(y^2 z + z^3) \int_0^{2\pi} \sin\phi' \exp\bigl[-is_1 \cos(\alpha - \phi')\bigr] d\phi' \Biggr] \hat{\mathbf{y}} \Biggr\} .
\end{aligned}
\tag{3.46}
$$

After finding the solution of integrals and further simplification gives us

$$
\mathbf{H}_e(\mathbf{r}) = \frac{k_o n_o I_0 a \varepsilon_d}{2(y^2 + z^2)} \frac{\exp(ik_o n_o r\Phi)}{r^2 \Phi^2} (y\hat{\mathbf{z}} - z\hat{\mathbf{y}}) \Bigl[xy \cos\alpha + (y^2 + z^2) \sin\alpha \Bigr] J_1\left(\frac{k_o n_o a\eta \sin\beta}{r\Phi} \right) ,
\tag{3.47}
$$

which can be further simplified with the use of Eq. (3.34) as

$$
\mathbf{H}_e(\mathbf{r}) = \frac{k_o n_o I_0 a \varepsilon_d}{2(y^2 + z^2)} \frac{y \exp(ik_o n_o r\Phi)}{r\Phi \rho_d \sin\theta} (y\hat{\mathbf{z}} - z\hat{\mathbf{y}}) J_1\left(\frac{k_o n_o a\rho_d \sin\theta}{\Phi} \right) .
\tag{3.48}
$$

Similarly the ordinary part of the magnetic field can be extracted from Eq. (3.45) by substituting Eqs. (3.6) and (3.7) in the numerator, Eq. (3.42) in the exponential term, and Eq. (3.37) with $\tilde{R} \approx r$ in the denominator, and retaining only the terms proportional to $1/r$ as

$$
\mathbf{H}_o(\mathbf{r}) = \frac{ik_o n_o I_0 a}{4\pi(y^2 + z^2)} \frac{z \exp(ik_o n_o r)}{r^2} \Bigl[-(y^2 + z^2)\hat{\mathbf{x}} + xy\hat{\mathbf{y}} + xz\hat{\mathbf{z}} \Bigr] \int_0^{2\pi} \cos\phi' \exp\bigl[-i\tau \cos(\phi - \phi')\bigr] d\phi' .
\tag{3.49}
$$

Further simplification gives

$$
\mathbf{H}_o(\mathbf{r}) = \frac{k_o n_o I_0 a}{2(y^2 + z^2)} \frac{z \exp(ik_o n_o r)}{r^2} \Bigl[-(y^2 + z^2)\hat{\mathbf{x}} + xy\hat{\mathbf{y}} + xz\hat{\mathbf{z}} \Bigr] \cos\phi J_1\left(k_o n_o a \sin\theta \right) .
\tag{3.50}
$$

Hence, we see that both the ordinary and the extraordinary waves are radiated when the axis of the loop is perpendicular to the optic axis.

Since the electric field and magnetic field satisfy the orthogonality relations given in Eq. (1.58), we can find the total radiated power by adding the radiated power of ordinary and extraordinary wave separately as given in Eq. (1.59).

Substituting the expressions for $\mathbf{E}_o$ and $\mathbf{H}_o$ from Eqs. (3.44) and (3.50) into Eq. (1.60) and converting into spherical coordinates, we get

$$\frac{dP_o}{d\Omega} = \frac{k_o^2 \mu_o \mu_b n_o I_0^2 a^2 c}{8} \frac{\cos^2\theta \cos^2\phi}{(\sin^2\theta \sin^2\phi + \cos^2\theta)} J_1^2(k_o n_o a \sin\theta) \,. \tag{3.51}$$

Similarly, by substituting the expressions for $\mathbf{E}_e$ and $\mathbf{H}_e$ from Eqs. (3.40) and (3.48) in Eq. (1.61) and converting into spherical coordinates, we get

$$\frac{dP_e}{d\Omega} = \frac{k_o^2 \mu_o \mu_b n_o I_0^2 a^2 c \varepsilon_d^2}{8\Phi \rho_d^2} \frac{\sin^2\phi}{(\sin^2\theta \sin^2\phi + \cos^2\theta)} J_1^2\left(\frac{k_o n_o a \rho_d \sin\theta}{\Phi}\right) \,. \tag{3.52}$$

The total time-averaged power radiated per unit solid angle by the current loop is given by substituting Eqs. (3.51) and (3.52) into Eq. (1.59) as

$$\frac{dP}{d\Omega} = \frac{k_o^2 \mu_o \mu_b n_o I_0^2 a^2 c}{8(\sin^2\theta \sin^2\phi + \cos^2\theta)} \left[\cos^2\theta \cos^2\phi J_1^2(k_o n_o a \sin\theta) + \frac{\varepsilon_d^2 \sin^2\phi}{\Phi \rho_d^2} J_1^2\left(\frac{k_o n_o a \rho_d \sin\theta}{\Phi}\right) \right] \,. \tag{3.53}$$

When we substitute $\varepsilon_d = 1$ (giving $\Phi = 1$ and $\rho_d = 1$), Eqs. (3.28) and (3.53) reduce to the exactly same results of circular current loop in isotropic material [25, 98].

3.4   Electrically small current loop (point-magnetic dipole)

An electrical small current loop is effectively a point-magnetic dipole. For an electrically small loop, the radius a is small enough that $|k_o n_o a| \ll 1$. Then $J_1\left(k_o n_o a \sin\theta\right)$ can be approximated by $\left(k_o n_o a/2\right)\sin\theta$ so that Eq. (3.20) simplifies to

$$\mathbf{E}(\mathbf{r}) = k_o^2 n_o \mu_o \mu_b \pi I_0 a^2 c g_o(\mathbf{r}) \sin\theta\,\hat{\mathbf{y}}\,, \tag{3.54}$$

and Eq. (3.27) can be simplified as

$$\mathbf{H}(\mathbf{r}) = k_o^2 n_o^2 I_o \pi a^2 g_o(\mathbf{r}) \left(\sin\theta\hat{\mathbf{z}} - \cos\theta\hat{\mathbf{x}}\right) \sin\theta\,. \tag{3.55}$$

From Eqs. (3.54) and (3.55), we see that electric field and magnetic field is independent of ϕ and these have the same spatial dependence as given for point-magnetic dipole parallel to the optic axis in [25].

Similarly the expression from Eq. (3.28) can be simplified as

$$\frac{dP}{d\Omega} = \frac{k_o^4 n_o^3 I_o^2 a^4 \mu_o \mu_b c}{32} \sin^2\theta\,. \tag{3.56}$$

Also for small radius of the loop $|k_o n_o a| \ll 1$, $J_1\left(k_o n_o a \rho_d \sin\theta/\Phi\right)$ can be approximated by $\left(k_o n_o a \rho_d \sin\theta/2\Phi\right)$ so that Eq. (3.40) simplifies to

$$\mathbf{E}_e(\mathbf{r}) = \frac{k_o^2 n_o \mu_o \mu_b \pi I_0 a^2 \varepsilon_d c}{r\Phi} g_e(\mathbf{r}) \frac{y\left[-(y^2+z^2)\hat{\mathbf{x}} + xy\hat{\mathbf{y}} + xz\hat{\mathbf{z}}\right]}{y^2+z^2}\,, \tag{3.57}$$

and Eq. (3.44) can be simplified as

$$\mathbf{E}_o(\mathbf{r}) = \frac{k_o^2 n_o \mu_o \mu_b \pi I_0 a^2 c}{y^2+z^2} g_o(\mathbf{r}) \left(-yz\hat{\mathbf{z}} + z^2\hat{\mathbf{y}}\right) \sin\theta\cos\phi\,, \tag{3.58}$$

whereas Eq. (3.48) simplifies to

$$\mathbf{H}_e(\mathbf{r}) = \frac{k_o^2 n_o^2 I_0 \pi a^2 \varepsilon_d}{y^2 + z^2} g_e(\mathbf{r}) y \left(y\hat{\mathbf{z}} - z\hat{\mathbf{y}} \right) , \tag{3.59}$$

and the simplified form of Eq. (3.50) is given by

$$\mathbf{H}_o(\mathbf{r}) = \frac{k_o^2 n_o^2 I_0 \pi a^2}{r(y^2 + z^2)} g_o(\mathbf{r}) \left[-(y^2 + z^2)\hat{\mathbf{x}} + xy\hat{\mathbf{y}} + xz\hat{\mathbf{z}} \right] z \sin\theta \cos\phi . \tag{3.60}$$

A comparison of the fields given in Eqs. (3.57)–(3.60) with the fields of point-magnetic dipole given in [25] shows that both the results agree when the dipole is taken perpendicular to the optic axis in Ref. [25].

Under the same approximation, the expression for the time-averaged Poynting vector of ordinary wave given in Eq. (3.51) can be simplified as

$$\frac{dP_o}{d\Omega} = \frac{k_o^4 \mu_o \mu_b n_o^3 I_0^2 a^4 c}{32} \frac{\cos^2\theta \cos^2\phi}{(\sin^2\theta \sin^2\phi + \cos^2\theta)} \sin^2\theta , \tag{3.61}$$

and the expression for extraordinary wave can be written as

$$\frac{dP_e}{d\Omega} = \frac{k_o^4 \mu_o \mu_b n_o^3 I_0^2 a^4 c \varepsilon_d^2}{32 \Phi^3} \frac{\sin^2\phi \sin^2\theta}{(\sin^2\theta \sin^2\phi + \cos^2\theta)} , \tag{3.62}$$

while the total power radiated by the point-magnetic dipole can be approximated from Eq. (3.53) as

$$\begin{aligned}
\frac{dP}{d\Omega} &= \frac{k_o^4 \mu_o \mu_b n_o^3 I_0^2 a^4 c}{32} \left(\cos^2\theta \cos^2\phi + \frac{\varepsilon_d^2 \sin^2\phi}{\Phi^3} \right) \\
&\quad \times \frac{\sin^2\theta}{(\sin^2\theta \sin^2\phi + \cos^2\theta)} .
\end{aligned} \tag{3.63}$$

When we substitute $\varepsilon_d = 1$ (giving $\Phi = 1$), Eqs. (3.56) and (3.63) reduce to exactly the same results, which is also the result for the point-magnetic dipole in the isotropic material.

3.5   Numerical results and discussion

The closed-form results obtained for the far-field radiation pattern are chief results of this chapter and are given in Eqs. (3.28) and (3.51)-(3.53). To illustrate their use, we present representative numerical results for radiations by current loops of different sizes in a common uniaxial material, rutile, with $I_0 = 0.1$ A, $\varepsilon_a = 8.427$, $\varepsilon_b = 6.843$, $\mu_b = 1$, and $\lambda_o = 0.584$ μm [29] for a current loop with radius $a = 0.1\lambda_o$, $a = 0.2\lambda_o$, and $a = 1.2\lambda_o$.
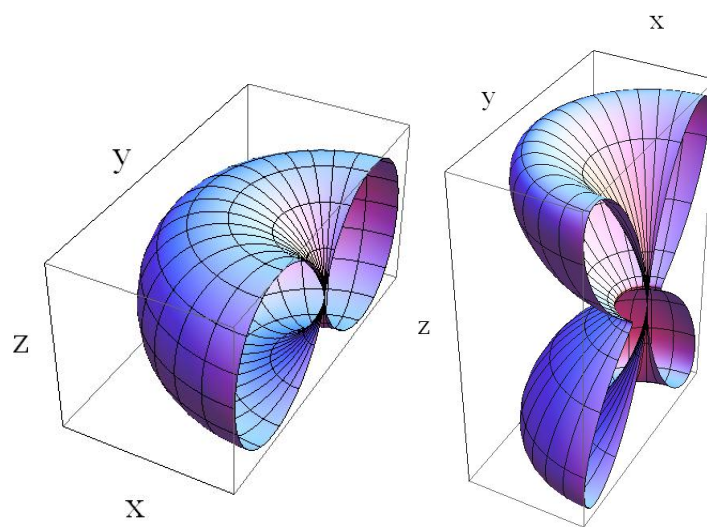
FIGURE 3.3: Far-field radiation pattern, Eq. (3.28), of ordinary waves emitted by a current loop with its axis parallel to the optic axis (z axis) in rutile. The plot is given for $0 \leq \theta \leq \pi$ and $\pi/2 \leq \phi \leq 3\pi/2$ with $I_0 = 0.1A$, $\varepsilon_a = 8.427$, $\varepsilon_b = 6.843$, $\mu_b = 1$, $\lambda_o = 0.584\,\mu$m [29], (left) $a = 0.1\lambda_o$ and (right) $a = 0.2\lambda_o$.

The far-field radiation patterns of ordinary waves emitted by a current loop with its axis aligned with the optic axis (z axis) are shown in Fig. 3.3. The loop is placed in uniaxial material (rutile) when $a = 0.1\lambda_o$ and $a = 0.2\lambda_o$. We have plotted Eq. (3.28) only for $0 \leq \theta \leq \pi$ and $\pi/2 \leq \phi \leq 3\pi/2$ because it is easier to visualize the pattern since it is independent of ϕ. The figure shows that the pattern is like that of a dipole in an isotropic material when $a = 0.1\lambda_o$. With the increase in the radius of the loop ($a = 0.2\lambda_o$) the radiation pattern compresses around the loop and becomes more directive along the axis of the loop. Let us note that no radiations exist along the optic axis which also happens to be the axis of the loop in this case.
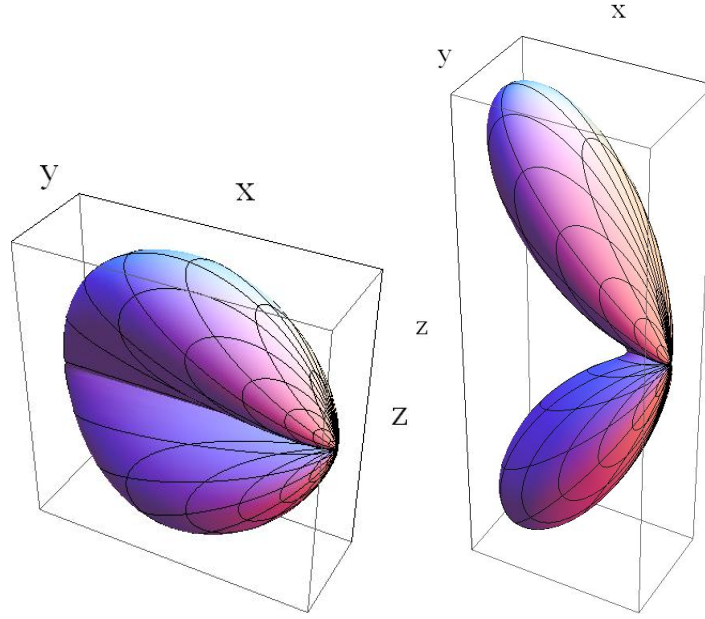
FIGURE 3.4: Far-field radiation pattern of ordinary waves given by Eq. (3.51) when the axis of the loop is oriented along z axis and the optic axis along x axis for a uniaxial material (rutile) with $\varepsilon_a = 8.427$, $\varepsilon_b = 6.843$, $\mu_b = 1$, $\lambda_o = 0.584\,\mu\text{m}$ [29], (left) $a = 0.1\lambda_o$, (right) $a = 0.2\lambda_o$ and $I_o = 0.1A$. The plot is given for $0 \leq \theta \leq \pi$ and $\pi/2 \leq \phi \leq 3\pi/2$. The plot is symmetric about yz plane.

When the axis of the current loop is perpendicular to the optic axis, the radiation pattern of the ordinary waves are shown in Fig. 3.4 when $a = 0.1\lambda_o$ and $a = 0.2\lambda_o$. Again we have plotted Eq. (3.51) for $0 \leq \theta \leq \pi$ and $\pi/2 \leq \phi \leq 3\pi/2$ because the pattern is symmetric about yz plane. Its clear from the figure that the radiations in the direction of optic axis are suppressed, though not zero.

The radiation pattern of the extraordinary wave, given by Eq. (3.52), for a current loop that have its axis perpendicular to the optic axis are shown in Fig. 3.5 when $a = 0.1\lambda_o$ and $a = 0.2\lambda_o$. When the loop size is small, the radiations are directed perpendicular to both the optic axis and the axis of the loop. But, when the dipole size is larger, the radiations are suppressed completely along the axis of the loop and the plane perpendicular to the this axis with the suppression strongest along a direction perpendicular to both the optic axis and the axis of the loop.

The radiation patterns for a large loop are given in Fig. 3.6 when $a = 1.2\lambda_o$. The major characteristic of these patterns are that they are all highly directive along the axis of the loop, though
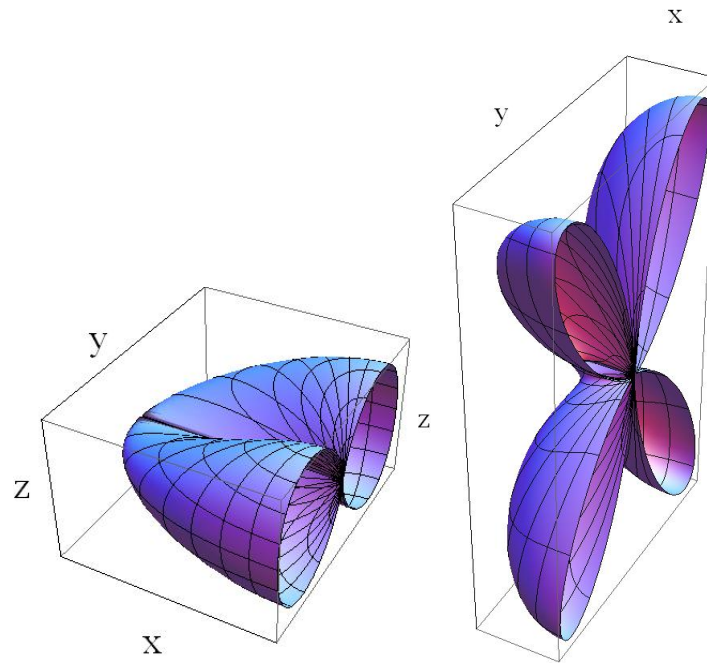
FIGURE 3.5: Same as Fig. 3.4 except that the pattern is that of extraordinary wave given by Eq. (3.52) with (left) $a = 0.1\lambda_o$ and (right) $a = 0.2\lambda_o$.

there are many side lobes now. Therefore, these radiation patterns show that the higher order multipoles [87] are also present in the radiation pattern when the radius of the loop is large.

3.6 Comparison with the point-magnetic dipole

To compare the results of the current loop with those of a point-magnetic dipole, let us consider a point-magnetic dipole with the electric current densities as given in Eq. (1.66) and the plots are given in Fig. 1.8 and 1.9. The following results are very helpful in comparing the finite-sized and the point-magnetic dipole:

- Let us note that $a \to 0$ in Eq. (3.28) results in the same form as that of Eq. (1.72). Similarly, the current loop results of Eq. (3.53) reduce to the same form as the point dipole of Eq. (1.75) when $a \to 0$ in Eq. (3.53).
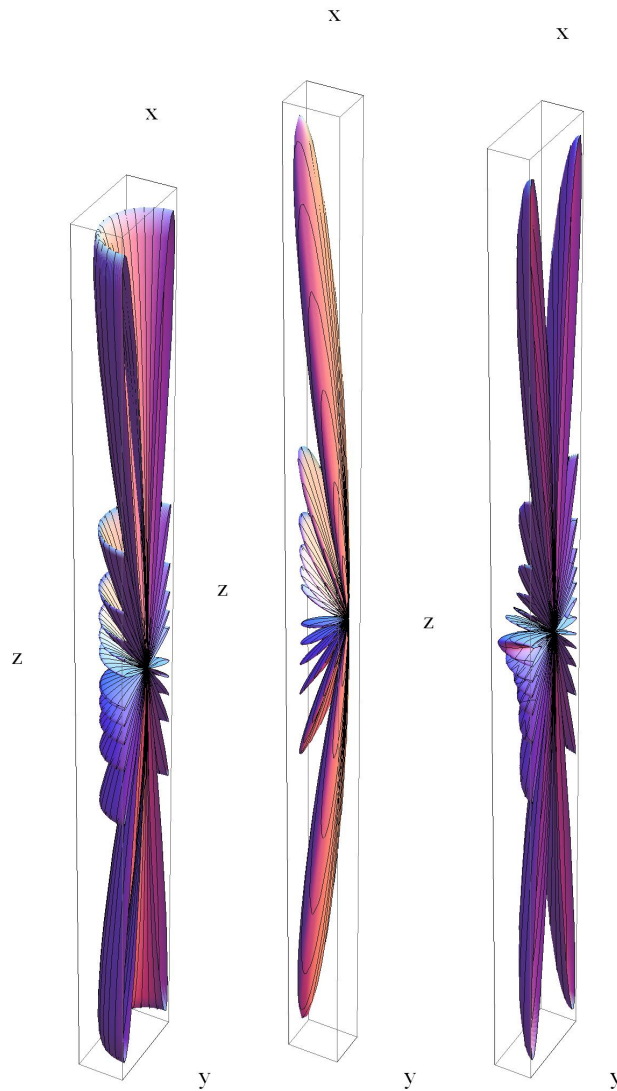
FIGURE 3.6: Far-field radiation pattern when $a = 1.2\lambda_o$ for (a) ordinary waves when the loop axis is parallel to the optic axis, and for (b) ordinary and (c) extraordinary waves when the loop axis is perpendicular to the optic axis.

- For comparison of the radiation patterns of the point-magnetic dipole and the current loop results, the far-field radiation pattern of the point-magnetic dipole are presented in Fig. 1.8 and 1.9 when the magnetic-dipole is, respectively, parallel and perpendicular to the optics axis, for the same parameters as those for the current loop. A comparison of Fig. 1.8 with Fig. 3.3 shows that the both pattern looks similar, but the directivity is enhanced by the increase in radius $2a$ of the current loop. The comparison of Fig. 1.9 with Figs. 3.4 and 3.5 draws the same conclusion that the current loop allows the control of directivity of the radiation by choosing the radius of the current loop.

3.7 Concluding remarks

The closed-form expressions for the far-field radiation pattern of a constant current loop in a uniaxial dielectric material were analytically derived and the representative numerical results were presented for a chosen uniaxial material. The approximate results for a point-magnetic dipole were also derived. The axis of the loop was taken to be along and perpendicular to the optic axis. When the axis of the loop was parallel to the optic axis, only ordinary wave was emitted. When the axis of the loop was perpendicular to the optic axis, both the ordinary and the extraordinary waves were emitted but the radiations along the optic axis were suppressed for both the ordinary and extraordinary waves. For all the cases, the directivity of the radiation pattern increased significantly with the increase in the size of the loop. When the radius of loop was very large (larger than the wavelength), the radiations were highly directive along the axis of the loop. A comparison of the radiation patterns of small loop ($a = 0.1\lambda_o$) with patterns of larger loops show that the current loop approximates the point-magnetic dipole only when the radius is small.

Chapter 4

Electric dipole in hyperbolic material

In this chapter, far-field radiation by a finite-length electric dipole is studied in the hyperbolic material. To account for the arbitrary orientation of the dipole, the results are presented when the dipole and the optic are parallel to each other and when they are perpendicular to each other. Analytical as well as numerical results for both the ordinary and extraordinary wave are presented. The results indicate a strong dependence upon the length of the dipole, in contrast to the case of the uniaxial dielectric material. When the dipole was parallel to the optic axis, radiations are emitted in a cone around the symmetry axis. When the dipole was perpendicular to the optic axis, extraordinary waves are emitted along only four directions, whereas ordinary waves are emitted in every direction perpendicular to the dipole.

The plan of the chapter is as follows: An introduction and the relevant literature review is presented in Sec. 4.1. The far-field radiation pattern by a finite-length dipole, when the dipole and the optic axis are parallel to each other, is discussed in Sec. 4.2. When the dipole is along the z axis and the optic axis is along x, the radiations are discussed in Sec. 4.3. The concluding remarks are presented in Sec. 4.4.

This chapter is based on "A. Hayat and M. Faryad, Radiation by a finite-length electric dipole in the hyperbolic media, *Phys. Rev. A* **101**, 013832 (2020)"

4.1 Introduction

Since the hyperbolic metamaterials [99, 100] are materials with strong dielectric anisotropy, these are also very promising for quantum nanophotonics [48, 101], because the density of states which is determined by the hyperboloid area is divergent. It means an infinite spontaneous decay rate of quantum emitters embedded in hyperbolic materials, i.e., infinite Purcell effect [10]. In the realistic case, the radiation rate is limited by certain cutoffs in the wave-vector space [102–106]; however, experimental observation of radiative enhancement is still possible [48, 107]. Several authors have studied the radiations emitted by a point dipole. For example, the radiations emitted by a point dipole in an unbounded uniaxial material was studied in Refs. [16–18]. The far-field radiation of a point dipole in hyperbolic material was studied in Ref. [47]. For the next order approximation, it is important to study the radiation from sources with finite length.

4.2 Dipole and optic axis parallel to z axis

Let us consider the situation in which the finite-length dipole and the optic axis are parallel to the z axis, and is placed in the hyperbolic material of type I as shown in Fig. 4.1. In this situation, it is observed that only an extraordinary wave is emitted as discussed in Ref. [86].

Since the dipole is parallel to the optic axis, the electric current density for that dipole is given by

$$\mathbf{J}_e(\mathbf{r}') = \begin{cases} -i\omega p_o \delta(x')\delta(y')\hat{\mathbf{z}}, & |z'| \leq L, \\ \\ 0, & |z'| > L. \end{cases} \tag{4.1}$$

The expressions for the electric and magnetic fields are given by [86]

$$\mathbf{E}(\mathbf{r}) = \frac{k_o \mu_b p_o \varepsilon_d}{2\pi\varepsilon_o n_o r} \frac{\exp(ik_o n_o r\Theta)}{\Theta^2} \left[\frac{\sin^2\theta}{\cos\theta}\hat{\mathbf{z}} - \sin\theta\cos\phi\hat{\mathbf{x}} - \sin\theta\sin\phi\hat{\mathbf{y}} \right] \sin\left(\frac{k_o L n_o \cos\theta}{\Theta} \right), \tag{4.2}$$
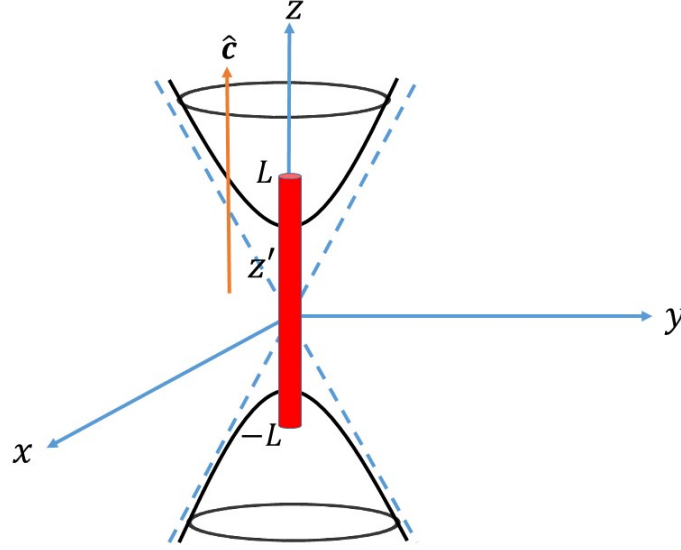
FIGURE 4.1: Schematic showing a finite-length dipole placed in the hyperbolic materials of type I with its optic axis aligned parallel to the direction of the dipole (z axis).

and

$$\mathbf{H}(\mathbf{r}) = \frac{k_o p_o c \varepsilon_d}{2\pi r} \frac{\exp(ik_o n_o r\Theta)}{\Theta \cos\theta} \left(-\sin\theta\cos\phi\hat{\mathbf{y}} + \sin\theta\sin\phi\hat{\mathbf{x}} \right) \sin\left(\frac{k_o L n_o \cos\theta}{\Theta} \right),$$ (4.3)

where

$$\varepsilon_d = \frac{\varepsilon_a}{\varepsilon_b} = \varepsilon_d' + i\varepsilon_d''.$$ (4.4)

Since we only have an extraordinary wave emitted by a finite-length dipole, the time-averaged power can be found by substituting Eqs. (4.2) and (4.3) into Eq. (1.54), and is given by

$$\frac{dP}{d\Omega} = \frac{dP_e}{d\Omega} = \frac{k_o^2 \mu_b p_o^2 c \left(\varepsilon_d'^2 + \varepsilon_d''^2 \right)}{8\pi^2 \varepsilon_o} \frac{\sin^2\theta}{\cos^2\theta} \mathrm{Re} \left[\frac{\sin\left(\frac{k_o L n_o \cos\theta}{\Theta} \right) \sin\left(\frac{k_o L n_o^* \cos\theta}{\Theta^*} \right)}{n_o \Theta^2 \Theta^*} \right].$$ (4.5)

We now present numerical results in the hyperbolic material with $\varepsilon_a = -3 + 0.2i$, $\varepsilon_b = 1 + 0.2i$ [47], as well as for a natural hyperbolic material hexagonal boron nitride (hBN) with $\varepsilon_a = -4.3 + 0.2i$, $\varepsilon_b = 2.8$ [108], $p_o = 1/\omega$, and $\mu_b = 1$ to understand the radiation in the hyperbolic material. The value
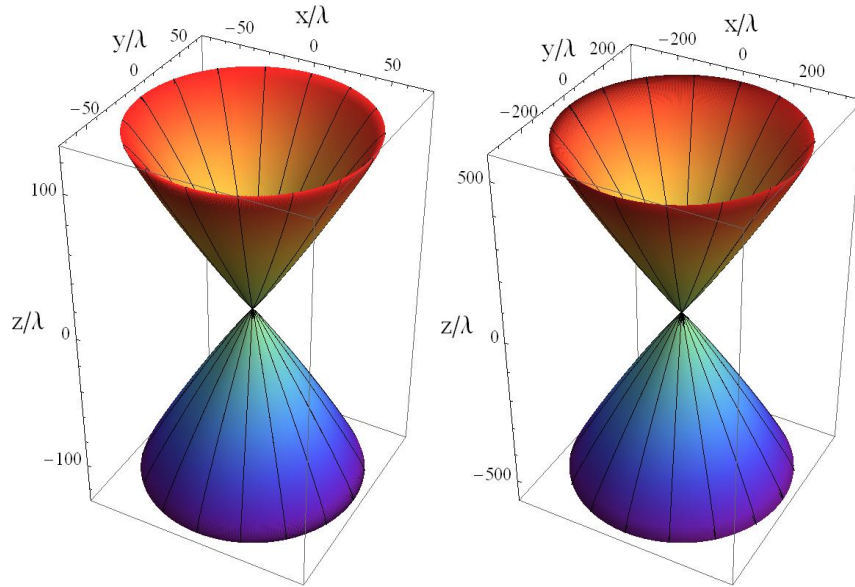
FIGURE 4.2: Far-field radiation pattern of a finite-length dipole, which is oriented parallel to the optic axis (z axis) and lying in the hyperbolic material with $\varepsilon_a = -3 + 0.2i$, $\varepsilon_b = 1 + 0.2i$, $p_o = 1/\omega$, $\mu_b = 1$, (left) $L = 0.1$, and (right) $L = 0.2$.
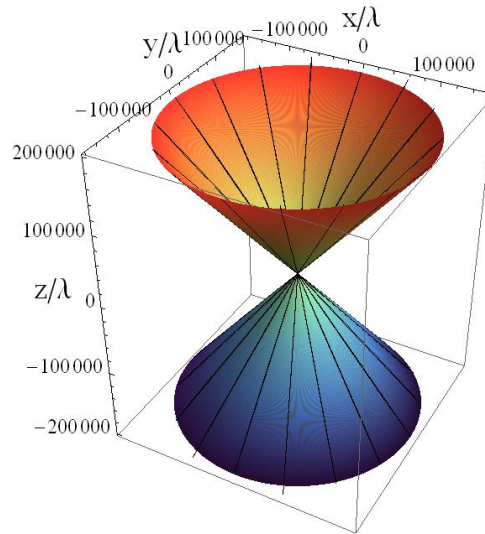
FIGURE 4.3: Same as Fig. 4.2 (left) except that the hyperbolic material is hBN with $\varepsilon_a = -4.3 + 0.2i$, $\varepsilon_b = 2.8$, $p_o = 1/\omega$, $L = 0.1$, and $\mu_b = 1$.

of permittivities for the hBN are taken at a wave number 1500 cm^{-1} from the data provided in Ref. [108].

The radiation pattern of the extraordinary wave given by Eq. (4.5) is shown in Fig. 4.2 (left) for $L = 0.1$ and Fig. 4.2 (right) for $L = 0.2$. It is observed that the radiation pattern is spread uniformly around the dipole and there is no radiation along the axis of the dipole. Furthermore, it is also noted that the rate of emission of radiation increases strongly when the length of the dipole increases. Moreover,

the radiation pattern is spread in a conical shape. If we compare these results with that of the uniaxial dielectric material [86], we see that the power radiated by a finite-length dipole strongly depends upon the length, i.e., a small change in the length produces a large change in the time-averaged radiated power in the hyperbolic material. Another difference observed between the uniaxial dielectric [86] and hyperbolic material is that the radiations are emitted in the plane perpendicular to the dipole in the uniaxial dielectric material, while in case of the hyperbolic material no radiations are emitted in the plane perpendicular to the dipole. The radiation pattern for the natural hyperbolic material hBN in Fig. 4.3 shows the same properties.

4.3 Dipole is along z axis and the optic axis is along x axis

Now, let us consider the case in which the dipole is placed perpendicular to the optic axis, i.e., the dipole is along the z axis and the optic axis is along the x axis as shown in Fig. 4.4. The current density for that dipole is given in Eq. (4.1). Now in this situation, both ordinary and extraordinary waves are emitted [86]. The expression of electric fields is given by [86]

$$\mathbf{E}_o(\mathbf{r}) = \frac{k_o \mu_b p_o}{2\pi\varepsilon_o n_o r}\left(-\hat{\mathbf{y}} + \tan\theta\sin\phi\hat{\mathbf{z}}\right)\frac{\exp(ik_o n_o r)\sin\theta\sin\phi}{(\sin^2\theta\sin^2\phi + \cos^2\theta)}\sin(k_o n_o L\cos\theta)\,, \qquad (4.6)$$

representing the ordinary wave and

$$\begin{aligned}\mathbf{E}_e(\mathbf{r}) &= \frac{k_o \mu_b p_o}{2\pi\varepsilon_o n_o r}\left[-(\sin^2\theta\sin^2\phi + \cos^2\theta)\hat{\mathbf{x}} + \sin^2\theta\cos\phi\sin\phi\hat{\mathbf{y}} + \sin\theta\cos\theta\cos\phi\hat{\mathbf{z}}\right]\\ &\quad\times\frac{\exp(ik_o n_o r\Phi)\sin\theta\cos\phi}{\Phi^2(\sin^2\theta\sin^2\phi + \cos^2\theta)}\sin\left(\frac{\varepsilon_d k_o n_o L\cos\theta}{\Phi}\right)\,,\end{aligned} \qquad (4.7)$$

representing the extraordinary wave.
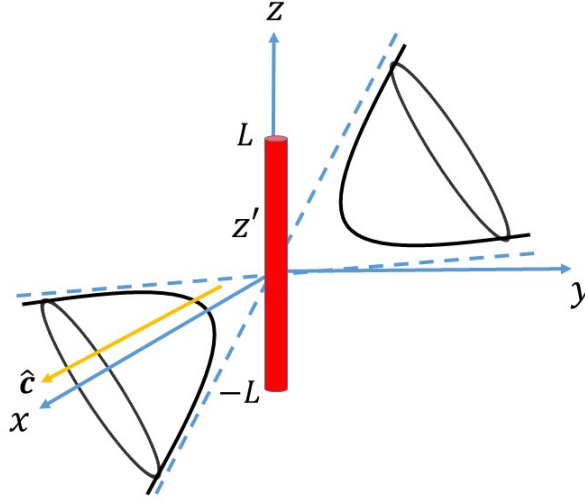
FIGURE 4.4: Schematic showing a finite-length dipole along the z axis placed in the hyperbolic material of type I with its optic axis along the x axis.

Similarly, the corresponding expressions for the magnetic fields are given by

$$
\begin{aligned}
\mathbf{H}_o(\mathbf{r}) &= \frac{k_o p_o c}{2\pi r}\Big[(\sin^2\theta\sin^2\phi + \cos^2\theta)\hat{\mathbf{x}} - \sin^2\theta\cos\phi\sin\phi\hat{\mathbf{y}} - \sin\theta\cos\theta\cos\phi\hat{\mathbf{z}}\Big] \\
&\quad \times \frac{\exp(ik_o n_o r)\sin\theta\sin\phi}{\cos\theta(\sin^2\theta\sin^2\phi + \cos^2\theta)}\sin(k_o n_o L\cos\theta)\,,
\end{aligned}
\tag{4.8}
$$

and

$$
\mathbf{H}_e(\mathbf{r}) = \frac{k_o p_o c}{2\pi r}\Big(-\cos\theta\hat{\mathbf{y}} + \sin\theta\sin\phi\hat{\mathbf{z}}\Big)\frac{\exp(ik_o n_o r\Phi)\sin\theta\cos\phi}{\Phi(\sin^2\theta\sin^2\phi + \cos^2\theta)}\sin\left(\frac{\varepsilon_d k_o n_o L\cos\theta}{\Phi}\right).
\tag{4.9}
$$

Now the expression for the time-averaged power radiated per unit solid angle by the finite-length dipole can be found by substituting Eqs. (4.6) and (4.8) into Eq. (1.60), as

$$
\frac{dP_o}{d\Omega} = \frac{k_o^2\mu_b p_o^2 c}{8\pi^2\varepsilon_o}\frac{\sin^2\theta\sin^2\phi}{\cos^2\theta(\sin^2\theta\sin^2\phi + \cos^2\theta)}\mathrm{Re}\left[\frac{\sin\left(k_o n_o L\cos\theta\right)\sin\left(k_o n_o^* L\cos\theta\right)}{n_o}\right],
\tag{4.10}
$$

for the ordinary wave. Similarly by substituting Eqs. (4.7) and (4.9) into Eq. (1.61), we get

$$\frac{dP_e}{d\Omega} = \frac{k_o^2 \mu_b p_o^2 c}{8\pi^2 \varepsilon_o} \frac{\sin^2 \theta \cos^2 \phi}{(\sin^2 \theta \sin^2 \phi + \cos^2 \theta)} \text{Re} \left[\frac{\sin \left(\frac{\varepsilon_d^* k_o L n_o \cos \theta}{\Phi} \right) \sin \left(\frac{\varepsilon_d^* k_o L n_o^* \cos \theta}{\Phi^*} \right)}{n_o \Phi^2 \Phi^*} \right] , \qquad (4.11)$$

for the extraordinary wave.

The far-field radiation pattern of the ordinary wave given by Eq. (4.10) is shown in Fig. 4.5 (top) for $L = 0.1$ and in Fig. 4.5 (bottom) for $L = 0.2$. Similarly the far-field radiation pattern of the extraordinary wave given by Eq. (4.11) is shown in Fig. 4.6 (top) for $L = 0.1$ and in Fig. 4.6 (bottom) for $L = 0.2$.
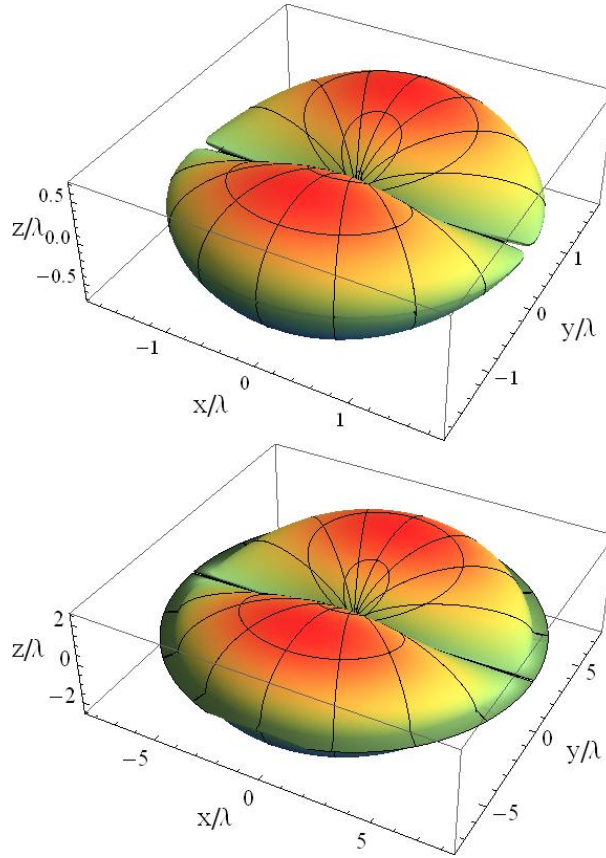
FIGURE 4.5: Far-field radiation pattern of ordinary waves given by Eq. (4.10), when the dipole is oriented along the z axis and the optic axis is along the x axis, and lying in the hyperbolic material with $\varepsilon_a = -3 + 0.2i$, $\varepsilon_b = 1 + 0.2i$, $p_o = 1/\omega$, $\mu_b = 1$, (top) $L = 0.1$, and (bottom) $L = 0.2$.

Figure 4.5 shows that the radiations are suppressed along the optic axis, though it is not zero. Also, it is observed that when we increase the length of the dipole, the directivity increases. If we compare with

that of the uniaxial dielectric material, we see that suppression of the radiation along the direction of the optic axis is a bit strong. However, the radiation pattern is the same for both the uniaxial dielectric and the hyperbolic material.
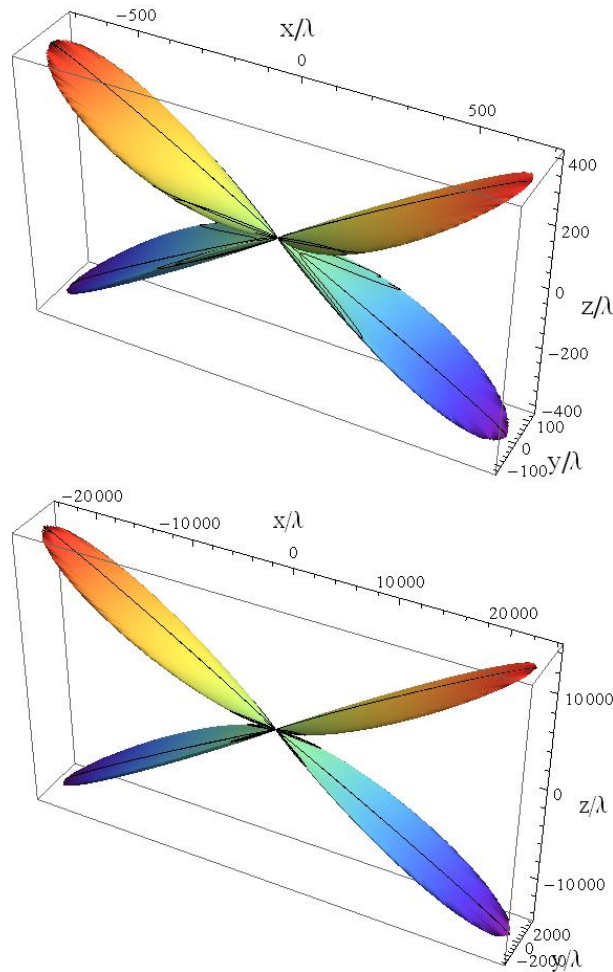
FIGURE 4.6: Same as Fig. 4.5 except that the pattern is that of the extraordinary wave.

Figure 4.6 shows that no radiations are emitted along the dipole, the optic axis, and perpendicular to the plane formed by the dipole and the optic axis. This is in contrast to the dipole in the uniaxial dielectric material [86] where the radiations were predominantly along a direction perpendicular to the optic axis and the dipole. When the length of the dipole is increased, Fig. 4.6 shows that the strength of the radiation increases very significantly. Let us note that the radiation patterns for the natural hyperbolic material have the same properties and show the same trends as in Figs. 4.5 and 4.6 and are not reproduced here.

4.4   Concluding remarks

Far-field radiations by an electric dipole of finite length are presented and analyzed when the dipole was parallel or perpendicular to the optic axis. When the dipole was parallel, only extraordinary waves are emitted, but both the ordinary and the extraordinary waves are emitted when the dipole was perpendicular to the optic axis. Furthermore:

- A comparison of the finite-length dipole in the hyperbolic material with that of the uniaxial dielectric material showed that the radiation patterns are very different for the extraordinary waves but the patterns for the ordinary waves are similar.

- The directivity of the radiation pattern is strongly dependent upon the length of the dipole.

- When the dipole and the optic axis were parallel, the extraordinary radiations are emitted along a cone with the optic axis as its axis.

- When the dipole was perpendicular, no extraordinary radiation is emitted along the dipole, the optic axis, and perpendicular to the plane formed by the dipole and the optic axis.

Let us note that the formulation presented in this chapter is valid for both the artificial as well as the natural hyperbolic material. Once the permittivity dyadic of the hyperbolic material is known, the results of this chapter can be used to find the electromagnetic fields and the radiation pattern of the radiations by the finite-length dipole.

Chapter 5

Electric dipole in wire material in zero-index regime

In this chapter, radiations by a finite-length dipole in a uniaxial zero-index materials (ZIMs) are studied. The wire material in the zero index regime is taken as the uniaxial ZIM. Analytical results are obtained for the wire material when the finite length dipole is parallel to the optic axis and when it was perpendicular to the same axis. When the dipole was parallel, only the near field was significantly present and no radiations were emitted in the far field. When the dipole was perpendicular, the near field negligible, but far field radiations were present, though only of the ordinary type.

The plan of the chapter is as follow: The introduction and the relevant literature review is presented in Sec. 5.1. The approximated dyadic Green functions for the wire material are discussed in Sec. 5.2. The radiation pattern by a finite-length dipole when the dipole and the optic axis are parallel to each other is discussed in Sec. 5.3. The fields due to a dipole that is perpendicular to the optic axis are presented in Sec. 5.4. The concluding remarks of this chapter are presented in Sec. 5.5.

5.1 Introduction

Electromagnetic metamaterials offer a wide range of electromagnetic properties that are otherwise not available in natural materials or not available in the desired spectral range [26, 34, 109, 110]. These metamaterials engender a wide range of extraordinary optical phenomena [111–114] and applications [115–117]. Zero-index metamaterials (ZIMs) or materials with refractive index near zero have various applications [83, 84, 118–128], for instance, to control transmission in a ZIM waveguide with defects [118–121], getting desired directive radiation or multi-beams [122–124], increasing radiation efficiency [83, 84, 125], compressing or bending electromagnetic wave in a sub-wavelength ENZ channel [126, 127], and unifacial transmission [128].

The ZIM materials are usually fabricated as a mixture of metallic and dielectric materials. A parallel assembly of metallic wires in a dielectric host an easier way of fabricating a ZIM if the size of the unit cell is much smaller than the operating wavelength [39]. In such a ZIM, the material is uniaxial, with one principle permittivity zero and the other non zero. A similar uniaxial ZIM can also be fabricated using an all-dielectric 2D photonic crystal operating at the Dirac-like point in its photonic band-structure [129]. This dielectric photonic crystal also has permittivity zero along one direction and non-zero along the other. These anisotropic ZIM materials have numereous applications: the subwavelength transmission of images [130], superlensing [131], biosensing[132], the strong enhancement of the Vavilov-Cherenkov radiation and peculiar dipole emission patterns has been also predicted for these material [133–135].

The growing list of applications of uniaxial ZIM materials require a theoretical framework to understand scattering and radiation properties of the foreign inclusions and obstacles inside these ZIM to either characterize scattering losses and to design efficient radiators. Therefore, we set out to delineate the radiation characteristics of a finite-size electric dipole inside these uniaxial ZIMs.

5.2 Dyadic Green functions of wire material in ZIM regime

Consider the wire material as shown schematically in Fig. 5.1 and also discussed in Sec. 1.1.3. If we take the direction of the metallic wire to be along the unit vector $\hat{\mathbf{c}}$, the permittivity dyadic for these wire material is given by Eq. (1.21), and the dyadic Green functions for the wire material in the ZIM regime, i.e., for $\varepsilon_a \approx 0$, can be obtained from Ref. [25, 26, 86, 136] as

$$
\begin{aligned}
\underline{\underline{G}}^{ee}(\mathbf{R}) \;=\; & \frac{\omega\mu_o\mu_b}{4\pi k_o n_o}\Bigg\{ \exp(ik_o n_o R_d)\left(1+\frac{i}{k_o n_o R_d}\right)\frac{2\hat{\mathbf{c}}\hat{\mathbf{c}}}{R_d^2} \\
& +\frac{ik_o n_o \exp(ik_o n_o R)}{R}\frac{(\mathbf{R}\times\hat{\mathbf{c}})\,(\mathbf{R}\times\hat{\mathbf{c}})}{\mid\mathbf{R}\times\hat{\mathbf{c}}\mid^2} \\
& +\frac{\exp(ik_o n_o R)-\exp(ik_o n_o R_d)}{\mid\mathbf{R}\times\hat{\mathbf{c}}\mid^2}\left[\underline{\underline{I}}-\hat{\mathbf{c}}\hat{\mathbf{c}}-\frac{2\,(\mathbf{R}\times\hat{\mathbf{c}})\,(\mathbf{R}\times\hat{\mathbf{c}})}{\mid\mathbf{R}\times\hat{\mathbf{c}}\mid^2}\right]\Bigg\},
\end{aligned}
\tag{5.1}
$$

where

$$
R_d =\mid \mathbf{R}\cdot\hat{\mathbf{c}}\mid,
\tag{5.2}
$$

and

$$
\begin{aligned}
\underline{\underline{G}}^{me}(\mathbf{R}) \;=\; & \frac{1}{4\pi}\left(\frac{\exp(ik_o n_o R_d)}{R_d}-\frac{\exp(ik_o n_o R)}{R}\right)(\mathbf{R}\cdot\hat{\mathbf{c}}) \\
& \times\frac{[\hat{\mathbf{c}}\times(\mathbf{R}\times\hat{\mathbf{c}})]\,(\mathbf{R}\times\hat{\mathbf{c}})+(\mathbf{R}\times\hat{\mathbf{c}})\,[\hat{\mathbf{c}}\times(\mathbf{R}\times\hat{\mathbf{c}})]}{[(\mathbf{R}\times\hat{\mathbf{c}})\cdot(\mathbf{R}\times\hat{\mathbf{c}})]^2} \\
& -\frac{\exp(ik_o n_o R)}{4\pi}\,(1-ik_o n_o R)\,\frac{[\mathbf{R}\times(\mathbf{R}\times\hat{\mathbf{c}})]\,(\mathbf{R}\times\hat{\mathbf{c}})}{R^3\,[(\mathbf{R}\times\hat{\mathbf{c}})\cdot(\mathbf{R}\times\hat{\mathbf{c}})]}.
\end{aligned}
\tag{5.3}
$$

Let us now consider the radiation from a finite-length electric dipole of length $2L$ along z axis and placed in a wire material. The electric current density of the finite-length dipole is given by

$$
\mathbf{J}_e(\mathbf{r}') = \begin{cases} -i\omega p_o\delta(x')\delta(y')\hat{\mathbf{z}}, & |z'|\le L, \\[2mm] 0, & |z'|>L. \end{cases}
\tag{5.4}
$$

In order to be able to find the radiation for the wire material with its optic axis oriented at an arbitrary angle with respect to the dipole, we consider the two cases: (a) When the optic axis is parallel to the dipole, and (ii) when it is perpendicular.

5.3 Optic axis parallel to the dipole
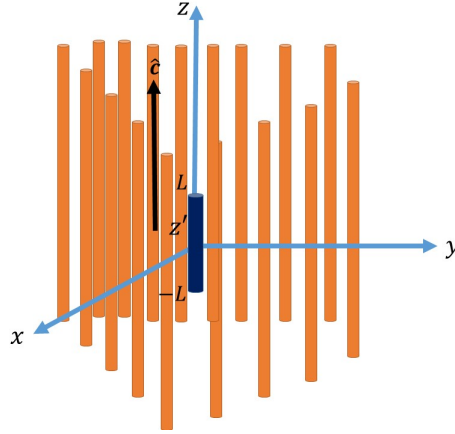
FIGURE 5.1: Schematic figure showing a finite length dipole placed in the zero-index wire material with $\varepsilon_a \approx 0$ with it's optic axis aligned with the dipole (z axis).

Consider a finite-length dipole of length $2L$ placed in a wire material as shown in Fig. 5.1. The dipole is aligned parallel to the direction of the optic axis (z axis). The radiated fields everywhere can be obtained by substituting the dyadic Green functions and the current density in Eqs. (1.27) and (1.28); however, the integrals cannot be evaluated analytically and numerical methods will be needed to solve the integral at any given position. But, in the near-field and the far-field, approximate analytical results can be obtained, as we see below.

5.3.1 Near field

In the near-field, $k_o n_o R_d \ll 1$ and $k_o n_o R \ll 1$, the electric field of the finite length dipole placed parallel to the optic axis in the wire material can be computed by substituting Eqs. (5.1) and (5.4) into Eq. (1.27)

by retaining the leading term:

$$\mathbf{E}(\mathbf{r}) = \frac{p_o}{2\pi\varepsilon_o\varepsilon_b} \int_{-L}^{L} \frac{\hat{\mathbf{c}}\hat{\mathbf{c}} \cdot \hat{\mathbf{z}}}{|\mathbf{R}_z \cdot \hat{\mathbf{c}}|^3} dz', \tag{5.5}$$

where

$$\mathbf{R}_z = x\hat{\mathbf{x}} + y\hat{\mathbf{y}} + (z - z')\hat{\mathbf{z}}. \tag{5.6}$$

Using Eq. (5.6) along with $\hat{\mathbf{c}} = \hat{\mathbf{z}}$ into Eq. (5.5) and evaluating integrals gives us

$$\mathbf{E}(\mathbf{r}) = \frac{p_o L}{\pi\varepsilon_o\varepsilon_b} \frac{z\hat{\mathbf{z}}}{\left(L^2 - z^2\right)^2}. \tag{5.7}$$

However, the magnetic field computed to the same order by substituting Eqs. (5.3) and (5.4) into Eq. (1.28) becomes

$$\mathbf{H}(\mathbf{r}) \approx 0. \tag{5.8}$$

From Eqs. (5.7) and (5.8) it is clear that the fields near the dipole will be present even if the dipole is static as the fields are dominantly electric and are independent of ω.

5.3.2 Far field

When we are very far away from the finite-length dipole, i.e., when $k_o n_o R_d \gg 1$ and $k_o n_o R \gg 1$, the electric and magnetic fields in the far zone can be computed by the substitution of Eqs. (5.1) and (5.4) into Eq. (1.27) by retaining the terms proportional to $1/r$ as

$$\mathbf{E}(\mathbf{r}) \approx \frac{k_o^2 \mu_b p_o}{4\pi\varepsilon_o} \int_{-L}^{L} \frac{\exp(ik_o n_o R_z)}{R_z} \frac{(\mathbf{R}_z \times \hat{\mathbf{c}})(\mathbf{R}_z \times \hat{\mathbf{c}}) \cdot \hat{\mathbf{z}}}{|\mathbf{R}_z \times \hat{\mathbf{c}}|^2} dz'. \tag{5.9}$$

With the use of Eq. (5.6) along with $\hat{\mathbf{c}} = \hat{\mathbf{z}}$ in Eq. (5.9), we get

$$\mathbf{E}(\mathbf{r}) = 0 . \tag{5.10}$$

Similarly the expression for the magnetic field can be computed by the substitution of Eqs. (5.3) and (5.4) along with $\hat{\mathbf{c}} = \hat{\mathbf{z}}$ into Eq. (1.28), and is given as

$$\mathbf{H}(\mathbf{r}) = 0 . \tag{5.11}$$

This means that no radiations are present in the far zone when both the optic axis and the dipole are parallel to each other.

5.4 Optic axis perpendicular to the dipole
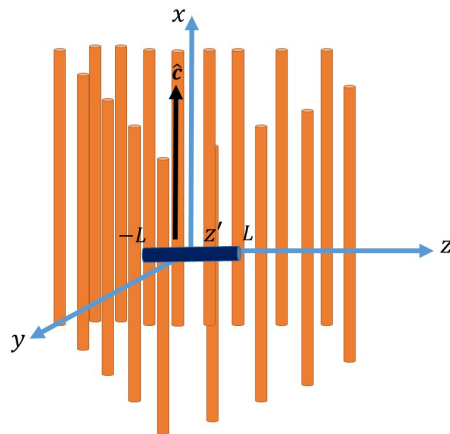
FIGURE 5.2: Schematic figure showing a finite length dipole placed in the zero-index wire material with $\varepsilon_a \approx 0$. The optic axis is along x axis and the dipole is along z axis.

Let us now consider the situation in which the optic axis is along x axis, and the finite-length dipole is along z axis and is placed in the zero-index wire material with $\varepsilon_a \approx 0$ as shown in Fig. 5.2.

5.4.1 Near field

The electric field in the near zone ($k_o n_o R << 1$) can be computed by substituting Eqs. (5.1) and (5.4) into Eq. (1.27) along with $\hat{\mathbf{c}} = \hat{\mathbf{x}}$, and retaining the terms proportional to $1/r^3$ give

$$\mathbf{E}(\mathbf{r}) = 0. \tag{5.12}$$

Similarly, the magnetic field obtained by substituting Eqs. (5.3) and (5.4) into Eq. (1.28) along with $\hat{\mathbf{c}} = \hat{\mathbf{x}}$ and retaining the terms proportional to $1/r^3$ gives

$$\mathbf{H}(\mathbf{r}) = 0. \tag{5.13}$$

Therefore, the near-field of the dipole negligible in this case also.

5.4.2 Far field

The electric field in the far zone can be computed from Eq. (5.9) by replacing $\hat{\mathbf{c}} = \hat{\mathbf{x}}$, to get

$$\mathbf{E}(\mathbf{r}) = \frac{k_o^2 \mu_b p_o}{4\pi\varepsilon_o r} \frac{\exp(ik_o n_o r)}{y^2 + z^2} \left[y^2 \hat{\mathbf{z}} \int_{-L}^{L} \exp\left(-iszz'\right) dz' - y\hat{\mathbf{y}} \int_{-L}^{L} (z - z') \exp\left(-iszz'\right) dz' \right], \tag{5.14}$$

where $s = k_o n_o / r$. In Eq. (5.14), we have used the following approximation for the exponential terms

$$R_z = \left[r^2 + z'(z' - 2z) \right]^{\frac{1}{2}} \approx r - \frac{zz'}{r} \tag{5.15}$$

since our observation point is far away from the dipole. In the denominator, however, just $R_z \simeq r$ was used. Furthermore, we approximated

$$y^2 + (z - z')^2 \sim y^2 + z^2 \tag{5.16}$$

since $y^2 + z^2 \gg L$ in the far field. Now by evaluating integrals and converting into spherical coordinates, we get

$$\mathbf{E}(\mathbf{r}) = \frac{k_o \mu_b p_o}{2\pi\varepsilon_o n_o r}\left(-\hat{\mathbf{y}} + \tan\theta\sin\phi\hat{\mathbf{z}}\right)\frac{\exp(ik_o n_o r)\sin\theta\sin\phi}{(\sin^2\theta\sin^2\phi + \cos^2\theta)}\sin(k_o n_o L\cos\theta)\,. \tag{5.17}$$

Similarly, the magnetic field was obtained by substituting Eqs. (5.3) and (5.4) into Eq. (1.28) along with $\hat{\mathbf{c}} = \hat{\mathbf{x}}$ and retaining the terms proportional to $1/r$, to get

$$\mathbf{H}(\mathbf{r}) = \frac{k_o^2 n_o p_o c}{4\pi}\int_{-L}^{L}\frac{\exp(ik_o n_o R_z)}{R_z^2}\frac{[-xy^2\hat{\mathbf{y}} + y^3\hat{\mathbf{x}} - xy(z - z')\hat{\mathbf{z}} + y(z - z')^2\hat{\mathbf{x}}]}{y^2 + (z - z')^2}dz'\,. \tag{5.18}$$

Using the approximations given in Eq. (5.15) for the exponential term, Eq. (5.16) and $R_z \simeq r$ in the denominator of Eq. (5.18), the expression for the magnetic field in spherical coordinate is found as

$$\begin{aligned}\mathbf{H}(\mathbf{r}) &= \frac{k_o p_o c}{2\pi r}\Big[(\sin^2\theta\sin^2\phi + \cos^2\theta)\hat{\mathbf{x}} - \sin^2\theta\cos\phi\sin\phi\hat{\mathbf{y}}\\ &\quad - \sin\theta\cos\theta\cos\phi\hat{\mathbf{z}}\Big]\frac{\exp(ik_o n_o r)\sin\theta\sin\phi}{\cos\theta(\sin^2\theta\sin^2\phi + \cos^2\theta)}\sin(k_o n_o L\cos\theta)\,.\end{aligned} \tag{5.19}$$

From the expression of the electric and magnetic field in the far zone, its clear that only ordinary wave is emitted by the dipole.

The time-averaged power radiated per unit solid angle by the finite length dipole can be found by the substitution of Eqs. (5.17) and (5.19) into Eq. (1.54), as

$$\frac{dP}{d\Omega} = \frac{k_o^2 \mu_b p_o^2 c}{8\pi^2\varepsilon_o n_o}\frac{\sin^2\theta\sin^2\phi}{\cos^2\theta(\sin^2\theta\sin^2\phi + \cos^2\theta)}\sin^2\left(k_o n_o L\cos\theta\right)\,. \tag{5.20}$$

The far-field radiation patterns of an ordinary wave emitted by a finite length dipole, given by Eq. (5.20), when the dipole is perpendicular to the optic axis and placed in zero index wire material with $\mu_b = 1$, $\varepsilon_b = 3.17$ [38], (left) $L = 0.01$, and (right) $L = 0.1$ are shown in Fig. 5.3. Such a zero index
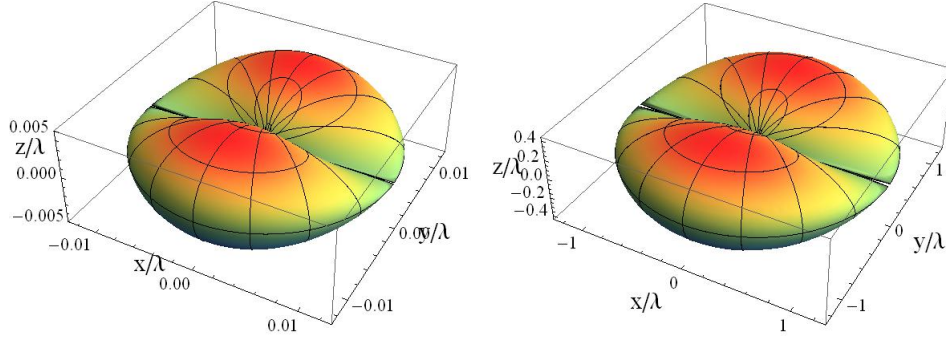
FIGURE 5.3: The far-field radiation pattern given by Eq. (5.20), when the dipole is along z axis and the optic axis is along x axis, and is placed in the wire material with $\mu_b = 1$, $\varepsilon_a = 0$, $\varepsilon_b = 3.17$ [38], (left) $L = 0.01$ and (right) $L = 0.1$.

materials can be obtained practically, for example by having a silver wires ($\varepsilon_i \approx -15$) of radius $R = 20$ nm in a glass host ($\varepsilon_h \approx 2.25$) arranged in a unit cell of period $a = 100$ nm in the middle of visible part of the spectrum. The radiation pattern shows that the radiation are strongly suppressed along the direction of the optic axis. Also, as the length of the dipole increases, the pattern becomes more directive in the plane perpendicular the the dipole.

5.5 Concluding remarks

The closed-form expressions for the near-field and the far-field electromagnetic fields of a finite-length electric dipole in the uniaxial zero-index material (ZIM) were analytically derived and the representative numerical results were presented for the wire material in the zero index regime. The optic axis of the material was taken to be parallel and perpendicular to the dipole. When the dipole was parallel, the far field radiations were also negligible but the electric field in the near-zone was significant. However, when the dipole was perpendicular to the optic axis, radiation were emitted in the far field, that also only of the ordinary type. Though, the near field were negligible in this case. The increase in the length of the dipole resulted in the increase in the directivity of the field pattern. This means that scatterer present in uniaxial ZIM does not scatter light if the excitations in it only has dipole mode parallel to the optic axis.

Chapter 6

Conclusions and future directions

The near-field and the far-field radiation pattern of a finite-sized electric dipole in uniaxial dielectric material were analytically derived and the far-field numerical results were presented for representative materials. The dipole was taken to be along and perpendicular to the optic axis so that fields for arbitrary orientations can be constructed. When the dipole was placed parallel to the to the optic axis, only extraordinary waves were emitted in the far field. When the dipole was taken perpendicular to the optic axis, both ordinary and extraordinary waves were emitted but the radiations along the optic axis were suppressed for both the ordinary and extraordinary waves. For the latter case, there was no emission of extraordinary waves perpendicular to the dipole and the optic axis in the far field. For all the cases, the directivity of the radiation pattern increased significantly with the increase in the length of the dipole. A comparison with the results of the point dipole showed that the length of the finite-sized dipole plays a significant role in the directivity of the radiation pattern. The magnetic dipole was modeled as a current loop and similar results were found except that the role of ordinary and extraordinary waves was reversed. The approximate results for a point-magnetic dipole were also derived from current loop that agreed with the direct results.

The radiation pattern of the finite-sized electric dipole were also derived when the dipole was placed in the hyperbolic material. When we compared the finite-length dipole in the hyperbolic material with that of the uniaxial dielectric material, it showed that the radiation patterns are very different for the extraordinary waves but the patterns for the ordinary waves were similar. The directivity of the radiation pattern was strongly dependent upon the length of the dipole.

The results for the finite-length electric dipole were also derived when it was placed in the uniaxial zero-index material (ZIM). When the dipole was taken parallel to the optic axis, the far field radiations were negligible but the electric field in the near-zone was significant. However, when the dipole was perpendicular to the optic axis, radiations were emitted in the far field, that also only of the ordinary type. Though, the near field were negligible in this case. The increase in the length of the dipole resulted in the increase in the directivity of the field pattern. This means that impurities/scatterers present in uniaxial ZIM does not scatter light if the excitations in it only has dipole mode parallel to the optic axis.

The work presented in this thesis provides the analytical results for finite-sized electric and magnetic dipoles in uniaxial material. This can provide foundations for an understanding of scattering and radiation in these media. Furthermore, radiations and scattering from more complicated geometries can be constructed using size-dependent results because bigger sources and scatterers can be assumed as assemblies of smaller parts. The results presented here can be used as a springboard to formulate radiation and scattering by finite-sized objects like spheres, cylinders, and other canonical geometries to model more realistic sources such as quantum dots, wires, and sheets. Furthermore, scattering from impurities present in uniaxial metamaterials can also be studied using the results in this thesis.

Bibliography

[1] F. E. Veiras, L. I. Perez, and M. T. Garea. "Phase shift formulas in uniaxial media: an application to waveplates". In: *Appl. Opt.* 49.15 (2010), pp. 2769–2777.

[2] W. P. Mason. "Applications and Production of Quartz Crystals". In: *Nature* 168.4287 (1951), p. 1098.

[3] G. W. Milton et al. "A proof of superlensing in the quasistatic regime, and limitations of superlenses in this regime due to anomalous localized resonance". In: *P. Roy Soc. A-Math, Phy* 461.2064 (2005), pp. 3999–4034.

[4] J. Zubin, L. V. Alekseyev, and E. Narimanov. "Optical Hyperlens: Far-field imaging beyond the diffraction limit". In: *Opt. Express* 14.18 (2006), pp. 8247–8256.

[5] A. V. Kabashin et al. "Plasmonic nanorod metamaterials for biosensing". In: *Nat. Mater.* 8.11 (2009), pp. 867–871.

[6] D. Schurig et al. "Metamaterial electromagnetic cloak at Microwave Frequencies". In: *Science* 314.5801 (2006), pp. 977–980.

[7] A. A. Govyadinov and V. A. Podolskiy. "Metamaterial photonic funnels for subdiffraction light compression and propagation". In: *Phys. Rev. B* 73.15 (2006), p. 155108.

[8] I. I. Smolyaninov and Y. Hung. "Modeling of time with metamaterials". In: *J. Opt. Soc. Am. B* 28.7 (2011), pp. 1591–1595.

[9]   X. Zhang and Y. Wu. "Effective medium theory for anisotropic metamaterials". In: *Sci. Rep.* 5.1 (2015), p. 7892.

[10]   E. M. Purcell. "Spontaneous Emission Probabilities at Radio Frequencies". In: *Phys. Rev.* 69 (1946), p. 681.

[11]   K. G. Balmain, A. A. E. Luttgen, and P. C. Kremer. "Resonance cone formation, reflection, refraction, and focusing in a planar anisotropic metamaterial". In: *IEEE Antennas Wirel. Propag. Lett.* 1 (2002), pp. 146–149.

[12]   T. Taubner et al. "Near-Field microscopy through a SiC superlens". In: *Science* 313 (2006), p. 1595.

[13]   J. Yao et al. "Three-dimensional nanometer-scale optical cavities of indefinite medium". In: *Proc. Natl. Acad. Sci.* 108.28 (2011), pp. 11327–11331.

[14]   U. Tumkur et al. "Control of absorption with hyperbolic metamaterials". In: *Appl. Phys. Lett.* 100 (2012), p. 161103.

[15]   Z. Liu et al. "Far-Field Optical Hyperlens Magnifying Sub-Diffraction-Limited Objects". In: *Science* 315.5819 (2007), pp. 1686–1686.

[16]   C. H. Chen. "Dyadic Green's function and radiation in a uniaxially anisotropic medium". In: *International Journal of Electronics* 35.5 (1973), pp. 633–640.

[17]   A. Lakhtakia, V. K. Varadan, and V. V. Varadan. "Radiation and canonical sources in uniaxial dielectric media". In: *Int. J. Electron.* 65.6 (1988), pp. 1171–1175.

[18]   L.A. Alexeyeva, I.A. Kanymgaziyeva, and S.S. Sautbekov. "Generalized solutions of Maxwell equations for crystals with electric and magnetic anisotropy". In: *J. Electromagnet. Wave.* 28 (Aug. 2014), pp. 1974–1984.

[19]   L. Tsang, E. Njoku, and J. A. Kong. "Microwave thermal emission from a stratified medium with nonuniform temperature distribution". In: *J. Appl. Phys.* 46.12 (1975), pp. 5127–5133.

[20] J. A. Kong. "Electromagnetic fields due to dipole antennas over stratified anisotropic media". In: *Geophys.* 37 (1972), pp. 985–996.

[21] Y. S. Kwon and J. J. H. Wang. "Computation of Hertzian dipole radiation in stratified uniaxial anisotropic media". In: *Radio Science* 21.06 (1986), pp. 891–902.

[22] C. M. Tang. "Electromagnetic fields due to dipole antennas embedded in stratified anisotropic media". In: *IEEE T. Antenn. Propag.* 27.5 (1979), pp. 665–670.

[23] S. Ali and S. Mahmoud. "Electromagnetic fields of buried sources in stratified anisotropic media". In: *IEEE T. Antenn. Propag.* 27.5 (1979), pp. 671–678.

[24] A. Eroglu and J. Kyoon. "Far field radiation from an arbitrarily oriented Hertzian dipole in the presence of a layered anisotropic medium". In: *IEEE T. Antenn. Propag.* 53.12 (2005), pp. 3963–3973.

[25] M. Faryad and A. Lakhtakia. *Infinite-Space Dyadic Green Functions in Electromagnetism*. 2053-2571. Morgan & Claypool Publishers, (2018).

[26] C. H. Chen. *Theory of Electromagnetic Waves: A Coordinate-free Approach*. McGraw-Hill, (1985).

[27] L. B. Felsen and N. Marcuvitz. *Radiation and Scattering of Waves*. Piscataway, N.J. : IEEE Press, (1994).

[28] T. G. Mackay and A. Lakhtakia. *Electromagnetic Anisotropy and Bianisotropy*. World Scientific, (2010).

[29] A. Yariv and P. Yeh. *Optical Waves in Crystals: Propagation and control of laser radiation*. John Wiley and Sons Inc., 1984.

[30] C. D. Gribble and A. J. Hall. *Optical Mineralogy:Principles and Practice*. Springer US, (1992).

[31] K. Korzeb, M. Gajc, and D. A. Pawlak. "Compendium of natural hyperbolic materials". In: *Opt. Express* 23.20 (2015), pp. 25406–25424.

[32] A. Poddubny et al. "Hyperbolic metamaterials". In: *Nat. Photonics.* 7 (2013), pp. 948–957.

[33] M. Born and E. Wolf. *Principles of Optics: Electromagnetic theory of propagation, interference and diffraction of light*. 1970.

[34] W. Cai and V. Shalaev. *Optical metamaterials, fundamentals and applications*. Springer, 2010.

[35] A. Lakhtakia. "Constraints on Effective Constitutive Parameters of Certain Bianisotropic Laminated Composite Materials". In: *Electromagnetics* 29.6 (2009), pp. 508–514.

[36] S. Jamil. *On the dispersion equation for electromagnatic plane wave propagation in uniaxial and biaxial metamaterials.* (2018).

[37] V. P. Drachev, V. A. Podolskiy, and A. V. Kildishev. "Hyperbolic metamaterials: new physics behind a classical problem". In: *Opt. Express* 21.12 (2013), pp. 15048–15064.

[38] B. M. Wells, A. V. Zayats, and V. A. Podolskiy. "Nonlocal optics of plasmonic nanowire metamaterials". In: *Phys. Rev. B* 89 (3 2014), p. 035111.

[39] C. R. Simovski P. A. Belov A. V. Atrashchenko Y. S. Kivshar. "Wire Metamaterials: Physics and Applications". In: *Adv. Mater.* 24.31 (2012), pp. 4229–4248.

[40] O. Kidwai, S. V. Zhukovsky, and J. E. Sipe. "Dipole radiation near hyperbolic metamaterials: applicability of effective-medium approximation". In: *Opt. Lett.* 36.13 (2011), pp. 2530–2532.

[41] M. Wubs W. Yan and N. A. Mortensen. "Hyperbolic metamaterials: Nonlocal response regularizes broadband supersingularity". In: *Phys. Rev. B* 86 (20 2012), p. 205429.

[42] S. Tse P. Ikonen M. G. Silveirinha C. R. Simovski S. Tretyakov Y. Hao P. A. Belov Y. Zhao and C. Parini. "Transmission of images with subwavelength resolution to distances of several wavelengths in the microwave range". In: *Phys. Rev. B* 77 (19 2008), p. 193108.

[43] S. Thongrattanasiri and V. A. Podolskiy. "Hypergratings: nanophotonics in planar anisotropic metamaterials". In: *Opt. Lett.* 34.7 (2009), pp. 890–892.

[44] A. Salandrino and N. Engheta. "Far-field subdiffraction optical microscopy using metamaterial crystals: Theory and simulations". In: *Phys. Rev. B* 74 (7 2006), p. 075103.

[45] A. V. Kabashin et al. "Plasmonic nanorod metamaterials for biosensing". In: *Nat. Mater.* 8 (2011), 867—871.

[46] A. Murphy J. McPhillips R. J. Pollard V. A. Podolskiy V. V. Yakovlev W. Dickson and A. V. Zayats. "Ultrasensitive Non-Resonant Detection of Ultrasound with Plasmonic Metamaterials". In: *Adv. Mater.* 25 (16 2013), pp. 2351–2356.

[47] P. A. Belov A. S. Potemkin A. N. Poddubny and Y. S. Kivshar. "Green functions for hyperbolic media". In: *Phys. Rev. A* 86 (2012), p. 023848.

[48] E. Narimanov I. Kretzshmar H. N. S. Krishnamoorthy Z. Jacob and V. M. Menon. "Topological transitions in metamaterials". In: *Science* 336 (2012), pp. 205–209.

[49] Y. Liu Y. Wang C. Sun G. Bartal A. M. Stacy J. Yao Z. Liu and X. Zhang. "Optical negative refraction in bulk metamaterials of nanowires". In: *Science* 321 (2008), p. 930.

[50] G. Zhu T. Tumkur H. Li M. A. Noginov Y. A. Barnakov and E. E. Narimanov. "Bulk photonic metamaterial with hyperbolic dispersion". In: *Appl. Phys. Lett.* 94 (2009), p. 151105.

[51] T. Tumkur H. Li Y. A.Barnakov L. V. Alekseyev E. E. Narimanov and M. A. Noginov. "Uniaxial epsilon-near-zero metamaterial for angular filtering and polarization control". In: *Appl. Phys. Lett.* 97 (2010), p. 131107.

[52] S. Molesky C. L. Cortes W. Newman and Z. Jacob. "Quantum nanophotonics using hyperbolic metamaterials". In: *J. Opt.* 14 (2012), p. 063001.

[53] J. B. Pendry. "Negative refraction makes a perfect lens". In: *Phys. Rev. Lett.* 85 (2000), pp. 3966–3969.

[54] D. R. Smith R. A. Shelby and S. Schultz. "Experimental verification of a negative index of refraction". In: *Science* 292 (2001), pp. 77–79.

[55] E. Hwang I. I. Smolyaninov and E. E. Narimanov. "Hyperbolic metamaterial interfaces: Hawking radiation from Rindler horizons and spacetime signature transitions". In: *Phys. Rev. B* 85 (2012), p. 235122.

[56] S. He Y. He and X. Yang. "Optical field enhancement in nanoscale slot waveguides of hyperbolic metamaterials". In: *Opt. Lett.* 37 (2012), 2907–2909.

[57] D. R. Smith and D. Schurig. "Electromagnetic Wave Propagation in Media with Indefinite Permittivity and Permeability Tensors". In: *Phys. Rev. Lett.* 90 (2003), p. 077405.

[58] P. Kolinko D. R. Smith and D. Schurig. "Negative refraction in indefinite media". In: *J. Opt. Soc. Am. B* 21 (2004), pp. 1032–1043.

[59] A. V. Kildishev W. Cai U. K. Chettiar and V. M. Shalaev. "Designs for optical cloaking with high-order transformations". In: *Opt. Express* 16 (2008), pp. 5444–5452.

[60] S. S. Howard K. J. Franz D. Wasserman V. A. Podolskiy E. E. Narimanov D. L. Sivco A. J. Hoffman L. Alekseyev and C. Gmachl. "Negative refraction in semiconductor metamaterials". In: *Nat. Mater.* 6 (2007), 946–950.

[61] D. R. Smith, P. Kolinko, and D. Schurig. "Negative refraction in indefinite media". In: *J. Opt. Soc. Am. B* 21.5 (2004), pp. 1032–1043.

[62] V. A. Podolskiy and E. E. Narimanov. "Strongly anisotropic waveguide as a nonmagnetic left-handed system". In: *Phys. Rev. B* 71.20 (2005), p. 201101.

[63] P. A. Belov, C. R. Simovski, and P. Ikonen. "Canalization of subwavelength images by electromagnetic crystals". In: *Phys. Rev. B* 71.19 (2005), p. 193105.

[64] M. Noginov et al. "Focus issue: hyperbolic metamaterials". In: *Opt. Express* 21.12 (2013), pp. 14895–14897.

[65] C L Cortes et al. "Quantum nanophotonics using hyperbolic metamaterials". In: *J. Opt.* 14.6 (2012), p. 063001.

[66] M. A. Noginov et al. "Controlling spontaneous emission with metamaterials". In: *Opt. Lett.* 35.11 (2010), pp. 1863–1865.

[67] J. Yao et al. "Optical Negative Refraction in Bulk Metamaterials of Nanowires". In: *Science* 321.5891 (2008), pp. 930–930.

[68] A. N. Poddubny, P. A. Belov, and Y. S. Kivshar. "Purcell effect in wire metamaterials". In: *Phys. Rev. B* 87.3 (2013), p. 035136.

[69] S.-A. Biehs, M. Tschikin, and P. Ben-Abdallah. "Hyperbolic Metamaterials as an Analog of a Blackbody in the Near Field". In: *Phys. Rev. Lett.* 109.10 (2012), p. 104301.

[70] I. S. Nefedov and C. R. Simovski. "Giant radiation heat transfer through micron gaps". In: *Phys. Rev. B* 84.19 (2011), p. 195459.

[71] R. W. Ziolkowski N. Engheta. *Metamaterials: Physics and Engineering Explorations*. Wiley, 2006.

[72] R. W. Ziolkowski. "Propagation in and scattering from a matched metamaterial having a zero index of refraction". In: *Phys. Rev. E* 70 (4 2004), p. 046608.

[73] N. Engheta. "Pursuing Near-Zero Response". In: *Science* 340 (6130 2013), pp. 286–287.

[74] M. W. Ashraf and M. Faryad. "On the mapping of Dirac-like cone dispersion in dielectric photonic crystals to an effective zero-index medium". In: *J. Opt. Soc. Am. B* 33.6 (2016), pp. 1008–1013.

[75] Z. W. Liu et al. "Far-field optical hyperlens magnifying subdiffraction- limited objects". In: *Science* 315.5819 (2007), pp. 1686–1686.

[76] S. A. Ramakrishna et al. "Imaging the near field". In: *J. Mod. Opt.* 50.9 (2003), pp. 1419–1430.

[77] P. A. Belov and Y. Hao. "Subwavelength imaging at optical frequencies using a transmission device formed by a periodic layered metal-dielectric structure operating in the canalization regime". In: *Phys. Rev. B* 73 (11 2006), p. 113110.

[78] W. Yan J. Hao and M. Qiu. "Super-reflection and cloaking based on zero index metamaterial". In: *Appl. Phys. Lett.* 96.10 (2010), p. 101109.

[79] L. Chen V. C. Nguyen and K. Halterman. "Total Transmission and Total Reflection by Zero Index Metamaterials with Defects". In: *Phys. Rev. Lett.* 105.23 (2010), p. 233908.

[80] W. X. Jiang Q. Cheng and T. J. Cui. "Multi-beam generations at pre-designed directions based on anisotropic zero-index metamaterials". In: *Appl. Phys. Lett.* 99.13 (2011), p. 131913.

[81] S. A. Maier F. Mao J. J. Yang Y. Francescato and M. Huang. "Mu and epsilon near zero metamaterials for perfect coherence and new antenna designs". In: *Opt. Express* 22.8 (2014), pp. 9107–9114.

[82] Y. Jin and S. He. "Enhancing and suppressing radiation with some permeability-near-zero structures". In: *Opt. Express* 18.16 (2010), pp. 16587–16593.

[83] S. Maci J. C. Soric N. Engheta and A. Alu. "Omnidirectional Metamaterial Antennas Based on ε-Near-Zero Channel Matching". In: *IEEE T. Antenn. Propag.* 61.1 (2013), pp. 33–44.

[84] A. M. Mahmoud and N. Engheta. "Wave–matter interactions in epsilon-and-mu-near-zero". In: *Nat. Commun.* 5 (1 2014), p. 5638.

[85] Z. Gu X. Zou Y. Li B. Liang and J. Cheng. "Unidirectional acoustic transmission through a prism with near-zero refractive index". In: *Appl. Phys. Lett.* 103.5 (2013), p. 053505.

[86] A. Hayat and M. Faryad. "On the radiation from a Hertzian dipole of a finite length in the uniaxial dielectric medium". In: *OSA Continuum* 2 (2019), pp. 1411–1429.

[87] J. D. Jackson. *Classical electrodynamics*. John Wiley and Sons Inc., 1999.

[88] A. Zangwill. *Modern electrodynamics, Ch. 20*. Cambridge, University Press, 2012.

[89] H. Kuzmany. *Solid State Spectroscopy*. Springer, 2009.

[90] N.S. Bellyustin and V.P. Dokuchaev. "Generation of electromagnetic waves by distributed currents in an anisotoipic medium". In: *Radiophys. Quantum Electron.* 18 (1975), pp. 10–17.

[91]   T. N. C. Wang and T.-L. Wang. "Radiation resistance of small electric and magnetic antennas in a cold uniaxial plasma". In: *IEEE T. Antenn. Propag.* 20 (1972).

[92]   T. Wang and Tzu-Li Wang. "Radiation resistance of small electric and magnetic antennas in a cold uniaxial plasma". In: *IEEE T. Antenn. Propag.* 20.6 (1972), pp. 796–798.

[93]   G. Alkina and S. Sautbekov. "Radiation of a magnetic dipole in hyperbolic uniaxial media". In: *ICEAA, 14614727, Palm Beach, Netherlands* (2014).

[94]   A.V. Kudrin T. M. Zaboronkova and E.Yu. Petrov. "Toward the theory of a loop antenna in an anisotropic plasma". In: *Quantum Electron.* 41 (1998), pp. 236–246.

[95]   T. M. Zaboronkova A. V. Kudrin and A. S. Zaitseva. "Electrodynamic characteristics of a loop antenna located on the surface of a uniaxial anisotropic cylinder". In: *2016 Days on Diffraction (DD), June 27-July 1, St. Petersburg, 16504249* (2016).

[96]   D. M. Pozar. "Radiation and scattering from a microstrip patch antenna on a uniaxial substrate". In: *Antennas Propag.* 35 (1987), pp. 613–621.

[97]   T. M. Zaboronkova, A. V. Kudrin, and E. Yu. Petrov. "Toward the theory of a loop antenna in an anisotropic plasma". In: *Radiophys. Quantum Electron.* 41.3 (1998), pp. 1573–9120.

[98]   M. A. Salem and C. Caloz. "Electromagnetic fields radiated by a circular loop with arbitrary current". In: *IEEE Trans. Antennas Prop.* 63 (2015), pp. 442–446.

[99]   V. A. Podolskiy and E. E. Narimanov. "Strongly anisotropic waveguide as a nonmagnetic left-handed system". In: *Phys. Rev. B* 71 (2005), p. 201101.

[100] J. Atkinson P. Shekhar and Z. Jacob. "Hyperbolic metamaterials: Fundamentals and applications". In: *Nano Convergence* 1 (2014), p. 14.

[101] Z. Jacob and V. M. Shalaev. "Plasmonics goes quantum". In: *Science* 334 (2011), pp. 463–464.

[102] P. A. Belov A. N. Poddubny and Y. S. Kivshar. "Spontaneous radiation of a finite-size dipole emitter in hyperbolic media". In: *Phys. Rev. A* 84 (2011), p. 023807.

[103] S. V. Zhukovsky O. Kidwai and J. E. Sipe. "Dipole radiation near hyperbolic metamaterials: Applicability of effective-medium approximation". In: *Opt. Lett.* 36 (2011), p. 2530.

[104] A. Orlov P. Belov I. Iorsh A. Poddubny and Y. S. Kivshar. "Spontaneous emission enhancement in metal–dielectric metamaterials". In: *Phys. Lett. A* 376 (2012), p. 185.

[105] W. Yan, M. Wubs, and N. A. Mortensen. "Hyperbolic metamaterials: Nonlocal response regularizes broadband supersingularity". In: *Phys. Rev. B* 86 (2012), p. 205429.

[106] P. Ginzburg A. V. Zayats A. N. Poddubny P. A. Belov and Y. S. Kivshar. "Microscopic model of Purcell enhancement in hyperbolic metamaterials". In: *Phys. Rev. B* 86 (2012), p. 035148.

[107] P. Ginzburg A. V. Zayats A. N. Poddubny P. A. Belov and Y. S. Kivshar. "Improving the radiative decay rate for dye molecules with hyperbolic metamaterials". In: *Opt. Express* 20 (2012), p. 8100.

[108] J. D. Caldwell *et al.* "ub-diffractional volume-confined polaritons in the natural hyperbolic material hexagonal boron nitride". In: *Nature Commun.* 5 (2014), p. 5221.

[109] J. B. Pendry D. R. Smith and M. C. K. Wiltshirei. "Metamaterials and negative refractive index". In: *Science* 305 (2004), pp. 788–792.

[110] N. Engheta. "Circuits with light at nanoscales: Optical nanocircuits inspired by metamaterials". In: *Science* 317 (2007), 1698–1702.

[111] J. B. Pendry. "Negative Refraction Makes a Perfect Lens". In: *Phys. Rev. Lett.* 85 (2000), pp. 3966–3969.

[112] D. C. Vier S. C. Nemat-Nasser D. R. Smith W. J. Padilla and S. Schultz. "Composite medium with simultaneously negative permeability and permittivity". In: *Phys. Rev. Lett.* 84 (2000), pp. 4184–4187.

[113] *et al.* D. Schurig. "Metamaterial electromagnetic cloak at microwave frequencies". In: *Science* 314 (2006), pp. 977–980.

[114]   A. Alù M. G. Silveirinha and N. Engheta. "Parallel-plate metamaterials for cloaking structures". In: *Phys. Rev. E* 75 (2007), p. 036603.

[115]   A. S. Schwanecke A. V. Rogacheva V. A. Fedotov and N. I. Zheludev. "Giant gyrotropy due to electromagnetic-field coupling in a bilayered chiral Structure". In: *Phys. Rev. Lett.* 97 (2006), p. 177401.

[116]   J. Valentine et al. "Three-dimensional optical metamaterial with a negative refractive index". In: *Nature* 455 (2008), 376–379.

[117]   H. Chen et al. "Design and experimental realization of a broadband transformation media field rotator at microwave frequencies". In: *Phys. Rev. Lett.* 102 (2009), p. 183903.

[118]   W. Yan J. Hao and M. Qiu. "Super-reflection and cloaking based on zero index metamaterial". In: *Appl. Phys. Lett.* 96 (2010), p. 101109.

[119]   L. Chen V. C. Nguyen and K. Halterman. "Total transmission and total reflection by zero index metamaterials with defects". In: *Phys. Rev. Lett.* 105 (2010), p. 233908.

[120]   Y. Xu and H. Chen. "Total reflection and transmission by epsilon-near-zero metamaterials with defects". In: *Appl. Phys. Lett.* 98 (2011), p. 113501.

[121]   Y. Wu and J. Li. "Total reflection and cloaking by zero index metamaterials loaded with rectangular dielectric defects". In: *Appl. Phys. Lett.* 102 (2013), p. 183105.

[122]   B. Wang and K. M. Huangi. "Shaping the radiation pattern with Mu and epsilon-near-zero metamaterials". In: *Prog. Electromagnetics Res.* 106 (2010), 107–119.

[123]   W. X. Jiang Q. Cheng and T. J. Cui. "Multi-beam generations at pre-designed directions based on anisotropic zero-index metamaterials". In: *Appl. Phys. Lett.* 99 (2011), p. 131913.

[124]   S. Maier F. Mao J. J. Yang Y. Francescato and M. Huang. "Mu and epsilon near zero metamaterials for perfect coherence and new antenna designs". In: *Opt. Express* 22 (2014), p. 9107.

[125] Y. Jin and S. He. "Enhancing and suppressing radiation with some permeability near-zero structures". In: *Opt. Express* 18 (2010), 16587–16593.

[126] M. Silveirinha and N. Engheta. "Design of matched zero-index metamaterials using nonmagnetic inclusions in epsilon-near-zero media". In: *Phys. Rev. B* 75 (2007), p. 075119.

[127] R. Liu et al. "Experimental demonstration of electromagnetic tunneling through an epsilon-near-zero metamaterial at microwave frequencies". In: *Phys. Rev. Lett.* 100 (2008), p. 023903.

[128] Z. Gu X. Zou Y. Li B. Liang and J. Cheng. "Unidirectional acoustic transmission through a prism with near-zero refractive index". In: *Appl. Phys. Lett.* 103 (2013), p. 053505.

[129] M. W. Ashraf and M. Faryad. "Dirac-like cone dispersion in two-dimensional core-shell dielectric photonic crystal". In: *J. Nanophoton.* 9 (2015), p. 093057.

[130] P. A. Belov et al. "Transmission of images with subwavelength resolution to distances of several wavelengths in the microwave range". In: *Phys. Rev. B* 77 (2008), p. 193108.

[131] M. Fink F. Lemoult and G. Leroseyi. "A polychromatic approach to far-field superlensing at visible wavelengths". In: *Nat. Commun.* 3 (2012), p. 889.

[132] S. Pastkovsky W. Hendren G. A.Wurtz R. Atkinson R. Pollard V. A. Podolskiy A. V. Kabashin P. Evans and A. V. Zayats. "Plasmonic nanorod metamaterials for biosensing". In: *Nat. Mater.* 8 (2009), p. 867.

[133] V. V. Vorobev and A. V. Tyukhtin. "Nondivergent Cherenkov Radiation in a Wire Metamaterial". In: *Phys. Rev. Lett.* 108 (2012), p. 184801.

[134] S. I. Maslovski D. E. Fernandes and M. G. Silveirinha. "Cherenkov emission in a nanowire material". In: *Phys. Rev. B* 85 (2012), p. 155107.

[135] M. G. Silveirinha and S. I. Maslovski. "Radiation from elementary sources in a uniaxial wire medium". In: *Phys. Rev. B* 85 (2012), p. 155125.

[136]   A. Hayat and M. Faryad. "On the radiation from a Hertzian dipole of a finite length in the uniaxial dielectric medium: erratum". In: *OSA Continuum* 2 (2019), pp. 2855–2855.